DISCRETE FUNCTIONALIZATION OF RESORCINARENES FOR APPLICATIONS IN SUPRAMOLECULAR CHEMISTRY

by

KWAKU TWUM

A dissertation submitted in partial fulfillment of the

requirements for the degree of

DOCTOR OF PHILOSOPHY IN BIOMEDICAL SCIENCES: HEALTH AND ENVIRONMENTAL CHEMISTRY

2023

Oakland University

Rochester, Michigan

Doctoral Advisory Committee:

Ngong Kodiah Beyeh, Ph.D., Chair
Michael Sevilla, Ph.D.
Ziming Yang, Ph.D.
Gerard Madlambayan, Ph.D.

To my mum and dad

ACKNOWLEDGMENTS

To God be all the glory.

I want to first acknowledge the mentorship of Dr. Ngong Kodiah Beyeh throughout my graduate studies at Oakland University.

A special thank you also to my committee members, Dr. Michael Sevilla, Dr. Ziming Yang, and Dr. Gerard Madlambayan, Ph.D. program coordinator Dr. Xiangqun Zeng, and research collaborator Dr. John F. Trant (University of Windsor, ON, Canada) for their immense contributions to this dissertation research.

To my lab mates, past and present, thank you.

Finally, to the entire Twum family and my wife, Rosemond Badu, this is for you.

Kwaku Twum

PREFACE

The chemistry of macrocycles has since become ubiquitous in the field of supramolecular chemistry. The persistent hydrophobic cavities afford unique two-dimensional pockets that are utilized in this thesis dissertation for fundamental and translational research applications. In the following chapters, this dissertation presents an introduction to supramolecular chemistry, types of macrocycles and a mini review of the past resorcinarene macrocyclic chemistry applications in the Beyeh Lab. Subsequently, this dissertation discusses cooperativity in non-covalent interactions that allows the self-assembly of three different molecules. Perhaps, the most common use of the resorcinarene macrocycle is for their molecular recognition potential as sensors. This dissertation discusses the functionalization of the resorcinarene framework to bind and sense N-alkyl ammonium cations, pyrophosphate anions. Finally, this dissertation highlights how a water soluble resorcinarene can also act as aggregation inhibitors for peptides that cause eye cataracts.

ABSTRACT

DISCRETE FUNCTIONALIZATION OF RESORCINARENES FOR APPLICATIONS IN SUPRAMOLECULAR CHEMISTRY

by

KWAKU TWUM

Adviser: Beyeh Ngong Kodiah, Ph.D.

Resorcinarenes are three dimensional cyclic oligomers obtained by acid-catalyzed condensation between resorcinol and an appropriate aldehyde. This doctoral thesis research presents basic and translational research studies that demonstrates the versatile functionalization and applications of the resorcinarene macrocycle.

In chapter one, this thesis introduces macrocyclic chemistry with a brief reflection of the history of the science and Beyeh Lab's use of the resorcinarene macrocycle in supramolecular chemistry. Chapter two presents a fundamental study of cooperativity in non-covalent interactions using a resorcinarene as anchor to a guest in solution that restricts its free rotation in solution. Chapter three explores the molecular recognition potential of functionalized resorcinarenes as sensors for ammonium cations and pyrophosphate anions. Last, chapter four presents functionalized water soluble resorcinarenes as aggregation inhibitors for peptides that cause eye cataracts.

These applications are all realized through the persistent hydrophobic cavity inherent in the basic resorcinarene cavitand and the synthetic functionalization of the macrocyclic ring which underscores the versatile use of resorcinarene compounds in supramolecular chemistry.

TABLE OF CONTENTS

TABLE OF CONTENTS-Continued

TABLE OF CONTENTS-Continued

LIST OF TABLES

LIST OF FIGURES

LIST OF ORIGINAL PUBLICATIONS

This dissertation is based on the following original publications with copyright permission notices in the appendices referred to by their number.

1. Kwaku Twum, S. Sadraej, J. Feder, S. M. Taimoory, K. Rissanen, J. F. Trant and N. K. Beyeh, *Sharing the salt bowl: Counterion identity drives N-alkyl resorcinarene affinity for pyrophosphate in water,* Organic Chemistry Frontiers, 2022, 9(5), 1267-1275.

2. Kwaku Twum, Avik Bhattacharjee, Erving T. Laryea, Josephine Esposto, George Omolloh, Shaelyn Mortensen, Maya Jaradi, Naomi L. Stock, Nicholas Schileru, Bianca Elias, Theresa M. McCormick, Sanela Martic, Ngong Kodiah Beyeh, *Functionalized resorcinarenes effectively disrupt the aggregation of αA66−80 crystallin peptide related to cataracts,* RSC Med. Chem*,* 2021, 12(12), 2022-2030.

3. Kwaku Twum, Mikko J. Rautiainen, Shilin Yu, Khai-Nghi Truong, Jordan Feder, Kari Rissanen, Rakesh Puttreddy and Ngong Kodiah Beyeh, *Host-Guest Interactions of Sodiumsulfonatomethyleneresorcinarene and Quaternary Ammonium Halides: An Experimental-Computational Analysis of the Guest Inclusion Properties,* Crystal Growth and Design, 2020, 20(4), 2367-2376.

4. S. Maryamdokht Taimoory, Kwaku Twum, Mohadeseh Dashti, Fangfang Pan, Manu Lahtinen, Kari Rissanen, Rakesh Puttreddy, John F. Trant, and Ngong Kodiah Beyeh, *Bringing a Molecular Plus One: Synergistic Binding Creates Guest-Mediated Three-Component Complexes*, Journal of Organic Chemistry, 2020, 85(9), 5884-5894.

The following are not part of this dissertation.

5. Kwaku Twum, Khai-Nghi Truong, Frank Boateng Osei, Carolina von Essen, Sanaz Nadimi, John F. Trant, Kari Rissanen and Ngong Kodiah Beyeh, Guest-mediated self-assembly of deprotonated 2-bromoresorcinarenes, Crystal Growth and Design, 2022.

6. Anna Karle, Kwaku Twum, Alise Haddad, S. Maryamdokht Taimoory , Małgorzata M. Szczęśniak, Evan Trivedi, John F. Trant, Ngong Kodiah Beyeh, *Development of High-Affinity and Selective Recognition Element for Kynurenic Acid Detection, The Analyst,* 2022, 147(10), 2264-2271.

7. Kwaku Twum, Kari Rissanen and Ngong Kodiah Beyeh, *Recent Advances in Halogen Bonded Assemblies with Resorcin [4] arenes*, The Chemical Record, 2021, 21(2), 386-395.

8. Kwaku Twum, Nicholas Schileru, Bianca Elias, Jordan Feder, Leena Yaqoo, Rakesh Puttreddy, Małgorzata M Szczesniak and Ngong Kodiah Beyeh, *Water Soluble Host–Guest Chemistry Involving Aromatic N-Oxides and Sulfonateresorcinarene*, Symmetry, 2020, 12(11), 1751.

9. Kwaku Twum, Nadimi, S., Osei, F.B., Puttreddy, R., Ojong, Y.B., Hayward, J.J., Rissanen, K., Trant, J.F. and Beyeh, N.K. (2023), *The "nitrogen effect": Complexation with macrocycles potentiates fused heterocycles to form halogen bonds in competitive solvents,* Chemistry Asian Journal, 2023, Just Accepted.

LIST OF ABBREVIATIONS

NMR	Nuclear Magnetic Resonance
MS	Mass Spectroscopy
IR	Infrared Spectroscopy
UV-VIS	Ultra-Violet Visible
ITC	Isothermal Titrations Calorimetry
TEM	Transmission Electron Microscopy
DLS	Dynamic Light Scattering
ESI	Electrospray Ionization
MALDI	Matrix Assisted Laser Desorption Ionization

CHAPTER ONE: INTRODUCTION TO SUPRAMOLECULAR CHEMISTRY

1.1 A historical perspective

Supramolecular chemistry is a branch of chemistry that studies chemical systems between discrete molecules.[1] Unlike traditional organic chemistry, supramolecular chemistry revolves around the reversibility of weak non-covalent interactions that have advanced concepts in self-assembly[2], molecular recognition[3], molecular folding[4], and molecular interlocked systems.[5] Interactions responsible for supramolecular systems and their applications are primarily weak attractions like hydrogen, halogen, van der Waal's, aromatic, and electrostatic interactions. Whiles scientists have postulated the existence of these interactions since the late 1800s, Nobel laureate Hermann Emil Fischer was the first to develop the principles that have since then shaped this branch of chemistry.[6] As a relatively younger science, supramolecular chemistry started to blossom about three decades ago with the first reports of crown ethers and their host-guest chemistry. Subsequent advancements in technology spared the gradual understanding of non-covalent interactions and their use for other applications discussed further in this and the following chapters.

Latimer and Rodebush's research paper in 1920 elucidated hydrogen bonding, then called electro-affinity, as a driving principle between the formation of complexes in solution.[7] This understanding spearheaded Watson and Crick's understanding of the complexity of the DNA double helical structure in 1948. This also led to a subsequent appreciation of protein folding and the influence of hydrogen bonds in protein misfolded

disease states.[8] Within similar frameworks, Robert Mulliken developed the charge transfer theory now known as halogen bonding between electronegative atom and a sigma hole.[9] Crystallographic studies by Odd Hassel, confirmed the halogen bond interaction that won the Nobel Prize in Chemistry in 1969.[10] These discoveries led to another explosion of supramolecular chemistry applications in crystal engineering, polymeric systems, biological macromolecules, and molecular recognition. One of these was in 1960s when Charles Pederson first reported crown ethers, organic macrocycle capable of ion complexation.[11] In 1987, Charles, alongside Donald Cram and Jean-Marie Lehn shared the Nobel Prize in Chemistry for synthesizing guest selective macrocyclic compounds for applications in supramolecular chemistry.[12] To this day clinicians use ion-selective crown ethers for selective detection of potassium ions using fluorescence spectroscopy.[13] In the 1990s, James Fraser Stoddart inspired another discipline in supramolecular chemistry with the discovery of molecular machines.[14] The discovery began an advent into giant supramolecules[15], interlocked structures[16], molecular motion[17], and molecular imprint polymers.[18] In recent times, the field has become increasingly even more complex with the advent of technology which has expanded the range of possibilities beyond what the pioneers even envisioned.

Supramolecular chemistry principles have hence taken root in materials chemistry, medicine, electrochemistry, pharmaceutical sciences, nanostructures, among many others. Nowadays, it is not enough to simply tell one that you are a supramolecular chemist. The contemporary understanding has evolved to encompass any science where there is intermolecular communication resulting in self-assembly. Scientists have used

these principles in (thin)films, gels, polymers, batteries, sensors, drugs, and even electronic systems.[19] This proliferation has also evolved to include adaptation and inspiration from nature. For example, enzymatic activity and selectivity inspired development of molecular recognition systems with catalytic activity[20] whilst hydrophobic cavities in protein structures have inspired synthetic systems with persistent hydrophobic cavities.[21]

Within historical perspective, it's safe to say the future of the supramolecular chemistry is unpredictably exciting.

1.2 Introduction to macrocyclic chemistry

Macrocyclic chemistry is a discipline in supramolecular chemistry revolving around the synthesis and applications of organic cyclophanes with persistent hydrophobic cavities.[22] The pioneering work of Cram, Lehn, and Pederson in the 1960s not only spearheaded development in the discipline but also the advancement of supramolecular chemistry principles in other scientific disciplines. Advances in technology, knowledge and synthetic methodologies also pushed the envelope on the types and possible applications of macrocycles.[23] Scientists have also engaged self-assembly processes to construct other supramolecular architectures including molecular dumb bells, nano channels, nano capsules from macrocyclic compounds.[2] Synthetic routes to macrocycles have varied with improved yields over the years. The most common is via ring-closure macrocyclization using high dilution synthesis to avoid kinetic traps or templates to form preferred thermodynamic products.[24]

1.3 Subdivisions and applications of macrocycles

Several macrocycles exist in literature that fall under few broad categories. The differences can also be the result of functionalizations that affords unique properties like guest selectivity, solubility, and light emissions. Macrocycles typically have greater affinity for guest compounds than their acyclic counterparts due to cooperativity in their attractive interactions. Organic macrocycles have generally been grouped under the following broad categories.

1.3.1 Crown ethers

Crown ethers are two-dimensional macrocyclic compounds made up of repeating units of ether groups (Figure 1.1).[25] They are called crown ethers because of the crown-like conformation the macrocycle adopts when it complexes metal cations. The naming convention for crown ethers is two numbers interspaced with the word 'crown' e.g., 12-crown-4. The first number denotes the number of atoms in the macrocycle whiles the last number denotes the number of oxygen atoms. Crown ethers are typically used for complexing cations with selectivity due mainly to size match and charge density of the ion. 12-crown-4, 15-crown-5, 18-crown-6, and 21-crown-7 have peculiar cation selectivity for lithium, sodium, potassium, and cesium respectively.[26] Crown ethers were first reported by Charles Pederson, but scientists have since reported other crown ethers based on nitrogen (aza crown ethers)[27], sulfur (thia crown ethers)[28] and other functional group additions for conformational rigidity or photophysical effects.[29]

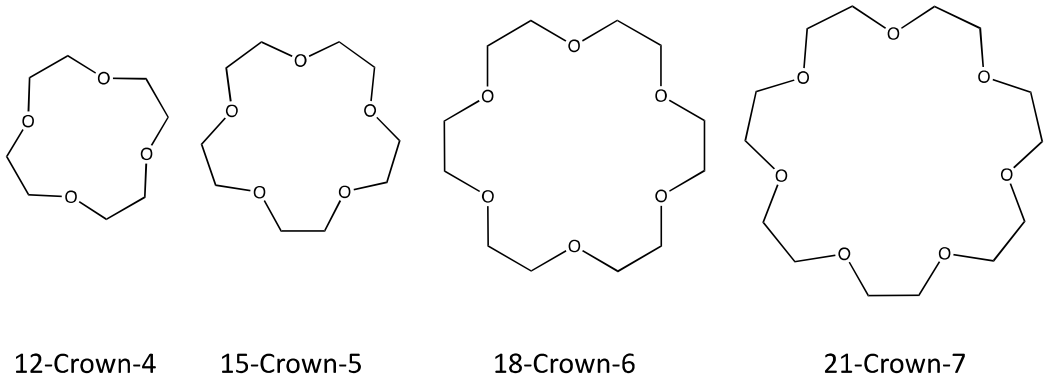

Figure 1.1: Structures of example crown ethers.

Crown ethers have traditionally been used for aqueous extraction of heavy metals with few quantitative studies on the extraction of other organic cations like amines[30] and amino acids.[31] Crown ethers have also been modified with chiral groups and derivatized on silica stationary phases for enantiomeric separations.[32] Metal complexation of crown ethers also enhances solubility in organic solvents enabling use as catalyst in organic reactions.[33] For metals too big to fit in the crown cavity, a 1:2 or 2:3 sandwich complex can form owing to the charge density and nucleophilicity of the counter-ion.[34] Crown ethers also have biochemical relevance as they have been reported for use as synthetic ionophores of sodium and potassium across the cellular membrane.[35] Lastly, crown ethers have also being explored for their antimicrobial activity due to their ability to complex signaling molecules necessary for bacterial proliferation.[36]

1.3.2 Cryptands

Cryptands are three dimensional macrocyclic compounds made from multidentate ligands for cationic guests (Figure 1.2).[37] Cryptands have an additional binding site for

chelating to a guest with better selectivity, affinity, and thermodynamic stability than crown ethers. Conventional naming of a cryptand is '[X.X.X]cryptand', where 'X' represents the number of ligand binding sites in each bridge between amine nitrogen atoms.

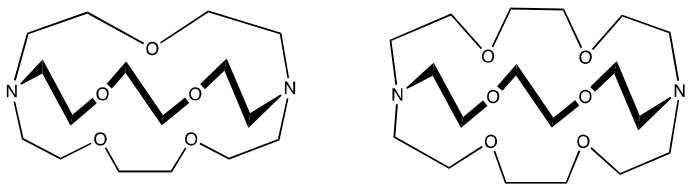

[1.2.2] cryptand [2.2.2] cryptand

Figure 1.2: Structure of example cryptands.

Historically, cryptands were first reported by Donald Cram, Jean-Marie Lehn, and Charles Pedersen which earned them the Nobel Prize in Chemistry in 1987.[12] Cryptands, like crown ethers, are popularly being used for binding cationic guests. Researchers have used cryptands to selectively monitor levels of potassium in blood under controlled pH levels.[37] Protonation of the macrobicyclic cryptand creates a cationic cage also capable of encapsulating anionic guests.[38] The lipophilic cryptand [2.2.2, C_{14}] has been reported as a catalyst for nucleophilic substitutions in chlorobenzene-water system via phase transfer.[39] Complexes of metal-ion and cryptands have also been used to extract metal ions from water into organic solvents.[40]

1.3.3 Calix[n]arenes

Calixarenes are macrocyclic compounds made from acid-catalyzed condensation of a phenol with an appropriate aldehyde.[41] Naming of calixarenes is generally based on the number of repeating units of the phenol in the macrocyclic ring e.g., calix[4]arene refers to a calixarene molecule with four repeating units. Typically, calixarenes can be substituted at the meso position based on the length of aldehyde used for the condensation reaction. This is added to the naming of the compound as a prefix 'C-', for example, C_{ethyl} calix[4]arene or C3-calix[4]arene.

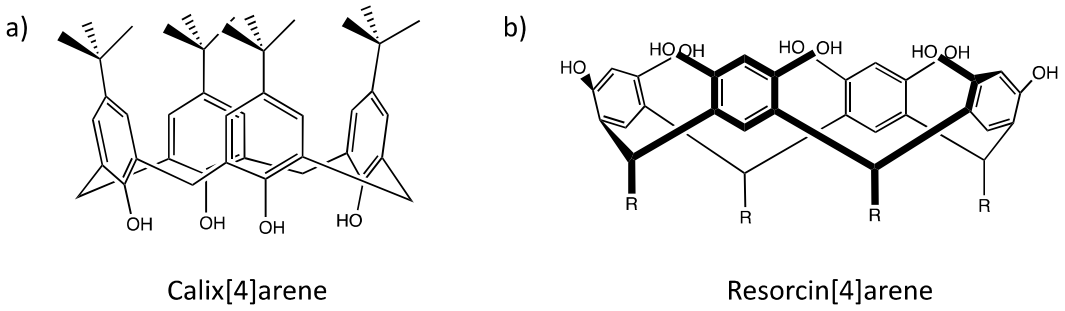

Calix[4]arene Resorcin[4]arene

Figure 1.3: Structure of example a) calix[4]arene and b) resorcin[4]arene

Resorcin[4]arenes are related calixarenes synthesized from acid-catalyzed condensation of resorcinol(1,3 dihydroxy benzene) and an appropriate aldehyde.[42] The choice of aldehyde forms the lower rim of the resorcinarene which also influences the solubility of the compound. Calixarenes in their parent form are notoriously insoluble in water until functionalized with water soluble functional groups like sulfonic acids or ammonium salts. The versatility of functionalized calixarenes and resorcinarenes have

created considerable applications in drug delivery, sensory recognition elements, fluorescent detectors and molecular self-assembly.[43]

This thesis discusses different applications of functionalized resorcinarenes.

1.3.4 Cyclodextrins

Cyclodextrins are arguably the most popular of cavitands especially in terms of research work and industrial applications (Figure 1.4). Cyclodextrins consist of oligosaccharide units joined by 1,4 glycosidic bonds as a macrocyclic compound.[43] There are three main types of cyclodextrins depending on how many repeating units of sugars make up the macrocycle including alpha-cyclodextrin, beta-cyclodextrin and gamma-cyclodextrin for 6, 7 and 8 glucose subunits respectively.

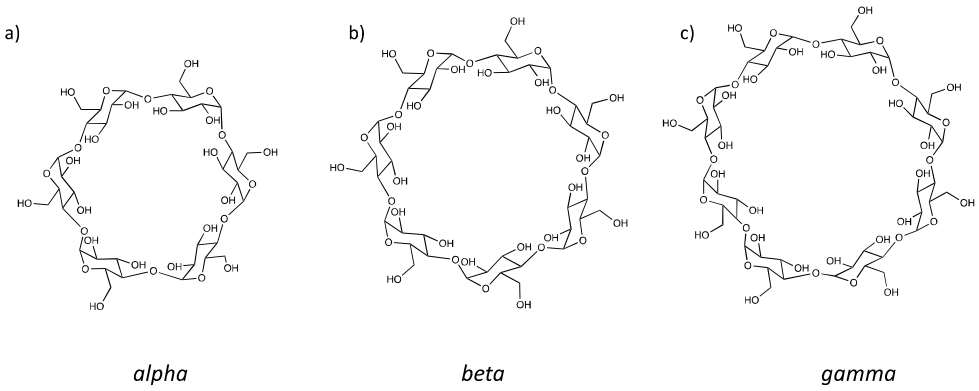

Figure 1.4: Structures of example cyclodextrins.

Their main synthetic route is through enzymatic treatment of starch to form a complex of mixtures which is subsequently purified using chromatography.[44] In supramolecular chemistry, cyclodextrins are noticeably used as solubilizing groups on hydrophobic complexes[45–47], capping units on mechanically interlocked systems[48],

coordination complexes[49] and stationary phase materials for HPLC separations[50]. In the pharmaceutical sector, cyclodextrins have also been employed as colorants, drug delivery aids and food preservatives.[51]

1.3.5 Pillar[n]arenes

Pillararenes are another class of macrocyclic cavitands composed of para-linked difunctionalized benzene units with methylene bridges (Figure 1.5).[52] The number of repeating units of benzene is used in naming pillararenes, e.g., pillar[5]arene is made up of five repeating benzene units. As a macrocycle, pillararenes are most famous for their host-guest chemistry applications but unlike other cavitands such as calixarenes and resorcinarenes, their internal hydrophobic cavity is accessible from both sides of the macrocycle.

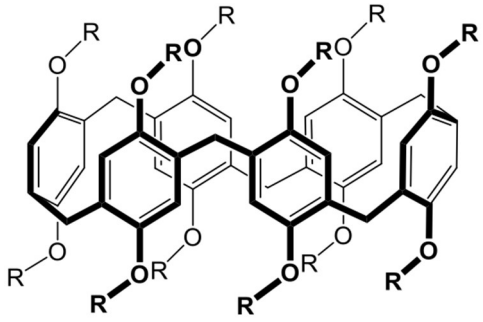

Figure 1.5: Structure of a pillar[6]arene macrocycle.

Pillar[5]arene is the most thermodynamically stable pillar[n]arene generated in synthesis but larger ring sized pillararenes have been reported using templates[53], bulky functional groups on the benzene monomer[54] or ring expansion of pillar[5]arene.[55] Like most cavitands, functionalization of the macrocycle generates functional applications.

Water soluble pillararenes have been used as drug delivery aids, bio-diagnostic sensory recognition elements and artificial ionophores.[56]

1.3.6 Cucurbiturils

Cucurbit[n]urils (CBs, figure 1.6) are also named according to the number of repeating units that forms the macrocyclic ring. They are synthesized from glycoluril units that are covalently linked by methylene bridges. The peculiar spatial orientation of the oxygen units on the linked monomer creates a partially enclosed hydrophobic cavity that is also bimodal (accessible from two directions).[57] Cucurbit[6]uril is the most stable macrocyclic of this group, however other different sized macrocycles have been reported using temperature control and template synthesis.[58] Like all the cavitands previously discussed, cucurbiturils are most famous for their host-guest chemistry applications.

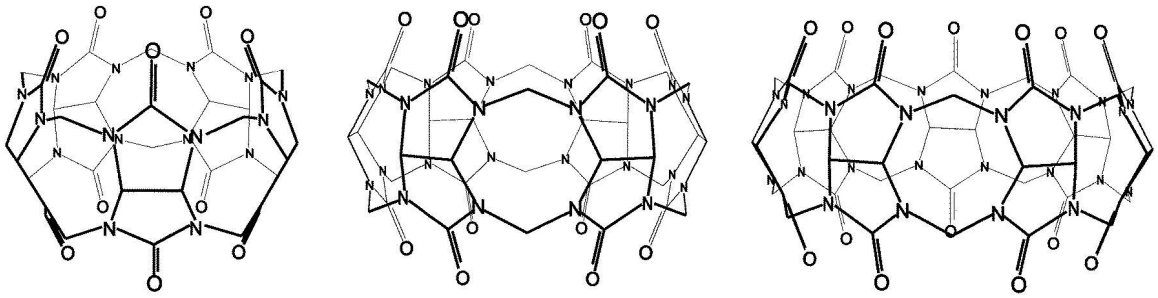

Cucurbit[5]uril Cucurbit[6]uril Cucurbit[7]uril

Figure 1.6: Structure of example cucurbit[n]urils. Adapted from ref. 59 [59]

Neutral and cationic guests are complexed via hydrophobic interactions and/or cationic-pi non-covalent attractions. Owing to the partially enclosed cavitand behavior, suitable guests can have high association constants. Functionalization of the cavitand has

been reported for pharmaceutical and biomedical applications including drug delivery, rotaxane synthesis, molecular recognition, and catalysis.[60]

1.3.7 Porphyrins

Porphyrins are macrocyclic compounds composed of pyrrole units interconnected at the alpha-carbon via methine bridges (Figure 1.7).[61] Porphyrins are also naturally occurring compounds. Their metal complex is the major component of hemoglobin in the blood that stores and transports iron.[62] Porphyrins are also conjugated systems that absorb light in plant leaves, impacting intense visible coloration and useful for photosynthesis.[63] In supramolecular chemistry, derivatives of porphyrins have been synthesized with pyrrole and an appropriate aldehyde. Like other cavitands, their functionalization has created important biomedical applications in photodynamic therapy, biomimetic systems, molecular recognition sensors and electron materials.[64]

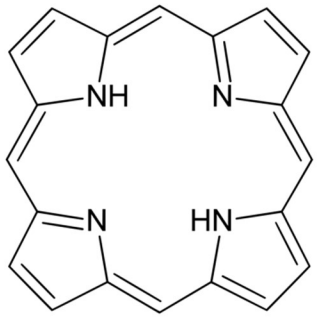

Figure 1.7: Base structure of a porphyrin macrocycle.

1.4 Beyeh Lab's research with macrocyclic compounds

The next dissertation chapters discuss applications of resorcinarenes compounds in supramolecular chemistry. The research was inspired by the versatility of the macrocycle and the synthetic organic functionalizations that affords unique properties. However, this subsection is a very brief review of previous research conducted with the resorcinarene framework prior to this dissertation. This discussion will focus on the specific applications and not on synthesis or their characterization.

Resorcin[n]arene can self-assemble with guests in solid, solution and the gas-phase to form bi-molecular complexes.[65] For example, the C_{ethyl}-2-methylesorcinarene forms strong binary host-guest complex with pyridine and quinoline N-oxides in solution. This relationship has long been characterized in resorcinarene chemistry and formed the framework of several analytical and materials chemistry applications of the organic macrocycle. In certain circumstances, the self-assembly must be aided by templating to the thermodynamically preferred complexes. For example, the Beyeh lab reported resorcinarenes based hexameric capsules using tetrabutylammonium and ruthenium bipyridine metal complex cations as templates.[65] Regardless of the nature of their self-assembly, capsules are typically characterized and identified using soft ionization mass spectrometry like Matrix Assisted Laser Desorption Ionization (MALDI) or Electrospray Ionization (ESI) MS. In that space, the Beyeh Lab has also employed a clever use of hydrogen/deuterium exchange solution experiments to examine the gas-phase structure of a hydrogen-bonded dimeric capsules.[66]

The popularity of the resorcinarene is also largely due to the ease of functionalization that affords different macrocycles with persistent hydrophobic cavities. In fact, that versatility is the inspiration behind this dissertation. One of those functionalization avenues is through alkylation of the 1,3 dihydroxyl groups. It has been well documented that the intramolecular hydrogen bonding between those adjacent hydroxyl groups creates a highly symmetrical resorcinarene with C_{4v} conformation. However, reaction of the resorcinarene with dancyl chloride in the presence of a base can create regioselective tetra (C_{2v}) and octa (C_{4v}) dansylated resorcinarenes also capable of forming guest inclusion complexes.[67] Cationic guests like tetramethylphosphonium and tetramethylammonium are appropriately sized guests for stable inclusion in those functionalized macrocycles using non-covalent cation-pi interactions.[68] Lower rim functionalized tetraethyl and tetraphenyl resorcinarenes can also form stable host guest complexes in the gaseous phase with hexose, pentose, and deoxyhexose sugars.[69] However, functionalized resorcinarene recognition of sugars in water has so far proved elusive.

Halogenation at the C2 position of the resorcinarenes also creates other desirable properties including a highly directional halogen bond donating potential. The halogenated resorcinarene can form stable complexes with ion-pairs, the cation sits in the cavity while the halogen atom renders the hydroxyl group more acidic to bond to the nucleophilic counterion.[70] As a result, in halogenated resorcinarenes, appropriate ammonium quaternary and di-quaternary guests can be synergistically bonded to the macrocycle using cation-π, hydrogen, and electrostatic interactions. The synergistic

attraction of multiple non-covalent interactions working together affords a strong binding affinity.[71] The Beyeh Lab also first reported the synthesis of tetraiodoethynyl resorcinarene cavitands as multivalent halogen bond donors.[72] The iodoethynyl moiety is a very potent donor that can form halogen bonds with oxygen, nitrogen, and halide acceptors. The tetraiodoethynyl cavitands also forms halogen bonded solvates with acetone, chloroform, acetonitrile, DMF and DMSO.[73] The inclusion behavior of the solvates in the cavitand is highly dependent on the length of the bridging unit between the resorcinarene arms. A unique capsule from tetrakis(3-pyridyl) ethylene resorcinarene cavitand was reported through N···I^+···N halogen bonded capsule.[74] A halogen bond donor like bromotrichloromethane can also form potent halogen bonds resulting in an extended, deep-cavity macrocyclic cavitand also capable of host-guest complexation.[75]

The C2-position of a resorcinol is also highly active for nucleophilic addition reactions. This is the basis for Mannich condensation reaction between formaldehyde, piperazine and the resorcinarene to create a dimeric helical cage with permanent cavity capable of conformational flexibility to accommodate small guests.[76] Moreover, it is not unusual for resorcinarenes to form self-inclusion complexes where the lower tails of one macrocycle sits in the cavity of another in a near linear fashion. This is typical of a family of hydrogen bond-stabilized *N*-alkyl ammonium resorcinarene salts. *N*-alkyl ammonium resorcinarenes have an extended cavity through Mannich condensation of the resorcinarene with excess formaldehyde and a primary amine to create a tetrabenzoxazine intermediate. The intermediate tetrabenzoxazine ring can be cleaved using a dilute mineral acid to create the *N*-alkyl ammonium resorcinarene salt. Using picric, triflate and

nitrate acid creates a tetra-array of counter-ions sandwiched between each arm of the cavitand, held together by hydrogen bonds. However, the bulky size of these anions distorts the stable conformation of the cavitand. As a result, guest exchange to suitably sized anions like chloride and bromide are enthalpically favored. This has been employed as a sensor mechanism for these anions.[77] The extended cavity cavitands can also form self-inclusion dimers but in the presence of an appropriate guest, spontaneously rearranging to 1:1 host-guest complexes. For example, a homoditopic hexyl amide forms a dimeric capsule with the cyclohexyl ammonium resorcinarene chloride through cooperative non-covalent interactions.[78] This phenomenon is also true for ditopic halogen bond donors like iodine (I_2) and diiodo perfluorinated alkanes with the sandwiched anions between the cavitand arms which are very potent halogen bond acceptors.[79] These sandwiched anions can even form halogen bonded complex with functionalized halogen bond donating polymers.[80]

1.5 Conclusions

This dissertation seeks to build on the rich history of resorcinarene research in the Beyeh lab by continuing to pursue further supramolecular chemistry applications.

CHAPTER TWO: COOPERATIVITY IN NON-COVALENT INTERACTIONS, A CASE OF THREE COMPONENT ASSEMBLIES

2.1. Introduction

Cooperativity[81] among non-covalent interactions plays a crucial role in supramolecular chemistry.[82,83] When two components associate, each with multiple functional groups, the various non-covalent interactions will either reinforce or partially negate each other.[84] Advances in our understanding of these cooperative interactions has had a significant impact in diverse fields including pharmaceutical formulation,[85–89] energy,[90–94] and liquid crystalline materials.[95,96] These cooperative effects are further complicated in ternary systems and can include hydrogen[97] and halogen-bonded networks.[98,99] Complex multicomponent co-crystals have been primarily characterized by X-ray diffraction analysis,[100,101] however this provides less information about the solution-phase behavior of these materials which is often of greater interest and the highlight of this chapter.

Calixarenes, resorcinarenes and other macrocyclic cavitands extensively studied for host-guest applications,[102–105] are well known for their ability to bind molecular guests *via* non-covalent interactions within their shallow and well-defined bowl-shaped cavity.[106] Resorcinarenes have been proposed as useful fluorescent diagnostics: for example, guest encapsulation changes the emission spectrum and can be used to measure binding.[107] However, a major limitation is that the choice of guest is restricted: small heterocycles and salts are preferred. The utility of the systems would be greatly expanded

by taking advantage of the emergent changes in the electronics of a bound guest to bind a third component, an analyte. In a simple multi-component system, for example, binding a pyridine in the electron rich resorcinarene cavity should increase electron density on the nitrogen, potentially making it more basic; this could be exploited to bind a carboxylic acid, creating a guest-mediated ternary complex. This binding event would then further change the physical properties of the complex which could be observed. To the best of our knowledge this would be a new architecture for supramolecular constructs.

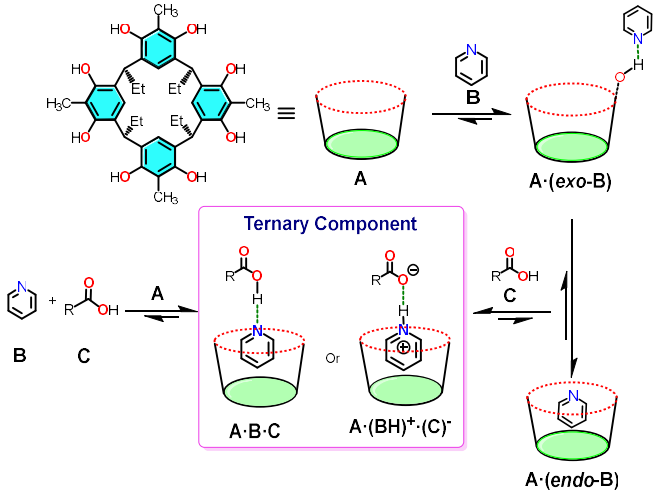

Figure 2.1: Representation of the stepwise assembly of ternary systems.

Defined ternary complex formation is the result of the interplay between a number of factors that determine the overall thermodynamics, and structure: pKa value of acidic protons, electronic effects, electrostatics, polarization, resonance-assistance, and dipole-dipole interactions.[108] Making ternary complexes requires the control of the non-covalent interactions in solution, particularly in protic polar solvents where hydrogen bonding is ubiquitous, and is rendered even more complicated as these properties, although derived

from the individual components, are true emergent properties of the complex itself. Two-component dimeric and hexameric capsules are common[109–111] but three-component all-organic structures involving macrocycles remain rare, and mostly involve either the host supported on a polymer or surface or polymer-like backbone,[112–115] or the host forming an inclusion complex with two guests simultaneously.[116–120]

Even though resorcinarene-guest constructs often dimerize to form stable self-inclusion complexes, this needs to be less favorable than forming a three-component system: 1) is it possible to keep the guest inside the host cavity, stabilized through multivalent interactions when a third component is added? 2) Will binding of the third component be synergistic? These questions inspired the current study on a simple model system (Figure 2.1).

2.2 Experimental

Combining C_{ethyl}-2-methylresorcinarene (A) with pyridine (B) makes a simple, and well-defined 1:1 dimeric *endo*-complex that have been documented in literature.[121–125] This was then titrated with ten different carboxylic acids (Cn; n = 1-10) which should initiate a single strong $_{B}(N)\cdots(H–O)_{Cn}$ interaction between B and Cn. Whether the ternary complex exists as hydrogen bonds and/or ion pairs depends on the specific pKa values of Cn (Figure 2.2). We examined the monomeric, binary, and ternary components and complexes using NMR spectroscopy and used isothermal titration calorimetry (ITC) to quantify and fully elucidate the thermodynamics of this possible ternary assembly.

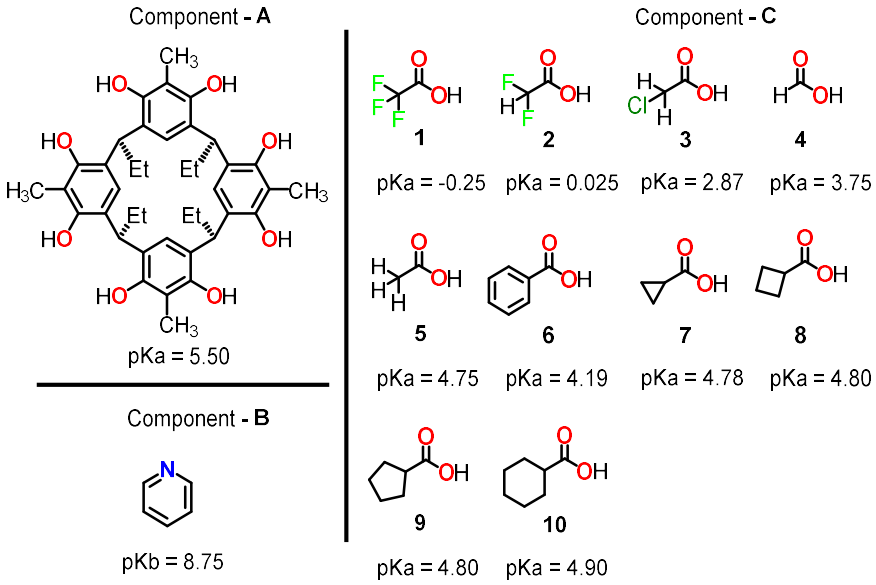

Figure 2.2. Components of the ternary complexes of C-ethyl-2-methylresorcinarene (A), pyridine (B), and carboxylic acids (Cn).

2.4 Results & Discussion

2.4.1 NMR Spectroscopy

Only one set of signals is present in NMR spectra of the mixtures, indicating that the complexes are likely in fast dynamic equilibrium with the individual components. For example, mixing the acid (C2) and pyridine (B) together induces the expected deshielding of the aromatic proton resonances due to a decrease in aromatic electron density (Figure 2.3c *vs* 2.3b). Similarly, the B resonances become increasingly shielded when mixed with A, consistent with *endo*-complexation[30] (Figure 2.3d *vs* 2.3b). The H_d difluoroacetic acid proton experiences H-F coupling (Figure 2.3g). Mixing C2 with A increases the splitting of the H_d signal but does not induce any significant changes in the chemical shift.This suggests that a weak hydrogen bond interaction induces asymmetry in

the fluorine atoms, but that the interaction with the phenol does not result in a deprotonation (Figure 2.3f *vs* 2.3g).

The same NMR experiments were conducted for all the other A·B·Cn complexes. The degree of deshielding induced on B by the formation of B·Cn was proportional to the pKa of Cn (Figure 2.2). Clear deshielding of the pyridine resonances was observed with strong acids trifluoroacetic acid C1, difluoroacetic acid C2, chloroacetic acid C3, and formic acid C4 (Appendix I-III, Figure 2.3). Negligible changes were seen with the weaker acids C5-C10 (Appendix IV – IX). Similarly, the increase in shielding of the B protons in A·B·Cn compared to A·B also increased as a function of pKa for C1-C4. For the weaker acids C5-C10, no significant increase in B shielding was observed between A·B and A·B·Cn suggesting that the pyridine's position and interactions within the host cavity is not hugely affected by binding to the weaker acids.

The ^{1}H NMR spectra of ternary complex A·B·C2 is clearly different from any of the binary systems it is derived from. In A·C2, the acid's H_d shows additional splitting but no significant shielding, suggesting that any interaction is *exo*. However, the change in the H_d chemical shift in the A·B·C2 assembly is greater than that observed for B·C2, suggesting a greater degree of hydrogen bonding is occurring in A·B·C2: the nitrogen has become more basic. Similarly, the pyridine resonances are shielded, indicating stronger *endo*-cavity interaction with A than in the binary system alone.[126] This is significant as protonation of B in B·C2 deshields the resonances. Increased shielding of B in the ternary complex (Figure 2.3e) over A·B, means that increasing the host-guest interaction has a

stronger impact on the chemical environment than the decrease in electron density arising from pyridinium formation. To further support these observations, ^{19}F NMR studies were carried out on A·B·C2 as fluorine's chemical shift is very sensitive to the chemical environment. The -CF_2H signal was shielded by 0.24 ppm in the equimolar mixture of A and C2 indicating some interaction between the components (Figure 2.4f). A significant deshielding of -1.85 ppm was observed for B·C2, indicating a strong $_B(N)\cdots(H–O)_{C2}$ hydrogen bond interaction (Figure 2.4g), while in A·B·C2, an even more significant deshielding (-2.60 ppm) of the fluorine signal was observed suggesting cooperativity (Figure 2.4h). A similar phenomenon but with much smaller shift changes of the fluorine signals was observed with the trifluoroacetic acid C1 in A·B·C1 (Figure 2.4a-d).

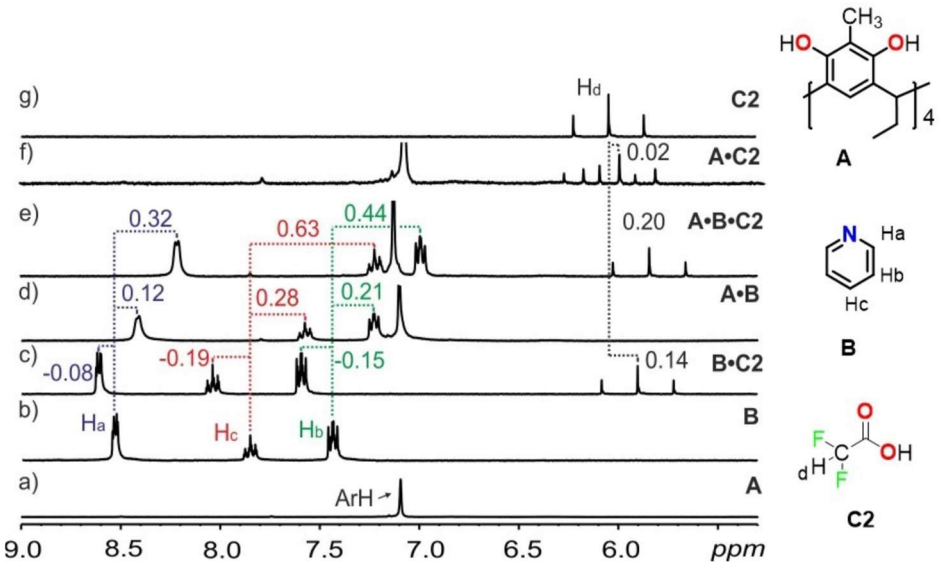

Figure 2.3. Expansions of the ^1H NMR (CD_3OD, 20 mM, 298 K, 300 MHz) of the three-component A·B·C2 assembly of host A, the pyridine guest B and difluoroacetic acid, C2 (pKa 0.025) and their dimeric and ternary complexes.

DOSY further supports the presence of these ternary complexes. The diffusion coefficient of a molecular species depends on its molecular weight, solvodynamic radius,

and interactions with solvent.[127–129] When comparing similar species in the same solvent at the same concentration and the same temperature, a smaller diffusion coefficient indicates a larger species. We studied a strong (C2) and a weak (C10) acid with monitorable protons (trifluoracetic acid C1 is not suitable due to the lack of a C–H bond). The diffusion coefficient of A (20 mM) in CD_3OD at 298 K was 0.63×10^{-9} m^2s^{-1} (Table 1, Figure 2.5),[130] consistent with other previously reported resorcinarene-derived values confirming that no dimeric or hexameric capsule is present.[128,129]

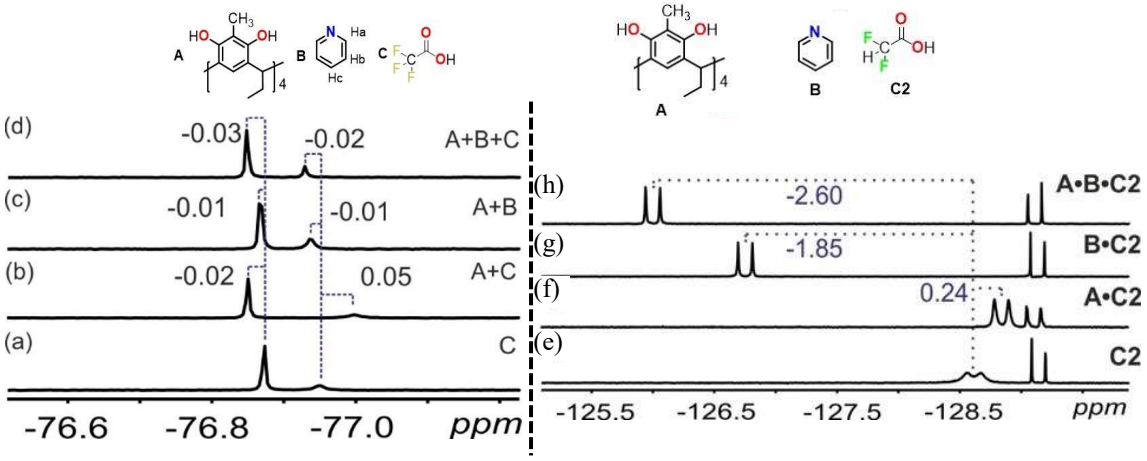

Figure 2.4. Sections of the ^{19}F NMR (CD_3OD, 298 K, 300 MHz) of the three-component ternary A·B·C1 complex between A, B and trifluoroacetic acid C1 (pKa -0.25). Spectra are produced from (a) C1. Equimolar mixture of: (b) A and C1, (c) B and C1, (d) A, B, and C1. Dashed lines highlight the observed shift changes of the resonances, labels are in ppm. Sections of the ^{19}F NMR of the three-component ternary A·B·C2 assembly between the host A, the pyridine guest B and difluoroacetic acid, C2 (pKa 0.025). Spectra are produced from (e) C2. Equimolar mixture of: (f) A and C2, (g) B and C2, (h) A, B, and C2.

The diffusion coefficients for the B and the acids (C2 and C10) also reflect their different solvodynamic radii in methanol (Table 1). When dimer and ternary structures are formed, the diffusion coefficients decrease, indicating slower movement, and likely a larger hydrodynamic radius. Taking the 1:1 host-guest mixture of A and B as an example,

the diffusion coefficients of host A, and B dropped to 0.59×10-9 m2s-1 and 1.91×10-9 m2s-1 respectively. In a capsular construct, the diffusion coefficients would be roughly the same. However, as an open inclusion complex it is in dynamic equilibrium with the monomeric species, and these different diffusion coefficients are expected. In the 1:1 mixture of B and C2, the decrease in the diffusion coefficients of both B and C2 show they both participate in a larger assembly; however, in the C10 and B complex, the diffusion coefficients resemble those of the free species consistent with a much weaker interaction (Table 1, Appendix XI).

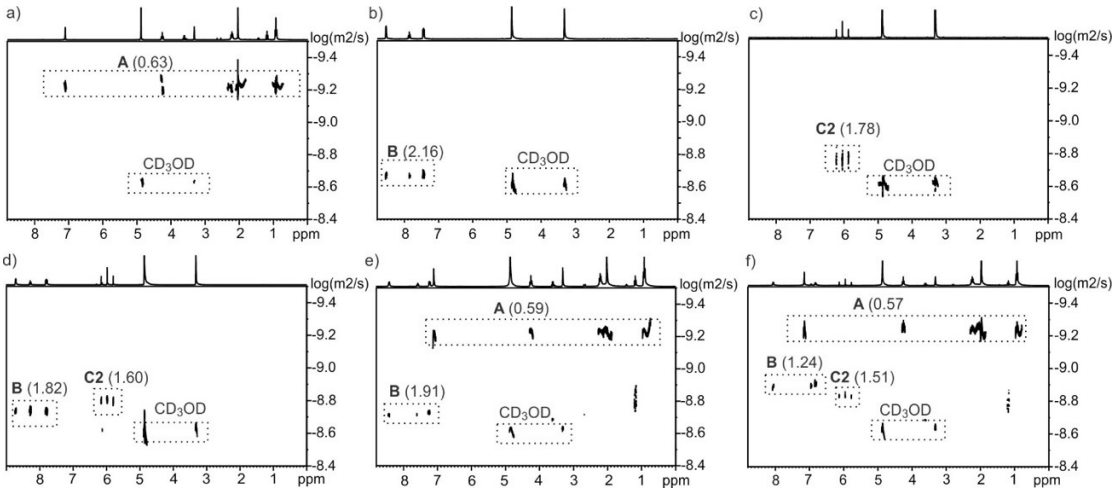

Figure 2.5. 2D DOSY NMR spectra (in CD3OD at 298 K) of a 20 mM sample of: a) A, b) B, c) C2, and equimolar mixtures of d) B+C2, e) A+B, f) A+B+C2 showing the chemical species present in the samples. The diffusion coefficient (×10-9 m2s-1) of each species is shown

Considering the host-acid dimers (A·C2 and A·C10), we see that the interaction is weak: addition of the acid has little to no effect on the diffusion coefficient of the host (Table 1). Considering A·B·C2 the diffusion coefficients of all components drop precipitously from all binary species: the size difference would not be significant (as can be seen by the minor change in A). This decrease in the values of B and C are consistent

with the equilibrium now lying more towards a ternary complex (Table 1, Appendix XI). In the case of the C10 ternary complex, the changes are far more subtle. The diffusion coefficients for C10 and B are lower than in their dimeric pair, but the decrease is not as significant, again consistent with the previous ^{1}H NMR data. The shifts are moderated as the process was measured in methanol, which competes for hydrogen bonds, decreasing affinity. In previous investigations of dynamic enclosed capsular resorcinarene-based assemblies, methanol was routinely used as a competing hydrogen bond solvent to break-up the capsular assemblies.[129] Seeing these effects in this solvent is strong evidence of the high affinity these components have for each other, especially in the presence of a competing solvent. In ternary complex A·B·C2, the pyridine and the host clearly show strong through space interactions that are only consistent with an *endo*-inclusion complex. The fluorine resonances on the acid show exchange peak behavior with respect to the host phenolic protons. This indicates either rapid changes in conformation, or rapid exchange between bound and unbound forms. Together, all the NMR evidence supports the formation of the proposed and innovative guest-mediated ternary system.

Table 1.0. Average diffusion coefficients ($\times 10^{-9}$ m^2s^{-1}) of the species in different combinations in CD_3OD at 298 K. The mixtures are all equimolar.

	A	B	C2	C10	CD3OD
A	0.63	–	–	–	2.61
B	–	2.16	–	–	2.39
C2	–	–	1.78	–	2.47
A+B	0.59	1.91	–	–	2.36
B+C2	–	1.82	1.60	–	2.35

Table 1.0 continued

	A	B	C2	C10	CD3OD
A+C2	0.58	–	1.80	–	2.38
A+B+C2	0.57	1.24	1.51	–	2.32

2.4.2. ITC Analysis

DOSY and ^{1}H NMR suggest the presence of a synergistic binding mode, but the gold-standard approach for measuring binding affinity is ITC, and for comparison the measurements were conducted in methanol (Appendix X – XI). The thermodynamic parameters of host-guest binding (K, ΔH, ΔS, and ΔG) for the binary components were determined by fitting the ITC data to a one-site binding model (Table 2). Negative ΔG values reveal the binding to be spontaneous at 303 K. The negative ΔH and TΔS values for the B·Cn and A·B·Cn systems indicate the complexation to be enthalpy driven, but entropy compensated. The negative ΔH and positive TΔS value for B·C10 indicates that the process is favored by both enthalpy and entropy (desolvation) driven. Resorcinarene A and pyridine B dimerize with a binding constant of 301 M^{-1}. The interaction between B and the carboxylic acids reveal a binding constant of 774 M^{-1} for strong acid C2 and 70 M^{-1} for the weak acid C10. This means that at equilibrium, A and B essentially exist as the dimer, while B and C2 also exist as the hydrogen-bonded ion pair, while in B·C10 the interaction is far weaker. ITC is designed to determine the thermodynamics of two-component systems; there is no method to compute the thermodynamics of a system consisting of three independent components interacting simultaneously. However, in the case of B·C2 we can assume that it behaves largely as a single component as the binding

is so strong. Titrating host A into an equimolar mixture of these compounds allowed the data to be fitted to a one-site binding model with a binding constant of 671 M^{-1}. The fact that this value is larger than the observed binding constant of A·B (301 M^{-1}) means that the protonated pyridinium is a far better guest than the neutral pyridine. Binding between B and C10 was insufficient for the required assumption that the mixture act like a single molecule: there is enough free B or A·B to prevent the mathematical model from providing a fit. This is not surprising; ITC is not designed to calculate three-component interactions, the fact that B·C2 form a strong enough dimer that it can be treated as a discrete single species is exceptional—we could not find any examples in the literature where it had been used for this previously. However, the assumption is clearly fair for C2 as the B·C2 system acted as a single unit, a prerequisite for ITC parameter calculation. The solution phase studies all strongly indicate that proposed guest-mediated complexes are formed, and that formation is synergistic with respect to all possible binary complexes.

Table 2. Binding constants *K* [M^{-1}] calculated for the A·B, B·Cn system, and A·B·Cn ternary system. [a]Data could not be fitted without large errors.

Entry	*K* [M^{-1}]	ΔH (kcal/mol)	TΔS (kcal/mol)	ΔG (kcal/mol)
A·B	301±80	-38.24±0.28	-34.89	-3.35
B·C2	774±81	-15.26±0.78	-11.32	-3.94
B·C10	70±0.97	-0.23±0.55	2.37	-2.60
A·(B·C2)	671±194	-7.65±0.81	-3.78	-3.87
A·(B·C10)	_[b]	_[b]	_[b]	_[b]

CHAPTER THREE: HOST-GUEST BINDING FOR SENSOR DEVELOPMENT

3.1 Introduction

Resorcinarenes as synthetic receptors are well-studied in the supramolecular host-guest (H-G) chemistry.[103,104,131,132] The development of aesthetic functionalization methods at the upper-rim such as alkylation/arylation of hydroxyl groups and the introduction of substituents at the C2-position between two hydroxyl groups of resorcinol has notably made resorcinarene an excellent building block to produce extended structures for host-guest sensor development and beyond.[133–135] The ability to modulate the properties of resorcinarenes by synthetic means has allowed the design of targeted molecules for this self-assembly processes.[136] However, the major structural feature of resorcinarenes is the electron-rich cavity, formed by the circular intramolecular O···H–O hydrogen bonding interactions between adjacent resorcinol units that can bind neutral and cationic guests through C−H···π, cation···π, and/or cooperative H-bond interactions.[137] In case of guest shape and size mismatch, the host's cavity stabilizes either by self-inclusion[138–140] or solvent encapsulation.[141,142] *Exo*-guest complex formation arises often via competitive H-bond interactions resulting in co-crystal complexes.[138,143,144] Nonetheless, strategic structural modification of the resorcinarene framework can afford development of highly selective, sensitive, and specific recognition elements to be used as sensors. Subchapter 3.2 analyses the guest encapsulation properties of one of the commonest functionalization of resorcinarenes in sensor development, using nine different *N*-alkyl ammonium cations. Subchapter 3.3 explores using extended cavity

resorcinarene frameworks for selective detection of a physiological anion implicated in disease diagnosis, prognosis, and clinical monitoring of therapeutic outcomes.

3.2 Guest binding in resorcinarene cavities: a case study with *N*-alkyl ammonium cations

Functionalized resorcinarenes have found use in nanoparticle synthesis,[145–148] optical[149,150] and chemosensors,[151] gels,[152] and separation applications.[153] In addition to the various potential applications of resorcinarenes, their use in rigorous quantitative H-G studies to extrapolate structure-property relationships and gain insights into fundamental principles e.g. guest binding affinities, size and shape, and conformational flexibility has always received wide attention in supramolecular chemistry research.[103] Unravelling such fundamental knowledge could help to build complex molecular systems using the bottom-up approach. The bottom-up approach in supramolecular chemistry has already created access for chemists to perform catalysis and organic reactions inside self-assembled hexamer and capsular structures [154–157] and has the potential for much more.

Sodiumsulfonatomethyleneresorcinarene is an example of a host that can interact with guests via multiple functionalities. Sulfonate substitution makes the resorcinarenes behave as amphiphiles. This amphiphilic behavior of tetra sulfonate derivatives (SR) has created new avenues for harnessing resorcinarenes in biological applications.[158,159] The representative examples of SRs studied in the literature include, methylenesulfonate groups appended at the upper-rim C2-positions (Type-1),[158–169] sulfonate and phenolic oxygens linked by methylene chains (Type-2),[170] and alkylated sulfonate derivatives at the lower-rim (Type-3).[171–173] The nature of their binding to neutral, singly and doubly charged aliphatic/*N*-heterocycle cationic guests are been studied in solution to understand

the sulfonate groups intricate role in H-G systems. For example, Liu *et al*. have shown that the H-G complexation between viologen type cationic guests and Type-2 receptor in water results from charge transfer interaction between electron-rich host and electron-deficient guest aromatic rings.[170] Additionally, the upper-rim longer alkyl chain sulfonates provide an elongated cavity to improve the binding affinity for rod-shaped guests such as *N*,*N*-dimethyl-4,4-bipyridinium ions. In another report by Aoyama *et al*., the recognition of sugars using Type-3 receptors in water resulted in very low binding constants due to the aggregation of lower-rim longer alkylsulfonate chains and competitive H-bonding interactions.[171] These findings demonstrate that the factors affecting the guest inclusion complexes depend on the inherent location of the sulfonate groups, and therefore, clearly understanding such principles governing the molecular recognition process is a valuable asset to H-G chemistry based applications.[161]

In this context, Type-1 receptors have been subjected to less systematic testing in H-G studies using cationic guests. Several of Type-1 host's intriguing properties and possibilities of their unique *endo*-cavity environments for molecular recognition in solid-state and solution have been underexplored. For rational design of H-G systems exploiting Type-1 receptors, it is crucial to understand their limitations particularly in terms of spatial constraints of their cavities and nature of their H-G interactions. In the present two-component approach, $A \cdot B_n$ we use a combination of ^{1}H NMR spectroscopy and isothermal titration calorimetry (ITC) to investigate the nature of H-G chemistry between sodiumsulfonatomethyleneresorcinarene (A) and a set of nine ammonium guests

(Bn, n = 1 - 9) shown in Figure 3.1. Our motivation for studying the Type-1 receptors stem from the following:

(i) the four sulfonate groups encompassing the upper-rim offer a deeper cavity compared to classic C_{ethyl}-2-H-resorcinarene, and these substituents should act as a lid rendering a narrow portal thus improving the guest selectivity,

(ii) the guests can be stabilized by both C−H···π and C−H···OSO_2 interactions from *endo*-cavity π-systems and sulfonate groups, respectively,

(iii) mixing host A and guest (Bn) components leads to desalination (meaning removal of sodium chloride or sodium iodide) and the formation of H-G complexes of the type $(An)^{-}\cdot(Bn)^{+}$, despite the strong electrostatic attractive interaction between sulfonate O-atom and sodium to form coordination complexes, and competitive hydrogen bond interactions between chloride ion and the ammonium cations' H-atoms, and

(iv) the type of H-G interactions favored in *endo*-guest complexes can be potentially tuned by changing the H-G size match and ammonium cation functional groups.

We investigate the preferred type of H-G interactions by using a series of ammonium cations $^{+}NH_2(R_1)(R_2)$ (R_1 = -methyl, -ethyl; R_2 = -ethyl, -butyl, -aryl) to determine whether the *endo*-guest complexation occurs rather by more acidic *N*-methyl, *N*-ethyl or through longer *N*-alkyl/*N*-aryl chains. The $^{+}N(CH_3)_4$ is used as reference species as it is expected to have the best size match fitting inside the cavity and strong binding due to acidic C−H protons that can take part in C−H···π interactions. Furthermore, we

investigate whether *N*-methylated heterocycles have the inclination to form *endo*-complexes via *N*-methyl or the aromatic π-system using guest B8 and B9.

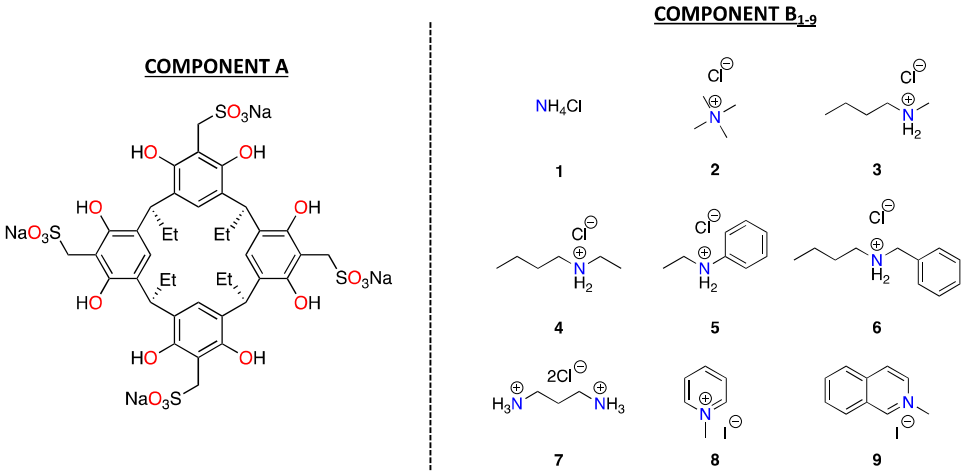

Figure 3.1: List of components, sodiumsulfonatomethyleneresorcinarene hosts (A), and quaternary ammonium halides Bn [n = 1-9].

3.2.1 Results and Discussion

3.2.1.1 ^{1}H NMR studies

The binding properties of the receptor A towards the guests were probed in solution through ^{1}H NMR analyses. In solution, the complexes are in rapid equilibrium with the free components, therefore, only one set of signals could be observed in the NMR spectra of the mixtures. Despite the dynamic system and fast exchange process, e*ndo*-cavity binding of the guests can be determined through monitoring the shielding effects of the guest signals. By following and comparing the degree of shielding, one could qualitatively determine which part of the $^+NH_2$(R1)(R2) guest (R1 or R2) is preferred and predominantly located in the cavity of the receptor. Strong increase in

shielding of the guest B2 protons was observed as would be expected considering the affinity of resorcinarenes towards quaternary ammonium ions. For the other guests, several parameters were investigated to understand the preferences of the host towards the guests B1-B9. First, we determined the maximum length of the alkyl group that could possibly be bound into the cavity of the receptor. For this process, the H-G complexes between A and B3-B7 were investigated. Taking A *vs* B3 as an example, the *N*-methyl group of B3 had the higher increase in shielding (1.62 ppm) when compared to the $–CH_3$ protons of the butyl group (0.14 ppm) clearly suggesting the *N*-methyl group sits deep into the cavity of the of A (Figure 3.2B). By the same analyses, it was observed that the *N*-ethyl groups of B4, B5 and B6 are also preferred for the *endo*-complexation (Figure 3.3, Appendix X - XII). Guest B7 is a particularly interesting example, since it has a butyl group on one side and a benzyl group on the opposite side of the nitrogen. Following the ^{1}H NMR changes, it was observed that neither the terminal $–CH_3$ signals of the *N*-butyl group (0.24 ppm) nor the aromatic signals of the *N*-benzyl group (*a-proton*: 0.31 ppm) had the highest change in shielding. Instead, the methylene protons closest to the ammonium group ($N\text{-}CH_2$-) showed the highest increase in shielding (0.64 ppm, 0.66 ppm). This suggests the receptor A interacts with the carbons adjacent to the positively charged nitrogen of the guest B7 as shown in Figure 3.2D.

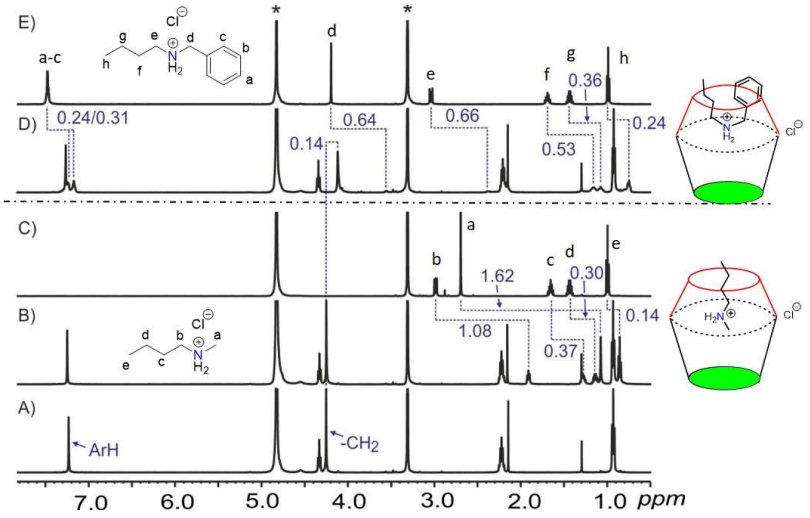

Figure 3.2: ^{1}H NMR spectra (CD_3OD, 303 K) of: (A) host A, (C) guest B3, (E) guest B7, and the equimolar mixtures of (B) A and B3, (D) A and B7. Star represents the residual CD_3OD solvent. The dash lines give an indication of the signal changes in ppm.

Secondly, we compared whether interaction with *N*-methyl group or the aromatic ring of pyridinium ion in B8 was preferred by the host. The changes in ^{1}H NMR of B8 in host equilibrium show that the aromatic protons were located deeper into the cavity of A than the *N*-methyl group (increase in shielding Ph_a: 1.63 ppm, *N*-CH_3: 0.95 ppm, Figure 3-3B). This is in contrast with the *N*-ethyl group preference shown by the *endo*-complexation of B5 or the preference toward shorter *N*-methyl or *N*-ethyl groups shown by the shallow cavity of host A with the B3-B7 guests. In case of B8 the different behavior can be explained by the better size match and stronger π–π interactions between the electron-deficient pyridinium ion and the electron-rich cavity of the host. Next, in case of guest *N*-methylquinolinium iodide B9, the higher increase in shielding of ^{1}H NMR signals of the *N*-methyl group show it to be in the cavity of the receptor (increase in shielding Qu_g: 0.87 ppm, *N*-CH_3: 1.69 ppm, Appendix XII). This preference could be explained by a better size match of *N*-methyl group than the quinoline moiety to the

cavity of the host. Additionally, the larger π-system of B9 is not as electron deficient as the aromatic ring in B8.

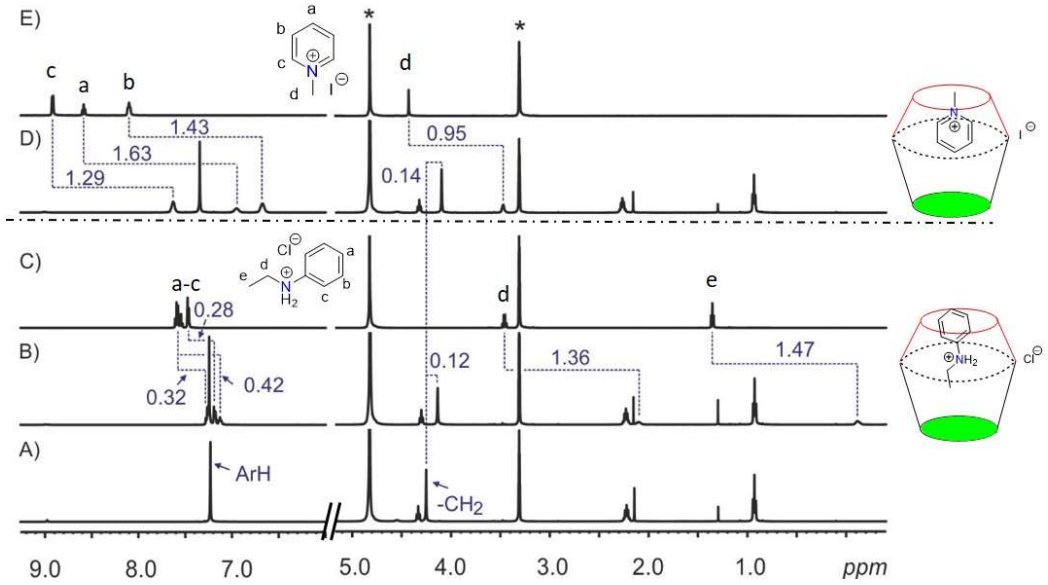

Figure 3.3: ^{1}H NMR spectra (CD_3OD, 303 K) of: (A) host A, (C) guest B5, (E) guest B8, and the equimolar mixtures of (B) A and B5, (D) A and B8. Star represents the residual CD_3OD solvent. The dash lines give an indication of the signal changes in ppm.

3.2.1.2 Isothermal Titration Calorimetry (ITC)

The complexation of the guests Bn by the host A were quantified through a series of ITC experiments in methanol (Appendix XIII - XV). The thermodynamic parameters of host-guest binding (K, ΔH, ΔS, and ΔG) between the host A and the guests Bn were determined by fitting the ITC data to a one-site binding model (Table 1). Complex formation between any combination of the host A and the guests Bn is spontaneous ($\Delta G < 0$) at the experimental temperature (303 K). The negative ΔH and positive $T\Delta S$ values indicate the complexation of the guests by A are both enthalpy and entropy driven. Solvation of the species and the counter ion releases are factors that explain the entropy

contribution. This has been previously observed for supramolecular binding interactions between poly(ammonium chlorides) and poly(sodium phosphates), and may be due to the particularly strong ion-pairs in the host.[174] The highest binding affinity among all the guests was observed with guest B2 (K_a = 909 M^{-1}). This is logical since tetramethylammonium cation is known to be a good fit for resorcinarene cavity through C–H···π and cation–π interactions.[175–178] This value is much higher when compared with basic resorcinarenes in methanol (K_a ~ 100-200 M^{-1}).[142,177,179]

Table 3.1. Thermodynamic binding parameters of formed complexes between the host A and the guests Bn by ITC.

Complex	K_a M^{-1}	ΔH kcal/mol	$T\Delta S$ kcal/mol	ΔG kcal/mol
B_1@A	173.00±7.19	-2.58±0.15	10.40	-13.00
B_2@A	909.10±191.60	-13.80±0.18	3.37	-17.20
B_3@A	-[b]	-[b]	-[b]	-[b]
B_4@A	196.10±21.90	-8.77±0.07	4.54	-13.30
B_5@A	-[b]	-[b]	-[b]	-[b]
B_6@A	546.40±123.60	-9.28±0.07	6.63	-15.90
B_7@A	207.90±53.80	-6.62±0.07	6.84	-13.50
B_8@A	326.80±38.60	-7.12±0.07	7.49	-14.60
B_9@A	80.00±7.10	-12.50±0.07	-1.48	-11.02

[a]ITC was done in methanol at 303 K. [b]Data could not be obtained due to large errors.

3.3 Resorcinarenes as molecular recognition sensors for pyrophosphate

A significant challenge in supramolecular chemistry is developing high-affinity receptors for anions in biologically relevant solvents,[180–184] and the design of such receptors has elicited considerable effort from the research community.[185–194] Primarily, this challenge has been addressed by leveraging the cooperative effect of non-covalent attractions.[195–197] One of such anions is pyrophosphate (PPi), a side product of ATP metabolism[198], that can quantitively be assessed for clinical diagnosis of disease states including crystal deposition[198,199] and other enzyme deficiency disorders. Therefore, chemosensors for qualitative and quantitative detection of PPi have been reported by several research groups featuring varying functional structures, including sensors relying on metal binding centers[193,200–204] and sensors for application only in organic media[205,206]. However, we recognize that any suitable application of a pyrophosphate sensor should be sensitive and selective in predominantly water systems. Unfortunately, anions have significantly high hydration energies in water that negatively affects complexation.[207,208]

In that space, the Beyeh Lab has previously reported the *N*-alkyl ammonium resorcinarene salts (NAR(X_4), consisting of a macrocyclic resorcinarene tetra-ammonium cation and four anions with a preference for chloride in NAR($Cl)_4$, over bromide, nitrate, triflate, or picrate in organic media.[209–211] This binding preference is due to the chloride's suitable size, the snug fit between two adjacent ammonium moieties, and its strong hydrogen bond acceptor behavior that generates the robust and circular [NH_2+…-Cl^- …NH_2+…-Cl^-…]$_2$ hydrogen-bonded seam along the upper rim of the macrocycle. The $NARX_4$ receptors are tetra-cationic, and by careful inspection, tetra-anionic

pyrophosphate (PPi) appeared to be the perfect guest due to size-charge complementarity and chelate cooperativity. As a result, the Beyeh Lab subsequently reported an *N*-alkyl ammonium resorcinarene chloride receptor capable of high affinity (10^7 M^{-1}) and selective binding of PPi in pure water.[212] Guest displacement assays further confirm the selectivity for PPi through absorbance measurements with 2-naphthalene sulfonic acid sodium salt as the guest. The binding motif is based on an intramolecular ionic seam where the four counter ions leave upon the complexation of PPi. Based on that mechanism, we recognized the potential to improve the affinity and selectivity of the receptor by employing the use of more weakly coordinating counter ions. Furthermore, we could simplify the determination of PPi binding by incorporating a fluorophore into the resorcinarene structure that would change optical behavior in the presence of a guest. This would bypass the need for guest displacement assays and allow for simple direct measurement. In this study, we hypothesized that, with weaker coordinating counter anions, the $NARX_4$'s affinity towards PPi would substantially increase. By integrating a fluorescent moiety into the receptor, we could develop a simple read-out high-affinity sensor for PPi.

3.3.1 Experimental

We synthesized ten new R-$NARX_4$'s (R = upper rim substituent, X = counter anion) receptors with three different counter anions, chloride, bromide, and triflate (OTf), and four different upper rim substituents; one with a flexible terminal hydroxyl propyl group (C3OHNARX_4, X = Cl, Br, and OTf), the second with a rigid cyclohexyl group at the upper rim (Cy$NARX_4$, X = Cl and Br), the third with a flexible benzyl group

(BnNARX, X = Cl and Br), and the fourth with a flexible and fluorescent napththalen-1-ylmethyl group ($NpNARX_4$, X = Cl, Br, and OTf). In addition to PPi, the binding properties of the receptors towards a tribasic monophosphate (K_3PO_4), and a dibasic monophosphate (AMP), diphosphate (ADP), and triphosphate (ATP) are also investigated. The binding was confirmed through ^{1}H and ^{31}P NMR experiments. Quantification and thermodynamics of the binding event were carried out through a series of Isothermal Titration Calorimetry (ITC) experiments.

3.3.2 Results & Discussion

Mannich condensation reaction between aliphatic amines and C-$_{hydroxyl}$-resorcinarene in the presence of excess formaldehyde generates tetrabenzoxazines.[213] Ring-opening of the six-membered tetrabenzoxazine ring is affected by refluxing in the presence of an acid (HCl, HBr, and triflic acid) to provide crude R-$NARX_4$s (Figure 3.4); these are purified through recrystallization to give the final products in 50 – 85% yields.

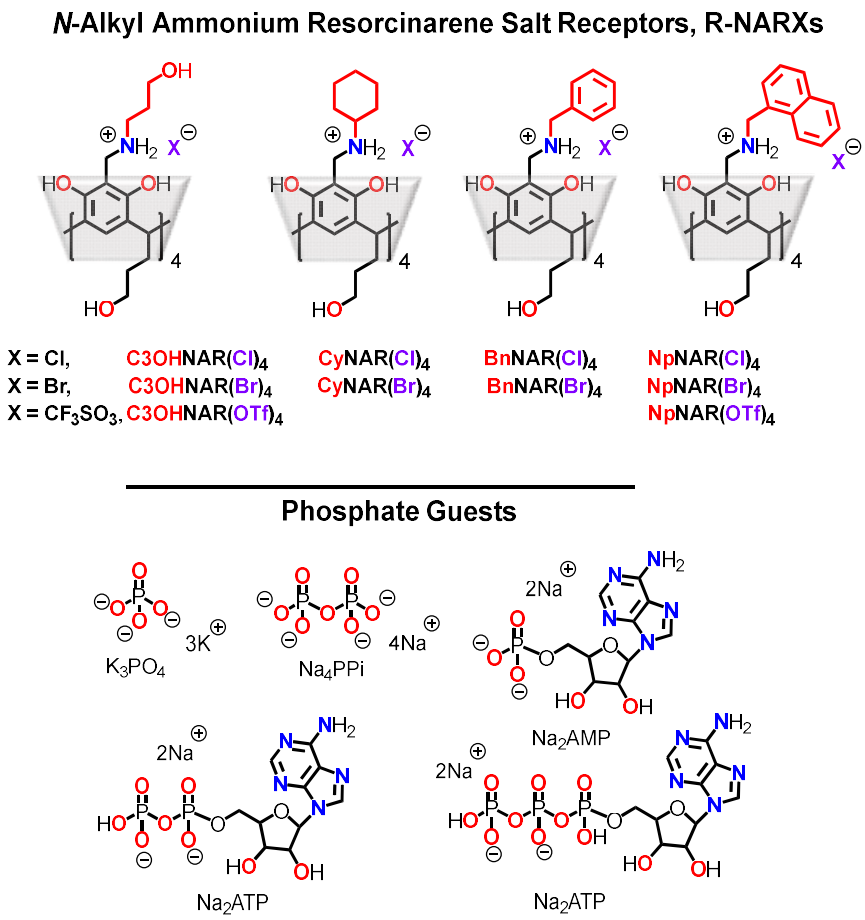

Figure 3.4: Synthesized resorcinarene salt receptors C3OHNAR(X)$_4$, CyNAR(X)$_4$, BnNAR(X)$_4$, NpNAR(X)$_4$ (X = Cl^-, Br^-, and $CF_3SO_3^-$), and the phosphate guests K_3PO_4, Na_4PPi, Na_2AMP, Na_2ADP, and Na_2ATP.

3.3.2.1 NMR Spectroscopy

The –OH and –NH_2 protons of the cationic core of the receptors form hydrogen bonds with the counter anions. When the R-NARX$_4$ receptors bind to pyrophosphate, the counter anions are displaced to accommodate PPi. This reorganization produces observable differences in the ^{1}H resonances of the –OH, –NH_2, and neighboring –CH_2– protons. To probe these receptors' binding capability, we performed a series of ^{1}H NMR

measurements of the pure phosphate guests, pure R-NARX$_4$ receptors, and equimolar mixtures of phosphate guests and R-NARX$_4$ receptors. The binding processes are fast on the NMR timescale; however, clear changes in the hosts' methylene signals confirm host-guest interaction between the NAR(X)$_4$s and the PPi (Figure 3.5). Due to the limited solubility of the R = napthyl receptors, the proton measurements were done in a D_2O/[D_6]DMSO (90%/10%) at 298 K. Hydrogen/ Deuterium exchange in this solvent mixture prevents the –OH and –NH_2 signals from being monitored. However, we observed changes in the chemical environment of the non-exchangeable methylene protons (Ar-CH_2N) closest to the –OH and –NH_2 groups. We also observed, by NMR, that the resorcinarene core distorts its bowl conformation, breaking C_{4v} symmetry to better accommodate PPi.

Take the binding of PPi by C3OHNAR(X$_4$) as an example; up to 0.09 ppm upfield shifts are realized by the methylene protons, and up to 0.22 ppm upfield shifts are observed for the aromatic protons of the resorcinarene core. The changes in the host's signals clearly support the host re-organizing the cavity during the binding process. No significant differences in the ^{1}H NMR of the receptor in PPi@R-NAR(X)$_4$ complex was observed between the chloride, bromide, or triflate counter ions once the counter anions are displaced to accommodate pyrophosphate. The final assembly is expected to be the same PPi@C3OHNAR(X)$_4$ where X represents the initial counterion that has now been fully displaced (Figure 3.5).

An even better way to access the binding process is to monitor the ^{31}P NMR signals of the phosphate guests upon complexation with the $NARX_4$ receptors. A series of ^{31}P NMR experiments of the phosphate anions and equimolar concentrations of pure phosphates and receptors were used to qualitatively probe the binding processes (Figure 3.6, Appendix 3.7 - 3.17). The magnitude of the upfield shift of the phosphorus isotopic signals upon binding the R-$NARX_4$ receptors qualitatively indicates the degree of guest shielding in the macrocyclic binding pocket. Of the different R-$NARBr_4$ receptors, PPi experienced the largest upfield movement with R = naphthalene This was followed closely by the benzyl (Bn)–$NARBr_4$ receptor and 1-propanol (C3OH)–$NARBr_4$ (Figure 3.6b). Qualitatively, the absence of an aromatic environment or a hydrogen bond potential of hydroxyl groups in the cyclohexyl upper rim modification may explain why it has the smallest effect on the PPi phosphate resonance.

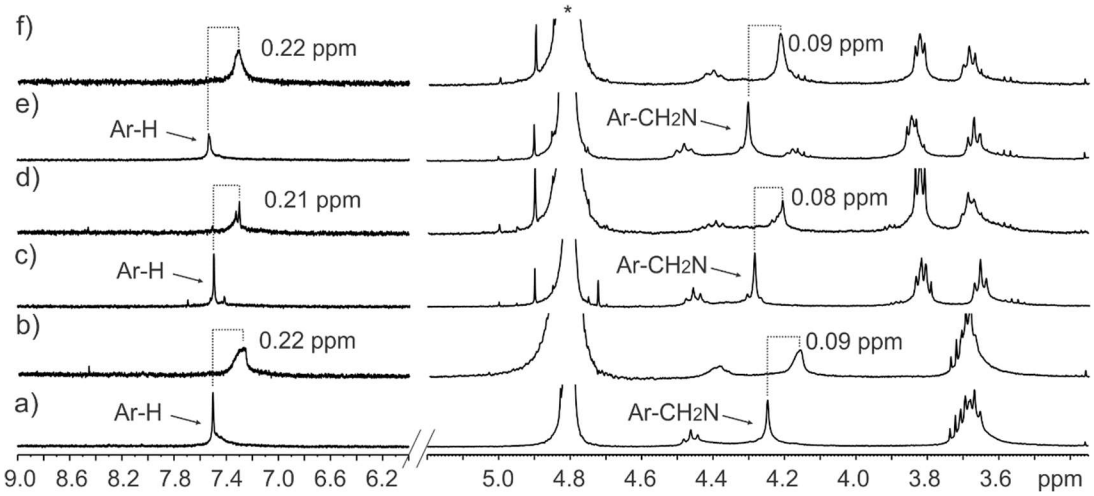

Figure 3.5: Sections of the ^1H NMR spectra in D_2O/[D_6]DMSO (90/10 v/v) at 298 K of (a) C3OHNAR$(Cl)_4$ and (b) the equimolar mixture C3OHNAR$(Cl)_4$ and PPi, (c) C3OHNAR$(Br)_4$, and (d) the equimolar mixture C3OHNAR$(Br)_4$ and PPi, (e) C3OHNAR$(OTf)_4$ and (f) the equimolar mixture C3OHNAR$(OTf)_4$ and PPi. The dashed

lines indicate the signal changes in ppm. Star represents the residual D_2O solvent. For clarity, the original counter anion is indicated in brackets.

Additionally, it is evident how the different counter ions contribute to the shielding of the pyrophosphate anions. The PPi signal was shielded by 1.14 ppm with C3OHNAR(Cl)$_4$, 1.76 ppm with C3OHNAR(Br)$_4$ and 1.85 ppm with C3OHNAR(OTf)$_4$. Larger up field shifts of 2.42, 2.50 and 2.72 ppm were observed upon switching from chloride to bromide or triflate with the NpNARX4 receptors. The magnitude of these shifts is a qualitative representation of the different affinities. As the product is identical in each case, the changes are better interpreted as a measurement of the population ratios between bound (upfield shifted) and free (unchanged) PPi. That the largest shifts are observed for triflate suggest that this salt shows the highest affinity, likely because the counterion is easiest to displace. Similar ^{31}P experiments were used to probe the binding of the receptors towards other phosphates: PO_4^{3-}, AMP, ADP, and ATP. PO_4^{3-} showed similar but much weaker upfield movement than PPi, while AMP showed greater field changes than PPi. Moderate, but measurable deshielding was observed for ADP and ATP. The interaction of ADP and ATP with the host might be through an exo-binding

mode, explaining the weaker effects, their larger size could be the main factor in this behavior.

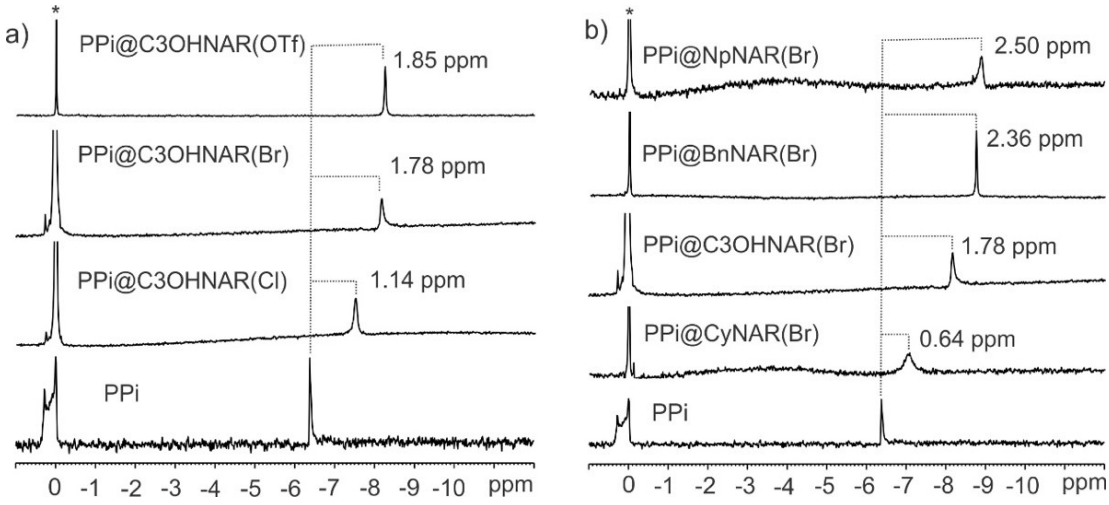

Figure 3.6: Sections of the ^{31}P NMR spectra in $D_2O/[D_6]DMSO$ (90/10 v/v) at 298 K. (a) Equimolar mixtures of PPi and $NpNAR(X)_4$ (X = Cl, Br, and OTf) as compared to pure PPi. (b) Equimolar mixtures of PPi and $CyNAR(Br)_4$, PPi and $C3OHNAR(Br)_4$, PPi and $BnNAR(Br)_4$, PPi and $NpNAR(Br)_4$ compared to pure PPi. The dashed lines indicate the signal changes in ppm. Star represents the residual H_3PO_4 as an external standard. For clarity, the original counter anion is indicated in brackets.

3.3.2.2 Isothermal Titration Calorimetry (ITC)

Thermodynamic parameters (K, ΔH, ΔS, and ΔG) between the $R\text{-}NAR(X)_4$ receptors and the different phosphate anions were measured by a series of ITC experiments in 90% H_2O/10% DMSO. A mixed solvent system was necessary to ensure the complete dissolution of the variable hydrophobic groups on the different $R\text{-}NAR(X)_4$ receptors. Probing different functionalization of the upper rim alkyl (R) substituent was necessary to underscore its importance in defining phosphate anion affinity (Table 2). All the data with a few exceptions were fitted to a two-set-of-sites binding model. Considering only one PPi guest can fit into the binding pocket, this two-set-of-sites binding model was puzzling at first. As a representative example, we did a ^1H NMR Job

plot experiment to understand the binding stoichiometry (Appendix 3.18). A closer inspection of a ^{1}H NMR titration of PPi to C3OHNAR(Cl)$_4$ revealed the secondary binding is likely happening at the four lower rim hydroxyl groups. This is indicated by the upfield shifts of the –CH_2– protons closest to the lower rim hydroxyl groups.

Upper rim substitution also offers an obvious role in the thermodynamic parameters of host-guest binding. The NAR(X)$_4$ with naphthalene groups show higher binding when compared to benzyl or cyclohexyl substituents due to the presence of a series of stacking interactions (Table 3.2). Interestingly, C3OH functionality overall provided the best affinity constant due to the extra hydrogen bond potential of the hydroxyl groups. In all, the trend of counter anion exchange on the Ka values is clear and consistent. K_1 values increased by 52.5% and 68.2% in the complexation of PPi to Np-NARX$_4$ upon switching counter-ion from chloride to bromide and triflate anion, respectively.

Table 3.2: Thermodynamic binding parameters of formed complexes between [PPi and R-NAR(Br)$_4$]

Complex	K_1 ($\times 10^5$) M^{-1}	ΔH_1 kcal/mol	$T\Delta S_1$ kcal/mol	ΔG_1 kcal/mol
PPi@C3OHNAR(Br)$_4$	5.30±1.08	-6.72±2.22	1.09	-7.81
PPi@CyNAR(Br)$_4$	2.62±0.54	-1.09±0.47	6.29	-7.38
PPi@BnNAR(Br)$_4$	3.12±0.24	-0.42±0.10	7.06	-7.48
PPi@NpNAR(Br)$_4$	3.02±0.22	-4.92±0.62	2.55	-7.47

Table 3.2 continued

Complex	K_2 ($\times 10^5$) M^{-1}	ΔH_2 kcal/mol	$T\Delta S_2$ kcal/mol	ΔG_2 kcal/mol
PPi@C3OHNAR(Br)$_4$	1.40±0.03	8.36±1.74	15.3	-6.94
PPi@CyNAR(Br)$_4$	0.18±0.01	26.6±0.84	32.2	-5.60
PPi@BnNAR(Br)$_4$	0.29±0.03	16.0±1.50	22.1	-6.10
PPi@NpNAR(Br)$_4$	1.13±0.01	32.6±2.11	39.6	-7.00

Negative ΔG values for all complexes of PPi with varying R-NAR(X)$_4$ suggest the association between the pair to be spontaneous at 298K. The ΔH and TΔS results also indicate the spontaneous association is exothermic and mostly enthalpy driven with a small entropic contribution. This is consistent with our understanding that PPi as an anion exists as a hydrated species in water, and this association must be disrupted upon complexation. The first binding event described as K_1 in table 3.3, reveals a generally higher binding constant for PPi over AMP, ADP, and ATP. As the cavity is committed to the binding of the first PPi molecule, this second interaction (described as K_2) is most likely an allosteric exo binding with the lower rim hydroxyl groups or in the case of C3OH-NARX4 the extra OH groups at the upper rims. From the NMR data, AMP is also highly shielded by the NARX receptors. We recognize that sometimes degree of shielding can also give a false sense of binding affinity. In the thermodynamic data of AMP complexation with the NAR(X)$_4$ receptors, the binding affinity is consistently one order of magnitude below PPi.

Table 3.3: Thermodynamic binding parameters of formed complexes between PPi, ATP, ADP, AMP, PO4 and C3OH-NAR(Br)4

Complex	K_1 ($\times 10^5$) M^{-1}	ΔH_1 kcal/mol	$T\Delta S_1$ kcal/mol	ΔG_1 kcal/mol
PPi@C3OHNAR$(Br)_4$	5.30±1.08	-6.72±2.22	1.09	-7.81
ATP@C3OHNAR$(Br)_4$	No Binding	-	-	-
ADP@C3OHNAR$(Br)_4$	No Binding	-	-	-
AMP@C3OHNAR$(Br)_4$	0.07±0.009	6.21±0.68	11.4	-5.19
PO4@C3OHNAR$(Br)_4$	No Binding	-	-	-

CHAPTER FOUR: MACROCYCLES FOR DEAGGREGATION OF CRYSTALLIN PEPTIDE RELATED TO CATARACTS

4.1 Introduction

Molecular aggregation is a phenomenon that occurs as a function of attractive non-covalent interactions in solution especially when concentration goes beyond the critical aggregation concentration (CAC). CAC refers to the minimum concentration above which molecules in solution begin to aggregate. This aggregation in human physiology is responsible for several disease pathologies including Alzheimer's disease, pulmonary embolism, deep-vein thrombosis, and eye cataracts.

Cataract disease remains without a cure and is caused by the clouding of the eye lens.[214] The onset of lens clouding is due to aging, protein post-translational modifications, and damage by radicals such as reactive oxygen species (ROS) generated by exogenous and endogenous factors.[214–216] The αA-crystallin, a heat-shock protein, maintains the solubility and stability of lens proteins and lens clarity by preventing protein aggregation, which may lead to lens clouding and eventually cataracts.[217–219] The chaperone property of αA-crystallin may be compromised with aging due to extensive chemical modifications and degradation of αA crystallin. The αA-crystallin protein level in the eye lens decreases significantly with aging leading to low molecular weight peptide (LMW) fragments.[220] The LMW fragments are present in aggregates of cataract lenses, pointing to their essential roles in the disease.[221] In particular, the αA66-80 peptide fragment of αA-crystallin, among others, was observed at a high level in cataracts eye

lenses.[218] The αA-crystallin peptide sequence has also been evaluated for its aggregation and ROS production.[222] The αA66-80 crystallin aggregation is a viable therapeutic target, and several small molecules have been assessed as aggregation inhibitors to include aspirin, flavonoids, orange G, among others.[222,223] Currently, there are no proven cures for cataracts other than surgery, which is performed at a later stage of the disease and continues to be debilitating to the people affected as they wait for the surgery.[224]

Cavity-containing macrocyclic compounds can be modified with specific functional groups and used as a target for biological materials.[225,226] Understandably, designing synthetic macrocycles that can target peptides or proteins offer a suitable avenue for applications in hybrid materials, diagnostics and potentially in this study as aggregation inhibitors. Receptors like molecular tweezers have been used to target aggregation of amyloidogenic peptides through their amino acid residues[227–229]; however, the crystallin aggregation has not been previously targeted using this approach. In this contribution, we hypothesize that receptors that can target specific amino acid sites on αA crystallin can disrupt the aggregation pattern inherent with its morphological changes. To this effect, we used three different resorcinarenes-based ionic macrocyclic receptors A, B and C (Figure 4.1). Receptors A and B are functionalized resorcinarenes with anionic sulfonate groups at the upper and lower rim respectively. Receptor C is a resorcinarene salt receptor with an extended cavity with four ammonium groups at the upper rim and four hydroxyl groups at the lower rim. Receptor C has a strong intramolecular circular hydrogen bond seam (⋯ NR'R"H2+ ⋯Cl^-⋯ NR'R"H2+ ⋯Cl^-⋯)$_2$ between the ammonium groups and the chloride anion referred to as the hydrogen bond analogs of

deep cavity cavitands.[213] The anionic receptors A and B have the potential to interact via electrostatic attractions to the cationic amino acids, arginine (R), lysine (K) and histidine (H) on the αA66−80 peptide while receptor C can interact with various amino acids including aspartic acid (D) and others through ionic and aromatic interactions.

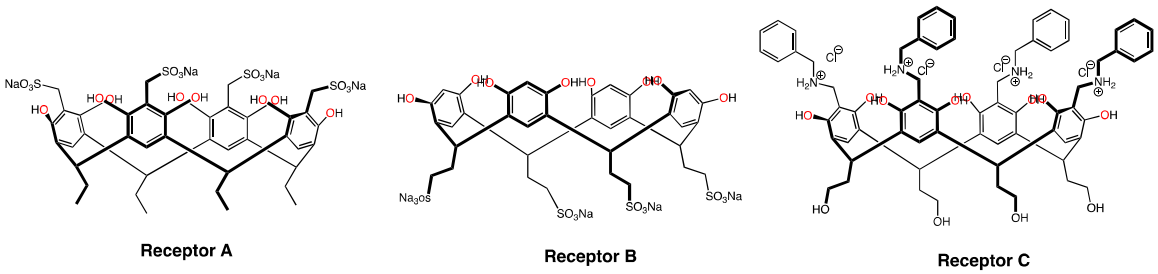

Figure 4.1. Structure of receptors A, B and C.

4.2 Experimental

The receptors used in this study were synthesized according to reported procedures.[230–233] The crystallin αA66-80 peptide was purchased from GenScript and used without further purification. All the receptors possess hydrophobic internal cavities that can accommodate neutral side groups based on size complementarity. The effect of the receptors on the aggregation/de-aggregation of αA66−80 peptide are investigated at the macroscopic level through Fluorescence Aggregation Assay, Dynamic Light Scattering (DLS), Transmission Electron Microscopy (TEM), and Mass Spectrometry. Interactions at the molecular level between the receptors and the individual amino acids are investigated qualitatively via NMR spectroscopy, and quantitatively via Isothermal Titration Calorimetry (ITC).

4.3 Results and discussion

4.3.1 Fluorescence Aggregation Assay

Resorcinarenes are notably weak fluorescent compounds which prompted the use of the proteostat detection kit for qualitative detection of peptide aggregates. This rotational proprietary dye specifically intercalates into quaternary protein structures typical of aggregated β-pleated sheet peptides and proteins, resulting in fluorescence emission enhancement.[234] The dye's free intramolecular rotation along a single central bond eliminates fluorescent emissions in the absence of aggregates. As a result, the dye has been reliably used as an indicator of β-pleated sheet formation during crystallin aggregation.[234–237] As shown in Figure 4.2, pure crystallin aggregation resulted in formation of dynamic structural assemblies that produced a high fluorescence intensity. To assess the level of aggregation of the peptide with the receptors, the mixtures of receptor: peptide ratios at 0.2, 0.4, 0.6, 0.8, 1.0 and 5.0 were incubated at 37 °C in 10 mM Tris buffer (pH 7.4) for seven days. Compared to the pure crystallin incubated for the same period, all ratios showed a concentration-dependent decrease in the extent of peptide aggregation (Figure 4.2a). From these results, receptors A, B and C all have an inhibiting effect on the extent of crystallin peptide aggregation in the seven days incubation period. To rule out any inconsistent fluorescence contributions from the proteostat dye, we also run positive and negative controls (Appendix 4.1) to make sure that, a) each freshly prepared dye solution is effective, b) there is little to no fluorescence contributions from free dye solutions and c) the receptors are not artificially quenching

fluorescence from the dye irrespective of peptide aggregation. In queries a) and b), we see high and minimal fluorescence intensities from the proprietary positive and negative controls respectively (Appendix 4.1).

4.3.2 Dynamic Light Scattering (DLS)

To clarify the effect of the receptors on peptide aggregation without another chemical dye, we resorted to Dynamic Light Scattering (DLS) experiments (Figure 4.2b). DLS is used for measuring the size distribution of small particles, peptides, cells, carbohydrates, nanoparticles, or polymers in solution.[238] These measurements were also carried out on increasing receptor: peptide molar ratios (0.0, 0.2, 0.4, 0.6, 0.8 and 1.0:1) after seven days of incubation at 37°C. The size (Z-) average in d.nm of triplicate measurements of the different concentration ratios reflects a similar inhibitory effect of receptors A, B, and C against aggregation of crystallin (Figure Appendix 4.2 – 4.4). In the incubations of pure αA66-80 crystallin peptide without any receptor, the Z-average size is (1.20±0.15) × 10^4 d.nm after seven days of incubation. All the incubations revealed substantially different size distribution profiles showing smaller average size intensity profiles compared to the crystallin peptide (Figure 4.2b). The mixture between receptor A, B and the peptide show some large size distributions on an average of replicate measurements, however, the overall sizes show substantially smaller distributions compared to the pure αA66-80 crystallin peptide. The average sizes from triplicate measurements of a 1:1 concentration ratio of receptor A, B, and C: crystallin are 1918±897, 3739±644, and 202±2.2 d.nm respectively. Receptor C, the deep cavity

cavitand, was most effective at disrupting the aggregation of the crystallin peptide in the DLS experiments.

4.3.3 Transmission Electron Microscopy (TEM)

Transmission electron microscopy (TEM) was used to virtually characterize αA66-80 crystallin peptide aggregates in the presence of the inhibitors. TEM analysis of pure αA66-80 crystallin peptide, peptide-receptor A, B and C complexes at 1:1 concentration ratio, and pure receptor A, B and C were performed after aging the samples for seven days. From the images, pure crystallin demonstrates large, fibrillar-like peptide aggregates congruent with the results from fluorescence and DLS experiments both initially and after seven days. The macrocycles show significant potential to disrupt the crystallin aggregation (Figure 4.2c). Additionally, TEM images also reveal receptor C, decorated with functional groups on both sides of the receptor, is superior to receptors A or B at equimolar concentrations regarding disrupting crystallin αA66−80 aggregation. αA66-80 Crystallin peptide: receptor C complex morphology showed significantly less fibrillar aggregates when compared to αA66-80 crystallin peptide: receptor A or B complex morphology, suggesting its superior inhibitory role. TEM imaging however shows amorphous small protein aggregates in the αA66-80 crystallin peptide: receptor A, B and C complexes with few branching fibrils. Overall, these results suggest that while

all receptors A, B, and C inhibit the aggregation of the crystallin peptide, receptor C acts as a more potent inhibitor to the peptide over time.

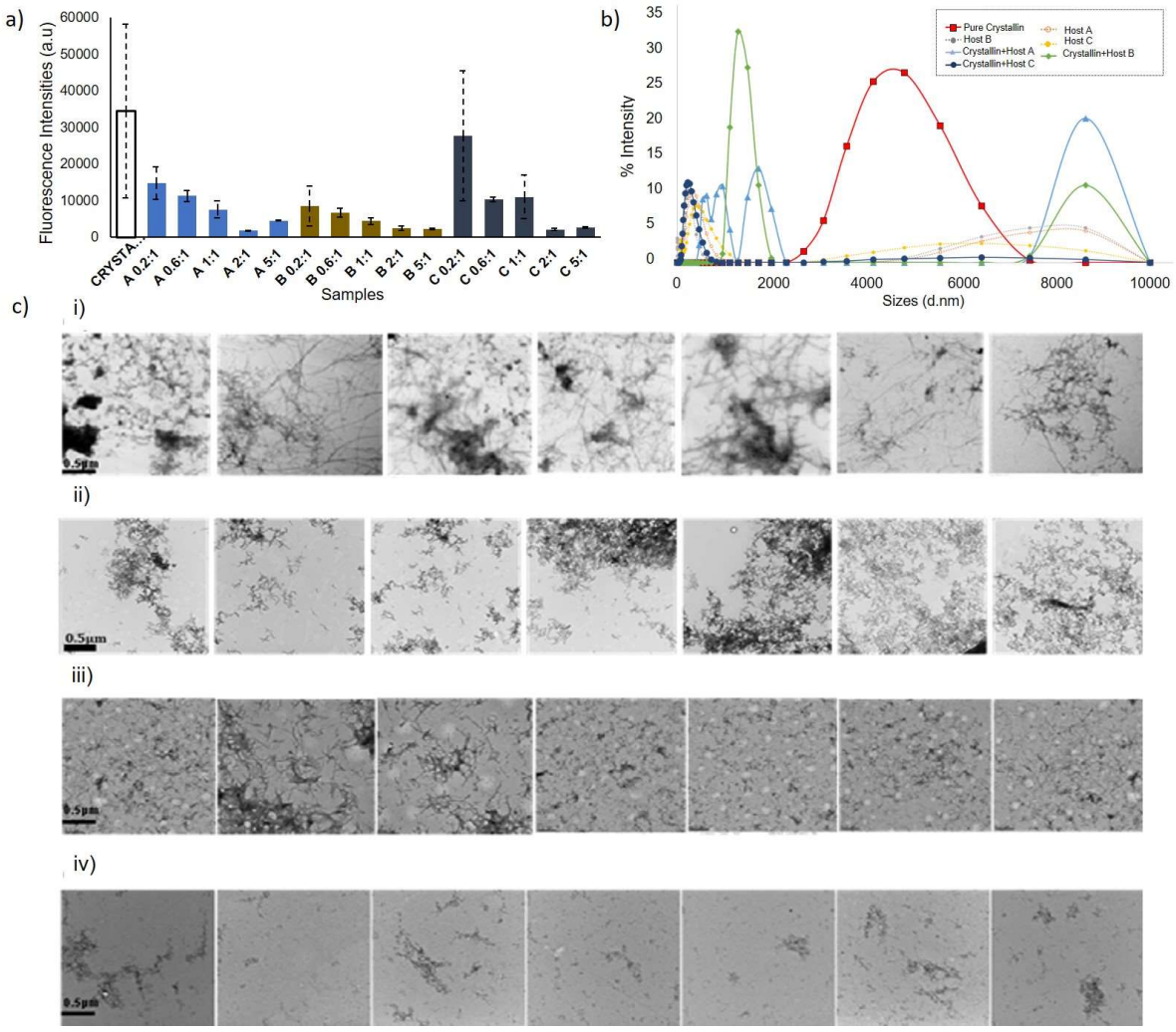

Figure 4.2. a) Bar chart showing results of fluorescence aggregation of crystallin peptide (5.4 mM) in different host ratios. Error bars represent standard deviations of the mean of repetitive measurements. b) Graph showing percent intensities of Z-average sizes in solution of pure crystallin (red), 1:1 αA66-80 crystallin peptide: receptor A (sea blue), 1:1 αA66-80 crystallin peptide: receptor B (green), 1:1 αA66-80 crystallin peptide: receptor C (dark blue), pure receptor B (grey), pure receptor A (orange) and pure receptor C (yellow). c) Transmission Electron Microscopy (TEM) imaging of one week incubated samples of pure crystallin, 1:1 αA66-80 crystallin peptide:receptor A, 1:1 αA66-80 crystallin peptide: receptor B, and 1:1 αA66-80 crystallin peptide: receptor C.

4.3.4 Mass Spectrometry

To further investigate this phenomenon of crystallin de-aggregation, we turned to gas phase measurements, devoid of solution interruptions to tease out possible host-αA66-80 crystallin peptide complexes. Electrospray ionization mass spectrometry (ESI-MS), a soft ionization method, was used to characterize each receptor and the peptide using freshly made sample solutions, as well as their respective complexes. In the positive ion mode, the mass spectrum for the peptide shows the $[M+3H]^{3+}$ peak at m/z 622.6646, associated with the triply charged peptide (Appendix 4.5a). The mass spectra for the receptor A, B, and C show peaks at m/z 1065.097 $[M+H]^{+}$, 1009.0296 $[M+H]^{+}$, and 599.3110 $[M-4HCl+2H]^{2+}$ respectively (Appendix 4.5b-d). The MS analysis of freshly prepared samples, compared to aged samples (72 h at 37°C), yielded more prominent receptor + peptide complexes. Figure 4.3a shows the observed and theoretical isotope patterns for doubly charged receptor A + peptide complexes as $[A+peptide-4Na+6H]^{2+}$ and $[A+peptide-3Na+5H]^{2+}$ (Figure 4.3b-c). In addition, the triply charged receptor A-peptide complexes were observed with increasing sodium loss. Figure 4.3 also shows the MS spectrum of the observed (Figure 4.3d) and theoretical isotope patterns of the doubly charged complexes of receptor B as $[B+peptide-4Na+6H]^{2+}$ and $[B+peptide-3Na+5H]^{2+}$ (Figure 4.3e-f). The receptor B + peptide complexes were also observed as triply and doubly charged ions. The multiply charged ions are expected due to the mass of the complexes, the multiple basic amino acids present in the peptide and the chosen ionization method. Equimolar receptor C and peptide solution were also analyzed, but no

peaks associated with receptor C + peptide complexes were observed under the same experimental conditions (Appendix 4.6). Receptor C is cationic and structurally different from the anionic receptor A and B. However, the receptor C + peptide complex could not be observed after optimization of the ionization methods.

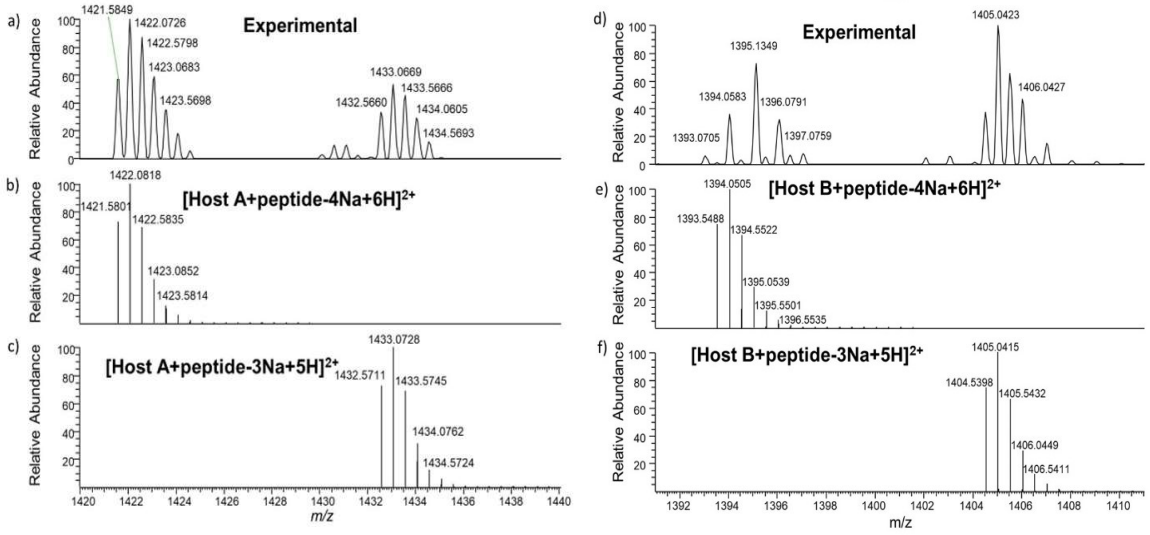

Figure 4.3. Positive mode ESI-MS spectra of a) doubly charged receptor A-peptide complexes showing $[A+peptide-4Na+6H]^{2+}$ and [A+peptide-3Na+5H]2+; d) Receptor B + peptide complexes showing $[B+peptide-4Na+6H]^{2+}$ and $[B+peptide-3Na+5H]^{2+}$ (experimental: a), d); theoretical isotope distribution: b), c), e), f).

4.3.5 NMR Spectroscopy

To further understand the interactions between the receptors and the αA66−80 crystallin peptide, we investigated the binding ability of the receptors towards the individual amino acids within the αA66-80 peptide through ^{1}H NMR experiments. This was done by monitoring the complexation-induced ^{1}H chemical shift changes of the receptor-amino acid mixtures and comparing that to the pure receptor and the amino acids. Guest complexation in the resorcinarene cavity is typically indicated by shielding

and broadening guests' signals while hydrogen bond interactions are generally observed as downfield shifts.[231] With receptors A and B, both upfield and downfield shifts of lysine and arginine signals were observed. While the receptors can encapsulate both amino acid residues, extra *exo*-cavity interactions are also observed with the de-shielded protons. No significant shift changes were also observed for the other amino acids, including histidine and aspartic acid (Appendix 4.7 – 4.32). If the association cannot be established with these individual amino acids, there is no reason to believe they are viable binding pockets on the crystallin peptide. Moreover, receptor C showed significant shift changes for complexation with lysine, arginine, histidine, and minor shift changes for aspartic acid (Appendix 4.25 – 4.32). These results indicate that these receptors have a peculiar preference for specific amino acids due to both size and complementarity of the weak interactions.

4.3.6 Isothermal Titration Calorimetry

If these interactions can translate into any consequential effect on the morphological changes in a peptide, we needed to understand the thermodynamics of those interactions under physiological conditions using isothermal calorimetric titrations (ITC). Individual amino acid experiments were limited to the arginine, lysine, histidine, and aspartic acid residues based on established supramolecular attraction to the receptors inferred from their ^{1}H-NMR chemical shift changes. Moreover, ITC experiments were also conducted between the receptors A, B, and C with αA66-80 crystallin peptide (Appendix 4.33 – 4.37, Table 4.1). The sodium sulfonate substitution pattern on receptors

A and B does not have a marked difference in the thermodynamic binding parameters with the amino acids from our initial experiments. However, the binding affinity and energy are highest with receptor A where the functional groups are closest to the macrocyclic cavity. Complexation was enthalpically favorable with entropic compensations except for histidine, enthalpically and entropically favorable in complexation with both receptors. The supramolecular attraction of the persistent hydrophobic cavity and the different functional groups on both sides of the receptor C are highlighted in the nonspecific nature of the ITC curvature with amino acids (Appendix 4.36). The multiple binding processes between receptor C and arginine, lysine could not be fitted to one or two sets of sites binding model without significant errors. However, complexation with histidine was found to be enthalpically favorable with minor entropic compensations. Aspartic acid, a negatively charged amino acid, was found to be both enthalpically and entropically favorable in complexation with receptor C. Ultimately, the binding event between C and the αA66−80 crystallin peptide is a one-to-one association. All the complexation experiments were found to be spontaneous at 298 K. It is worth mentioning that for the ITC measurements, the titrant is added, and the associated heat changes are measured immediately.[239] In effect, samples for these measurements cannot be aged, a limitation of the technique. Again, we recognize the unpredictable and three-dimensional folding of the crystallin peptide is the most predominating factor influencing peptide: receptor complexation and the subsequent disruption of aggregates. However, through ^{1}H-NMR and ITC experiments, we can predict possible binding pockets on the

crystallin aggregates that can effectively disrupt the peptide aggregation when or if accessible to the macrocycle.

Table 4.1. Thermodynamic parameters of binding between receptors A, B, and C with amino acids (arginine, lysine, histidine) and crystallin α66-80 peptide in 100% water. All the data shown were fitted to one set of sites binding model at 298K.

Complex	K ($\times 10^3$) M^{-1}	ΔH kcal/mol	TΔS kcal/mol	ΔG kcal/mol
A•				
Arginine	7.27±1.28	-15.70±3.85	-10.43	-5.27
Lysine	5.89± 0.88	-12.07±2.04	-6.45	-5.62
Histidine	2.94±0.39	-2.59±0.16	6.91	-9.50
Crystallin	1360 ± 490	-8.28 ± 0.21	0.092	-8.37
B•				
Arginine	3.64±0.47	-15.15±1.00	-10.25	-4.90
Lysine	4.45±0.69	-6.74±0.69	-1.76	-4.98
Histidine	3.44±0.51	-1.05±0.07	3.75	-4.80
Crystallin	380 ± 33	-3.23 ± 0.027	4.38	-7.61
C•				
Arginine	-	-	-	-
Lysine	-	-	-	-
Histidine	14.90±1.70	-7.53±0.34	-1.84	-5.69
Aspartic Acid	7.30±0.10	-1.00±0.06	2.90	-3.90
Crystallin	2.40 ± 0.95	4.89 ± 2.66	9.48	-4.59

CHAPTER FIVE: CONCLUSIONS

In conclusion, supramolecular chemistry principles are integral to the applications of organic, inorganic, environmental and analytical chemistry. Different types of macrocycles have been synthesized and reported for applications in this discipline. In the Beyeh Lab, we have extensive experience in calixarenes and pillararenes and have reported discrete functionalizations of the macrocycle for applications in experimental chemistry, materials science and as receptors for neutral guests, cations, anions, bio-analytes, and metals. In this thesis, we continued to explore the resorcinarene macrocycles and their discrete functionalizations for applications in ternary system assemblies, cataract de-aggregation, and as sensors for pyrophosphate and *N*-alkyl ammonium cations.

In chapter two, since Cn is the only component that differs between any two ternary systems, it would be unsurprising if the stability of the complexes is highly dependent on the pKa of the acid. This would be expected to be especially true if one is simply analyzing the interaction between the pyridine and the acid as a binary system. These results supports co-operativity: pKa is more important in the ternary system than in a simple binary acid-base system because the acidity and basicity behavior are enhanced. The presence of the resorcinarene, by increasing electron density on the pyridine and decreasing it on the acid, increases the affinity of the acid for the base. The reported pyridine-mediation of a resorcinarene-carboxylic acid interaction represents a new ternary supramolecular archetype. The presence of the carboxylic acid, located outside

the cavity, stabilizes the pyridine-resorcinarene inclusion complex. The electron-rich resorcinarene cavity makes the pyridine N-atom more basic via the host-guest C–H···π interactions. In the ternary systems, the strength of the O–H···N hydrogen bond between *exo*-carboxylic acid and *endo*-pyridine varies from −104.0 kcal/mol to −121.0 kcal/mol for carboxylic acids with pKa values ranging between −0.25 and 3.75; and −37.0 kcal/mol to −102.0 kcal/mol for acids with pKas between 4.19 and 4.90. The ITC derived thermodynamic parameters, negative ΔH and positive $T\Delta S$ values, for carboxylic acid-pyridine (binary) and ternary systems indicate that complexation is enthalpy driven and compensated by entropy. By broadening the pool of analytes for supramolecular diagnostic tools from those that fit in a macrocycle's cavity, to include those that interact with the guests in the cavity, these new guest-mediated ternary complexes could prove very useful as the basis for next-generation sensors in biomedicine and environmental science applications.

In chapter three, a comprehensive solution ^{1}H NMR study of the H-G complexation process between C_{ethyl}-tetrasodiumsulfonatomethyleneresorcinarene and ammonium halides was carried out in a hydrogen bond competing solvent, MeOH-d_4. In solution, despite the upper-rim host cavity being surrounded by hydrogen bond competing sulfonate oxygen atoms, the C−H···π contacts between guest and host are the key driving non-covalent interactions for 14 out of 16 observed *endo*-complexes. The exception being for *N*-butyl-*N*-benzylammonium cation, where the hydrogen bonding between -NH_2 and sulfonate oxygens restricts both *N*-butyl and *N*-benzyl groups from *endo*-complexation. Isothermal calorimetry titrations were carried out to quantify association constants. The

binding was spontaneous at 303 K. The highest binding constant observed for tetramethylammonium cation guest (K_a = 909.10 M^{-1}) reflects the perfect size match between the host and guest. Flexibility and size mismatch were also highlighted with lower binding constants of some of the guests. This work offers more fundamental insights into the unique properties of tetrasulfonatomethylene resorcinarenes and their potential as receptors for a variety of cationic guests in a highly competitive solvent. An extensive study in solution of ten *N*-alkyl ammonium resorcinarene salts with varying counter anions using ^{1}H and ^{31}P NMR, and ITC show the resorcinarene salts to be high-affinity receptors for PPi in aqueous media. The receptor with the terminal propyl hydroxyl groups C3OHNAR$(X)_4$ and the napththalen-1-ylmethyl group at the upper rim, both with weakly coordinating triflate counter anions, gave the best binding results with PPi. The results show that both the nature of the upper rim substituent and the coordinating strength of the counter anions play important roles in determining the affinity of binding. The C3OHNAR$(X)_4$ receptors provide extra hydrogen bond for enhanced binding, while the NpNAR$(X)_4$ provides a larger surface area for binding. Weakly coordinating counter anions such as triflate enhanced the binding affinity over more coordinating anions such as chloride. Our results also show good binding for AMP while PO_4^{3-} due to its smaller size was only weakly bound. The larger sizes of ADP and ATP suggest the binding to the receptor to be exo. These results show that modifying the upper rim and counter anions of the R-NAR$(X)_4$ enhances their affinity and sensor ability towards PPi. These results pave the way to using a supramolecular approach using cavity containing resorcinarene salts receptors as sensors for PPi in biological media.

Last, in chapter four, the present work demonstrates that three resorcinarene-based receptors can successfully disrupt αA66-80 crystallin peptide which is abundant in cataracts eye lenses. Two of the receptors possess anionic sulfonate groups at the upper and lower rim. The third receptor possesses cationic ammonium group and flexible benzyl groups. All three receptors possess internal hydrophobic cavities. Macroscopic experiments such as Fluorescence with a proteostat dye, dynamic light scattering, and TEM microscopy show the receptors to successfully interact and disrupt the aggregate of the αA66-80 crystallin peptide. These macroscopic experiments also show receptor C with the cationic ammonium groups and benzyl arms to be the optimum receptor for this process. Qualitative NMR experiments reveal the receptors prefer specific amino acids which are all part of the peptide backbone. Isothermal Titration Calorimetric experiments provide some thermodynamic data showing the interaction between the receptors and the amino acids, or the αA66-80 crystallin peptide to be spontaneous at the given temperature. We are currently expanding the library of these resorcinarene based receptors. We envision that based on these results, resorcinarenes can be developed into potential therapeutics for crystallin disruption.

Overall, resorcinarenes as macrocycles have incredible potential for applications in the chemical space. This dissertation highlights but a few of them. Advances in human chemical understanding and synthetic modalities will continue to open ways to functionalize resorcinarenes in novel and exciting ways for future applications.

APPENDIX

SUPPLEMENTARY DATA

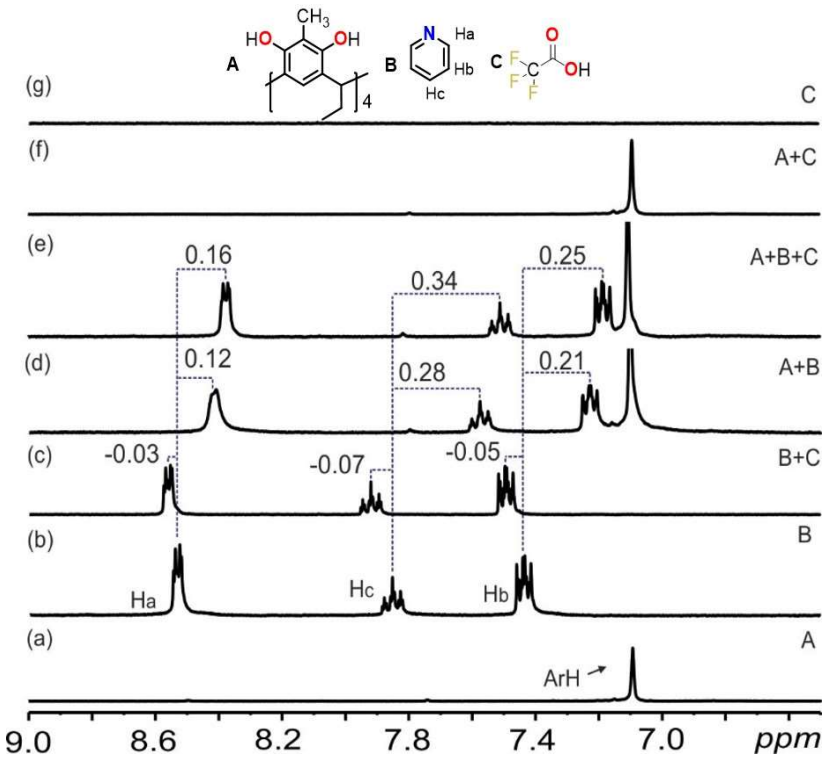

Appendix 2.1. Sections of the ^{1}H NMR (CD_3OD, 298 K, 300 MHz) of the ternary A·B·C1 complex between A, B and trifluoroacetic acid C1 (pK_a -0.25). Spectra are produced from (a) A, (b) B, (g) C1. Equimolar mixtures of: (c) B and C1, (c) A and B, (e) A, B, and C1, (d) A and C1. Dashed lines highlight the observed shift changes of the resonances, labels are in ppm.

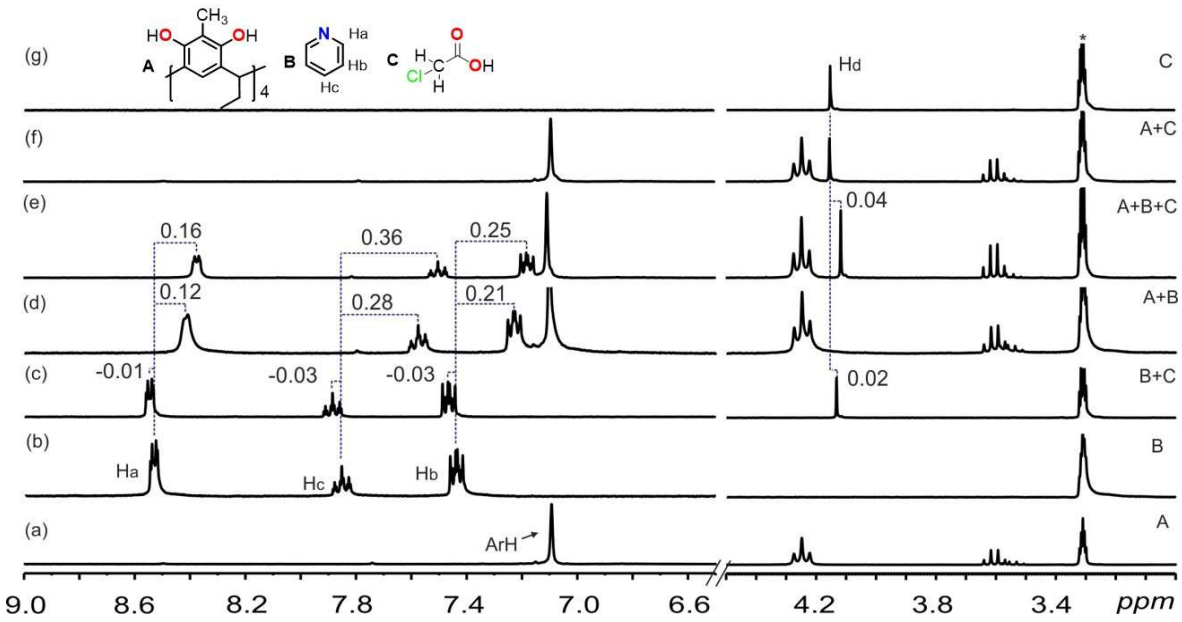

Appendix 2.2. Sections of the ^{1}H NMR (CD_3OD, 298 K, 300 MHz) of the three-component A·B·C3 complex between A, B and chloroacetic acid C3 (pK_a 2.87). Spectra are produced from (a) A, (b) B, (g) C3. Equimolar mixtures of: (c) B and C3, (c) A and B, (e) A, B, and C1, (d) A and C3. Dashed lines highlight the observed shift changes of the resonances, labels are in ppm.

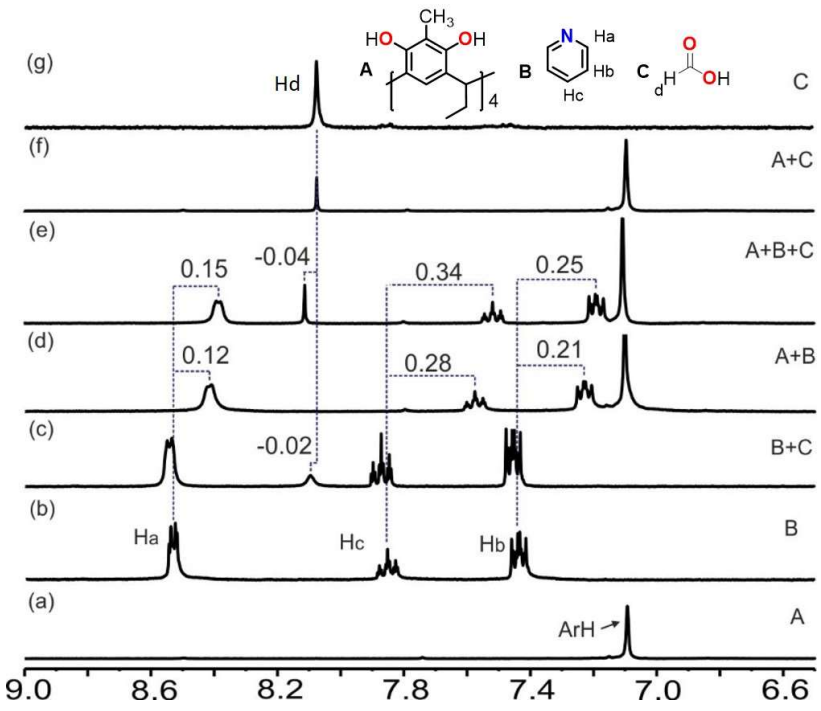

Appendix 2.3. Sections of the ^{1}H NMR (CD_3OD, 298 K, 300 MHz) of the three-component ternary A·B·C4 complex between A, B and formic acid C4 (pK_a 3.75). Spectra are produced from (a) A, (b) B, (g) C4. Equimolar mixtures of: (c) B and C4, (c) A and B, (e) A, B, and C4, (d) A and C4. Dashed lines highlight the observed shift changes of the resonances, labels are in ppm.

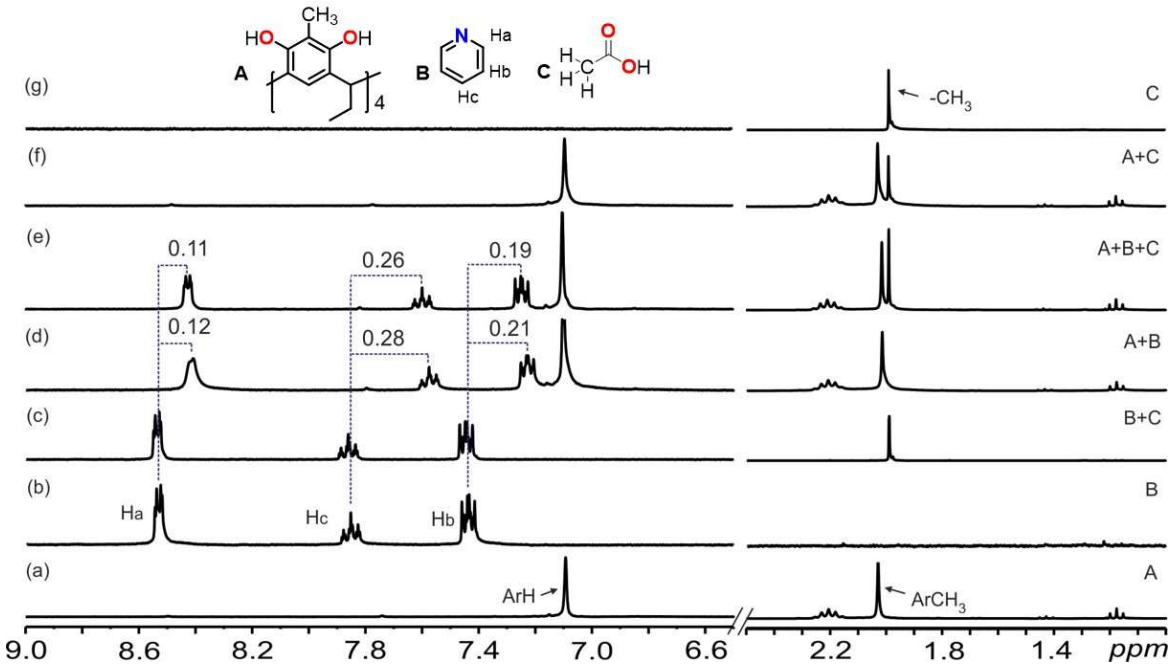

Appendix 2.4. Sections of the 1H NMR (CD_3OD, 298 K, 300 MHz) of the three-component ternary A·B·C5 complex between A, B and acetic acid C5 (pKa 4.75). Spectra are produced from (a) A, (b) B, (g) C5. Equimolar mixtures of: (c) B and C5, (c) A and B, (e) A, B, and C5, (d) A and C5. Dashed lines highlight the observed shift changes of the resonances, labels are in ppm.

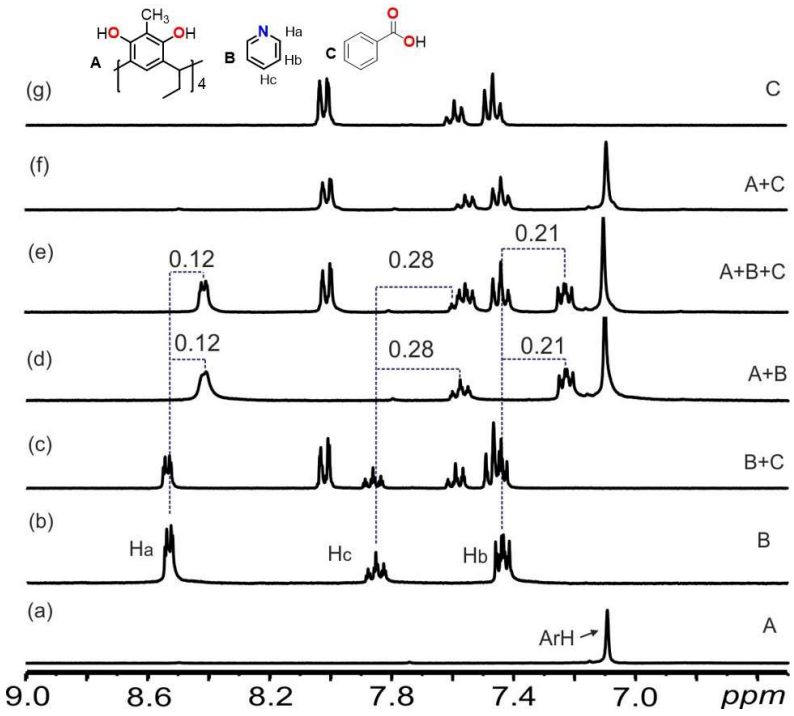

Appendix 2.5. Sections of the ^{1}H NMR (CD_3OD, 298 K, 300 MHz) of the three-component ternary A·B·C6 complex between A, B and benzoic acid C6 (pK_a 4.75). Spectra are produced from (a) A, (b) B, (g) C6. Equimolar mixtures of: (c) B and C6, (c) A and B, (e) A, B, and C6, (d) A and C6. Dashed lines highlight the observed shift changes of the resonances, labels are in ppm.

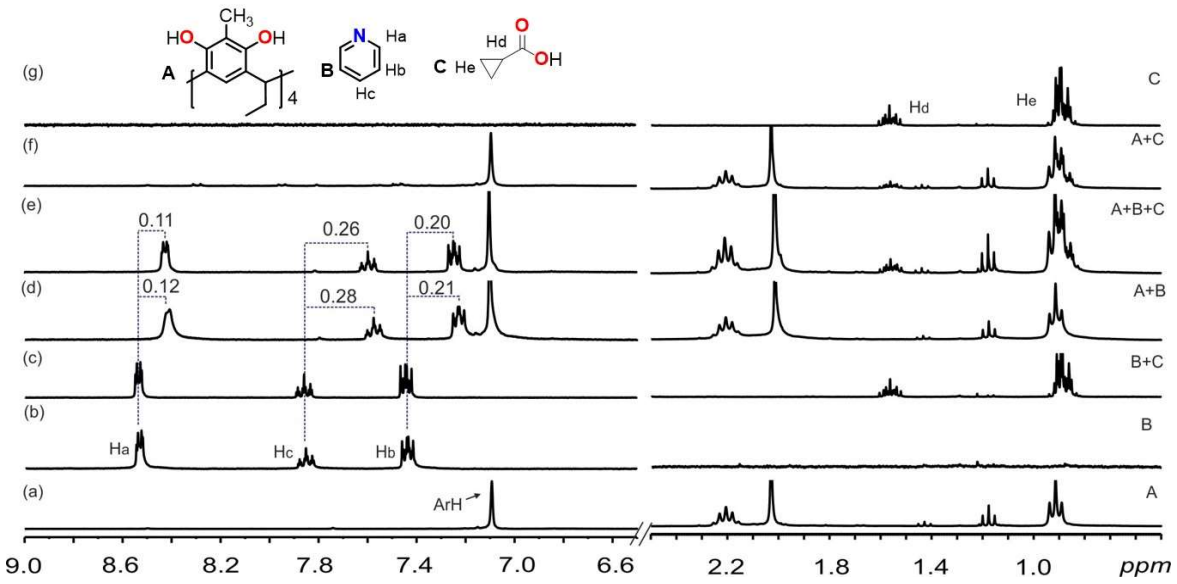

Appendix 2.6. Sections of the ^{1}H NMR (CD_3OD, 298 K, 300 MHz) of the three-component ternary A·B·C7 complex between A, B and cyclopropyl carboxylic acid C7 (pK_a 4.78). Spectra are produced from (a) A, (b) B, (g) C7. Equimolar mixtures of: (c) B and C7, (c) A and B, (e) A, B, and C7, (d) A and C7. Dashed lines highlight the observed shift changes of the resonances, labels are in ppm.

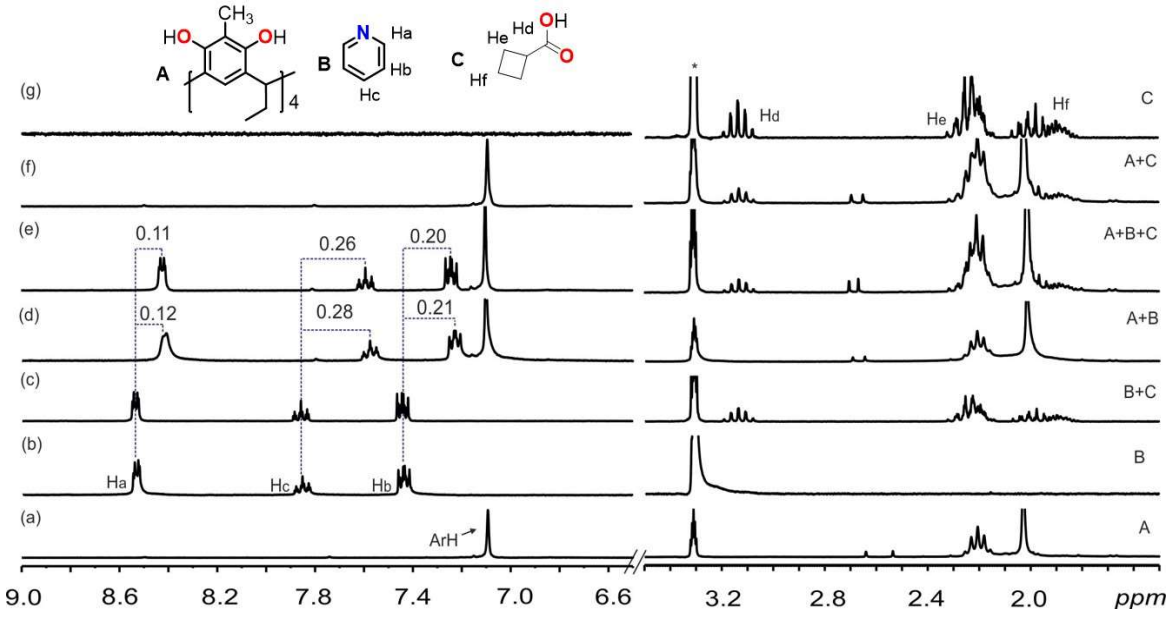

Appendix 2.7. Sections of the ^{1}H NMR (CD_3OD, 298 K, 300 MHz) of the three-component ternary A·B·C8 complex between A, B and cyclobutyl carboxylic acid C8 (pK_a 4.80). Spectra are produced from (a) A, (b) B, (g) C8. Equimolar mixtures of: (c) B and C8, (c) A and B, (e) A, B, and C8, (d) A and C8. Dashed lines highlight the observed shift changes of the resonances, labels are in ppm.

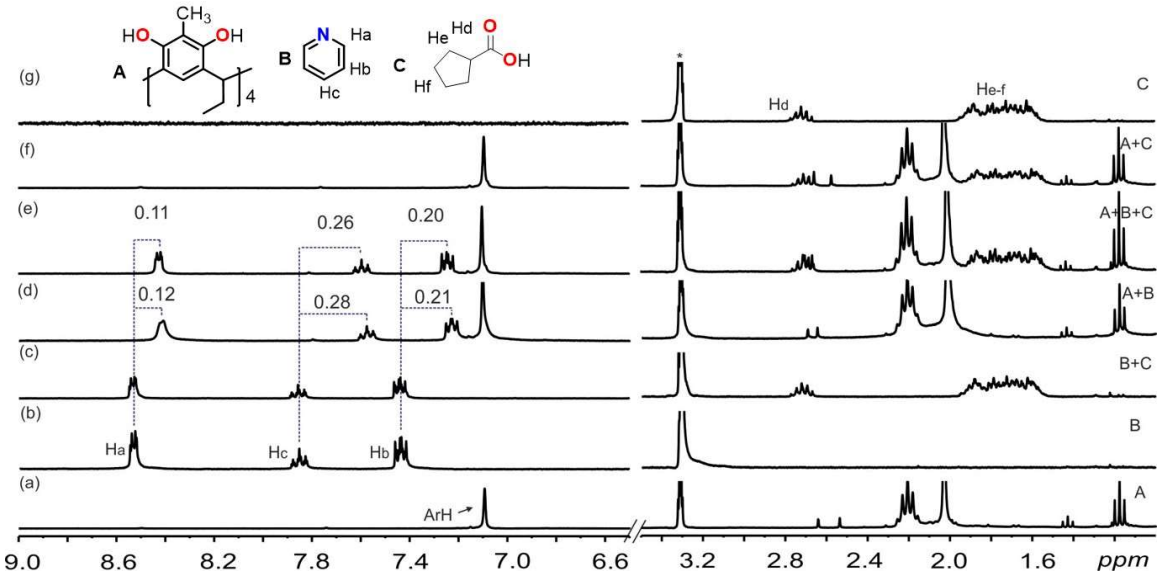

Appendix 2.8. Sections of the ^{1}H NMR (CD_3OD, 298 K, 300 MHz) of the three-component ternary A·B·C9 complex between A, B and cyclopentyl carboxylic acid C9 (pK_a 4.80). Spectra are produced from (a) A, (b) B, (g) C9. Equimolar mixtures of: (c) B and C9, (c) A and B, (e) A, B, and C9, (d) A and C9. Dashed lines highlight the observed shift changes of the resonances, labels are in ppm.

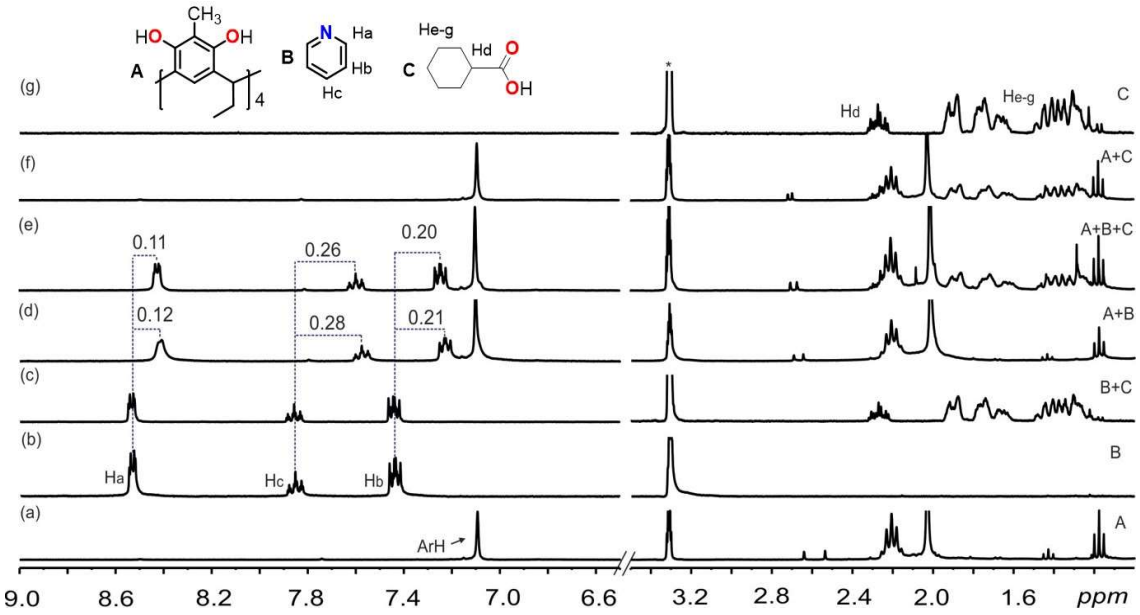

Appendix 2.9. Sections of the ^{1}H NMR (CD_3OD, 298 K, 300 MHz) of the three-component ternary A·B·C10 complex between A, B and cyclohexyl carboxylic acid C10 (pK_a 4.90). Spectra are produced from (a) A, (b) B, (g) C10. Equimolar mixtures of: (c) B and C10, (c) A and B, (e) A, B, and C10, (d) A and C10. Dashed lines highlight the observed shift changes of the resonances, labels are in ppm.

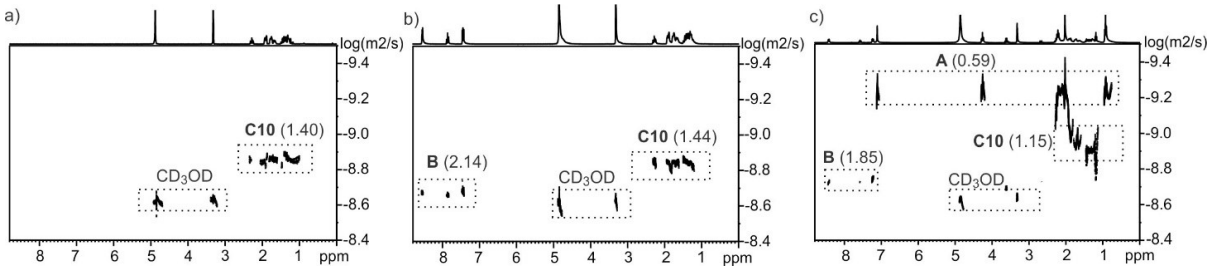

Appendix 2.10. 2D DOSY NMR spectra (in CD_3OD at 298 K) of a 20 mM sample of: a) C10, and equimolar mixtures of b) B·C10, c) A·B C10 showing the chemical species present in the samples. The diffusion coefficient ($\times 10^{-9}$ m^2s^{-1}) of each species is shown in brackets.

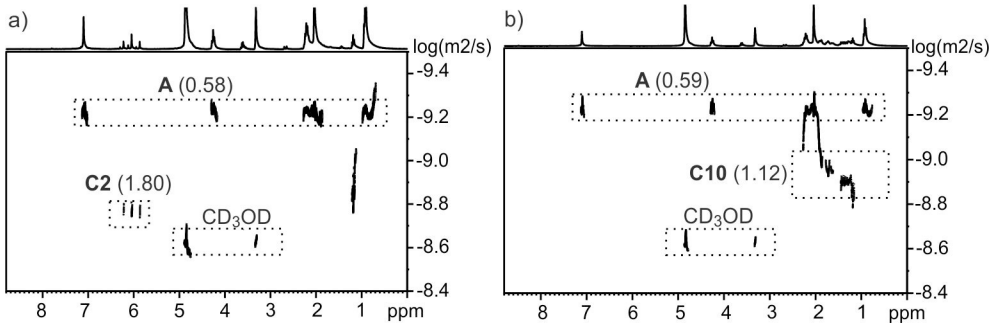

Appendix 2.11. 2D DOSY NMR spectra (in CD_3OD at 298 K) of a 20 mM equimolar sample of: a) A·C2, and b) A·C10 showing the chemical species present in the samples. The diffusion coefficient ($\times 10^{-9}$ m^2s^{-1}) of each species is shown in brackets.

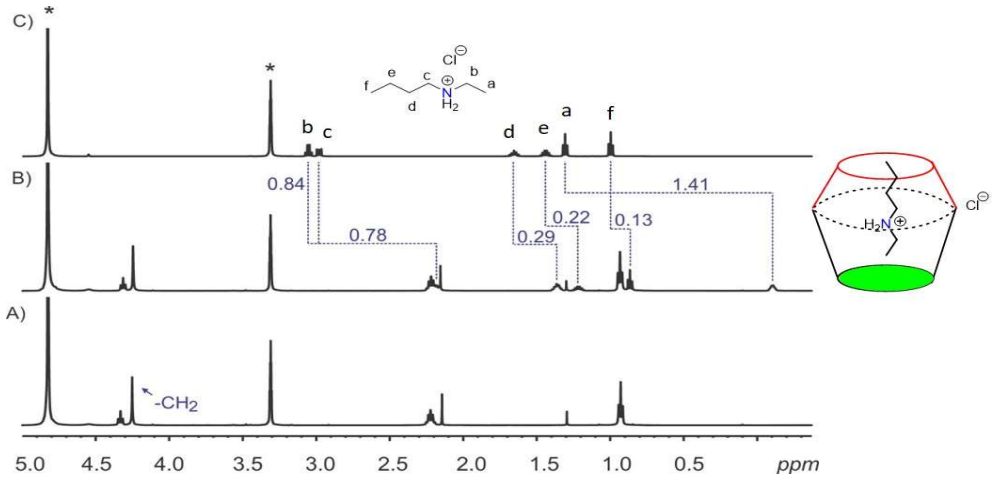

Appendix 3.1: ^{1}H NMR spectra (CD_3OD, 298 K) of: (A) host A_1, (C) guest B_4, and the equimolar mixture of (B) A_1 and B_4. Star represents the residual CD_3OD solvent. The dash lines give an indication of the signal changes in ppm.

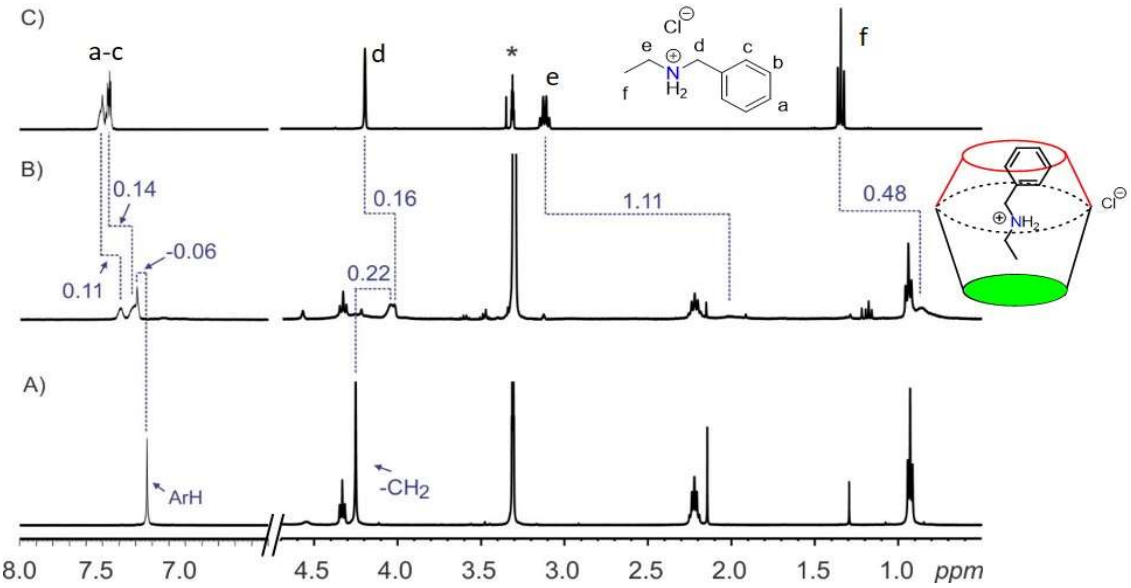

Appendix 3.2: ^{1}H NMR spectra (CD_3OD, 298 K) of: (A) host A_1, (C) guest B_6, and the equimolar mixture of (B) A_1 and B_6. Star represents the residual CD_3OD solvent. The dash lines give an indication of the signal changes in ppm.

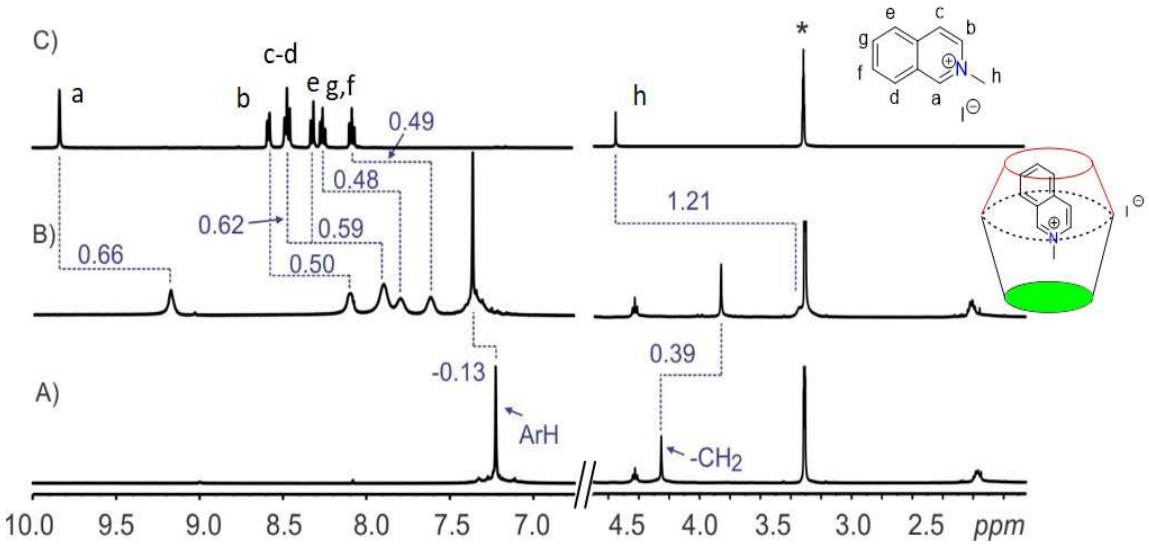

Appendix 3.3: ^{1}H NMR spectra (CD_3OD, 298 K) of: (A) host A_2, (C) guest B_9, and the equimolar mixture of (B) A_2 and B_9. Star represents the residual CD_3OD solvent. The dash lines give an indication of the signal changes in ppm.

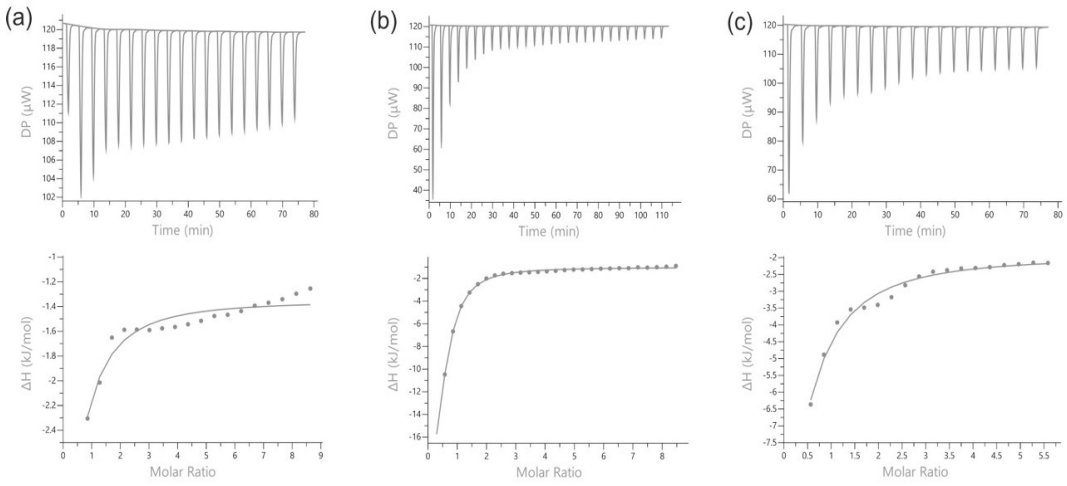

Appendix 3.4: ITC traces of the titration of the host A with the guests (a) B_1, (b) B_2 and (c) B_4 in CH_3OH at 298 K. The data were fitted into a one-site binding model.

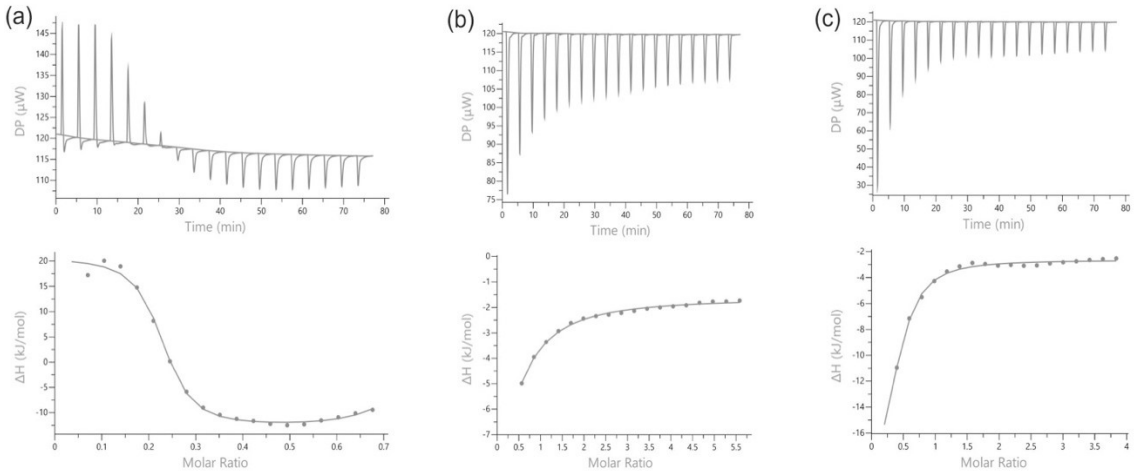

Appendix 3.5: ITC traces of the titration of the host A with the guests (a) B_5, (b) B_6 and (c) B_7 in CH_3OH at 298 K. The data for B_6 and B_7 were fitted into a one-site binding model. The data for B_5 could not be fitted correctly, with very large errors.

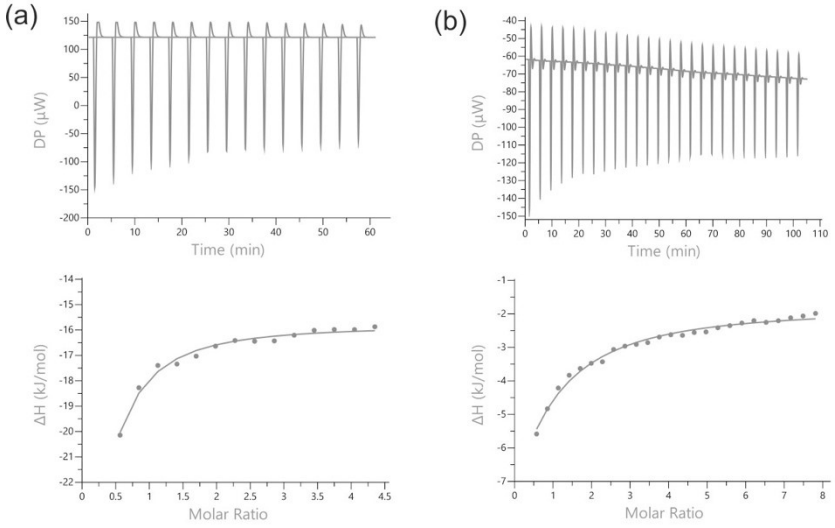

Appendix 3.6: ITC traces of the titration of the host A with the guests (a) B_8 and (b) B_9 in CH_3OH at 298 K. The data were fitted into a one-site binding model.

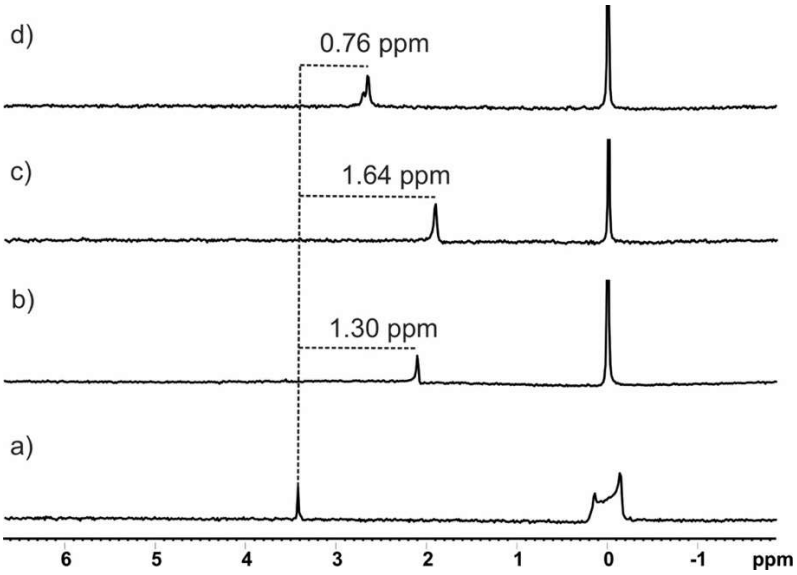

Appendix 3.7: ^{31}P NMR spectra (D_2O/[D_6]DMSO 9/1 v/v, 298 K) of (a) PO_4^{3-}, and equimolar mixtures of (b) PO_4^{3-}@C3OHNAR(Cl)$_4$, (c) PO_4^{3-}@C3OHNAR(Br)$_4$ and (d) PO_4^{3-}@C3OHNAR(OTf)$_4$. The displaced anions are represented in parentheses. The dash lines give an indication of the signal changes in ppm.

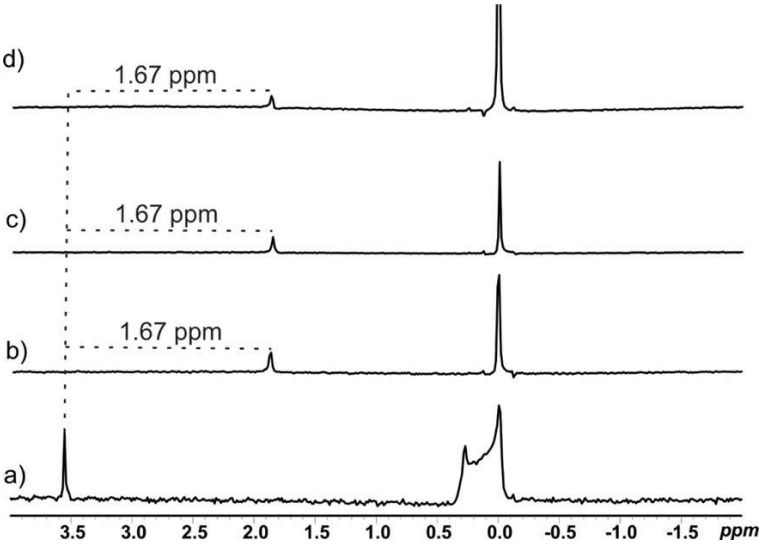

Appendix 3.8: ^{31}P NMR spectra (D_2O/[D_6]DMSO 9/1 v/v, 298 K) of (a) PO_4^{3-}, and equimolar mixtures of (b) PO_4^{3-}@NpNAR(Cl)$_4$, (c) PO_4^{3-}@NpNAR(Br)$_4$ and (d) PO_4^{3-}@NpNAR(OTf)$_4$. The displaced anions are represented in parentheses. The dash lines give an indication of the signal changes in ppm.

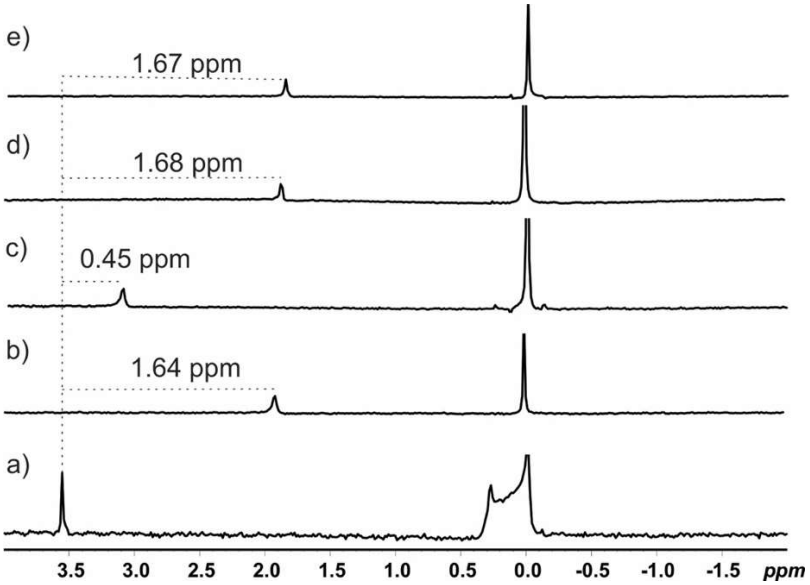

Appendix 3.9: 31P NMR spectra (D2O/[D6]DMSO 9/1 v/v, 298 K) of (a) PO43-, and equimolar mixtures of (b) PO43-@C3OHNAR(Br)4, (c) PO43-@CyNAR(Br)4, (d) PO43-@BnNAR(Br) 4 and (e) PO43-@NpNAR(Br)4. The displaced anions are represented in parentheses. The dash lines give an indication of the signal changes in ppm.

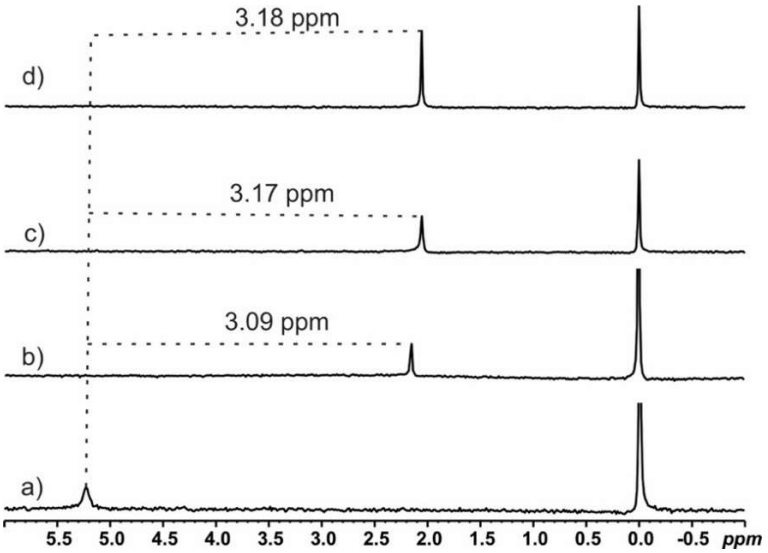

Appendix 3.10: ^{31}P NMR spectra (D_2O/[D_6]DMSO 9/1 v/v, 298 K) of (a) AMP, and equimolar mixtures of AMP@C3OHNAR(Cl)$_4$, (c) AMP@C3OHNAR(Br)$_4$ and (d) AMP@C3OHNAR(OTf)$_4$. The displaced anions are represented in parentheses. The dash lines give an indication of the signal changes in ppm.

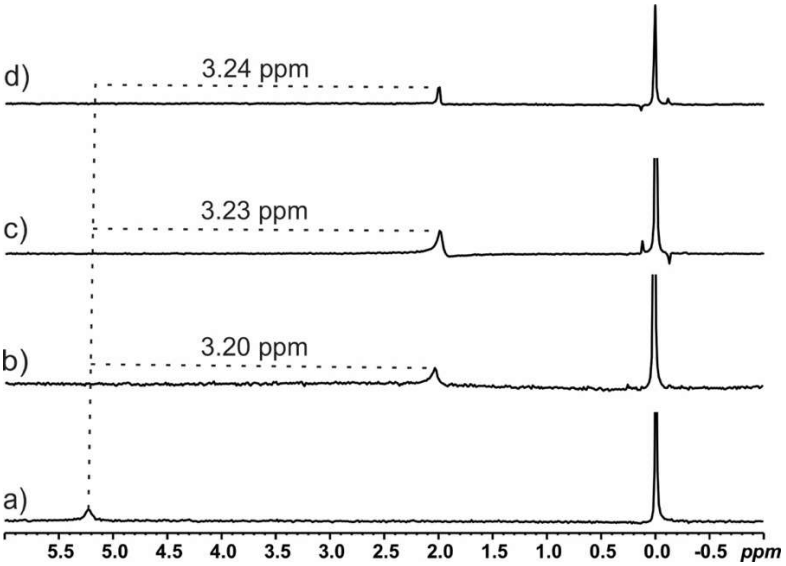

Appendix 3.11: ^{31}P NMR spectra (D_2O/[D_6]DMSO 9/1 v/v, 298 K) of (a) AMP, and equimolar mixtures of (b) AMP@NpNAR(Cl)$_4$, (c) AMP@NpNAR(Br)$_4$ and (d) AMP@NpNAR(OTf)$_4$. The displaced anions are represented in parentheses. The dash lines give an indication of the signal changes in ppm.

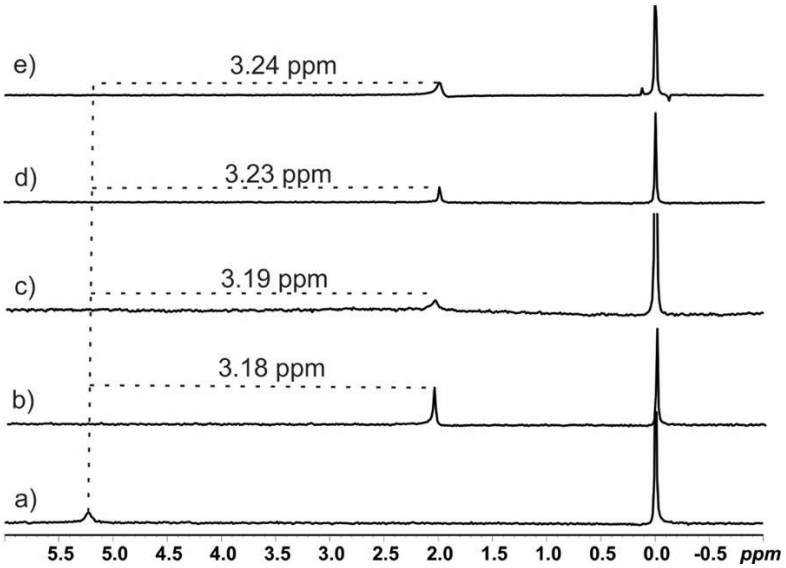

Appendix 3.12: ^{31}P NMR spectra (D_2O/[D_6]DMSO 9/1 v/v, 298 K) of (a) AMP, and equimolar mixtures of (b) AMP@C3OHNAR(Br)$_4$, (c) AMP@CyNAR(Br)$_4$, (d)

AMP@BnNAR(Br)$_4$ and (e) AMP@NpNAR(Br)$_4$. The displaced anions are represented in parentheses. The dash lines give an indication of the signal changes in ppm.

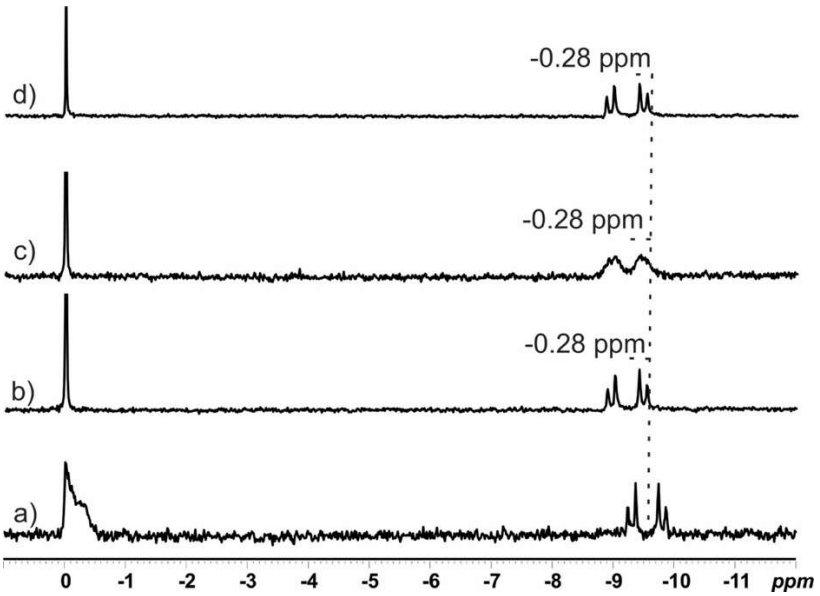

Appendix 3.13: ^{31}P NMR spectra (D_2O/[D_6]DMSO 9/1 v/v, 298 K) of (a) ADP, and equimolar mixtures of ADP@C3OHNAR(Cl)$_4$, (c) ADP@C3OHNAR(Br)$_4$ and (d) ADP@C3OHNAR(OTf)$_4$. The displaced anions are represented in parentheses. The dash lines give an indication of the signal changes in ppm.

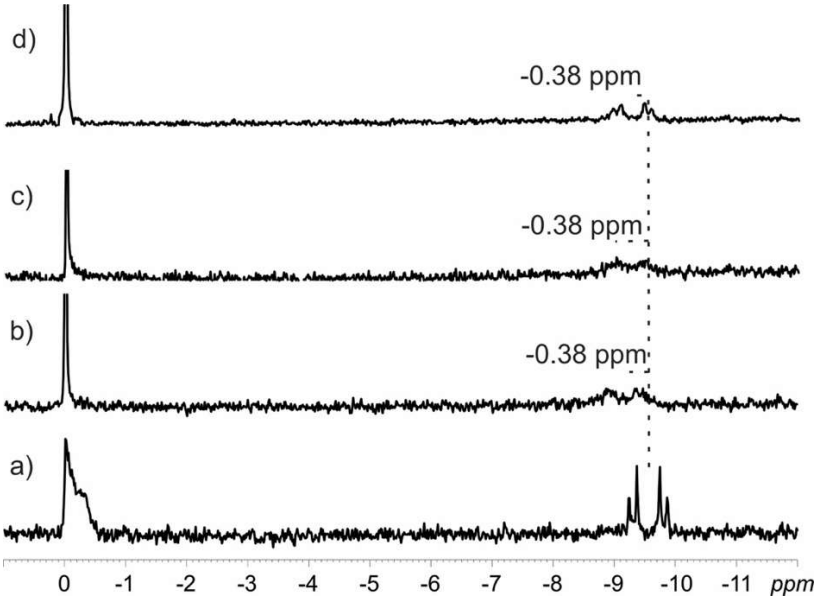

Appendix 3.14: ^{31}P NMR spectra (D_2O/[D_6]DMSO 9/1 v/v, 298 K) of (a) ADP, and equimolar mixtures of (b) ADP@NpNAR(Cl)$_4$, (c) ADP@NpNAR(Br)$_4$ and (d) ADP@NpNAR(OTf)$_4$. The displaced anions are represented in parentheses. The dash lines give an indication of the signal changes in ppm.

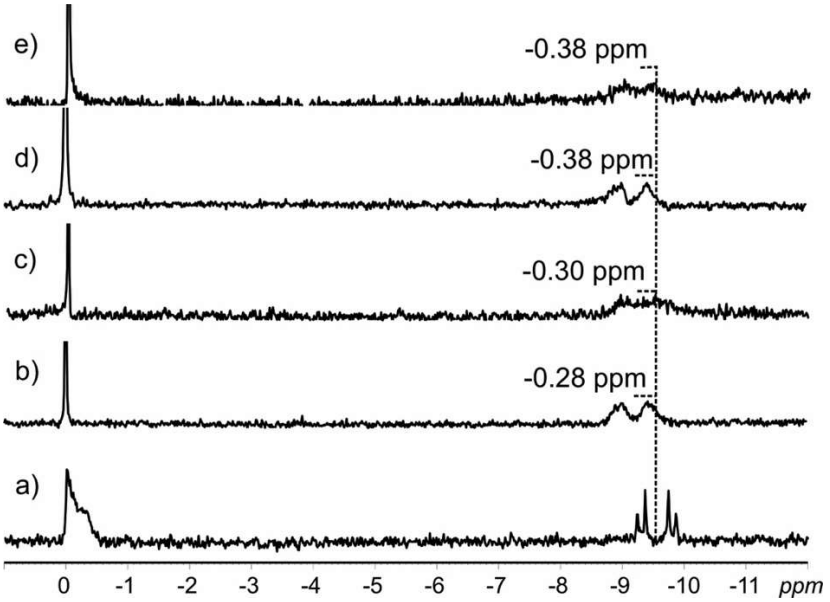

Appendix 3.15: ^{31}P NMR spectra (D_2O/[D_6]DMSO 9/1 v/v, 298 K) of (a) AMP, and equimolar mixtures of (b) ADP@C3OHNAR(Br)$_4$, (c) ADP@CyNAR(Br)$_4$, (d) ADP@BnNAR(Br)$_4$ and (e) ADP@NpNAR(Br)$_4$. The displaced anions are represented in parentheses. The dash lines give an indication of the signal changes in ppm.

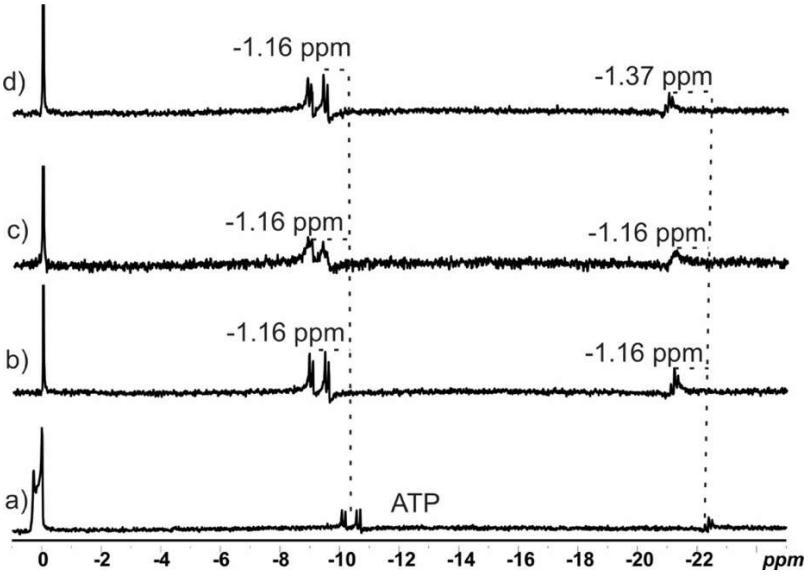

Appendix 3.16: ^{31}P NMR spectra (D_2O/[D_6]DMSO 9/1 v/v, 298 K) of (a) ATP, and equimolar mixtures of ATP@C3OHNAR$(Cl)_4$, (c) ATP@C3OHNAR$(Br)_4$ and (d) ATP@C3OHNAR$(OTf)_4$. The displaced anions are represented in parentheses. The dash lines give an indication of the signal changes in ppm.

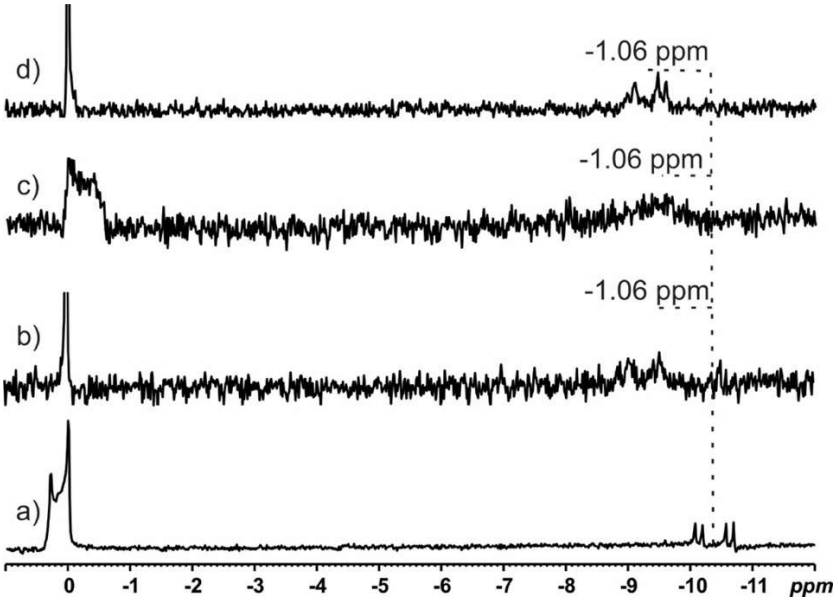

Appendix 3.17: ^{31}P NMR spectra (D_2O/[D_6]DMSO 9/1 v/v, 298 K) of (a) ATP, and equimolar mixtures of (b) ATP@NpNAR$(Cl)_4$, (c) ATP@NpNAR$(Br)_4$ and (d) ATP@NpNAR$(OTf)_4$. The displaced anions are represented in parentheses. The dash lines give an indication of the signal changes in ppm.

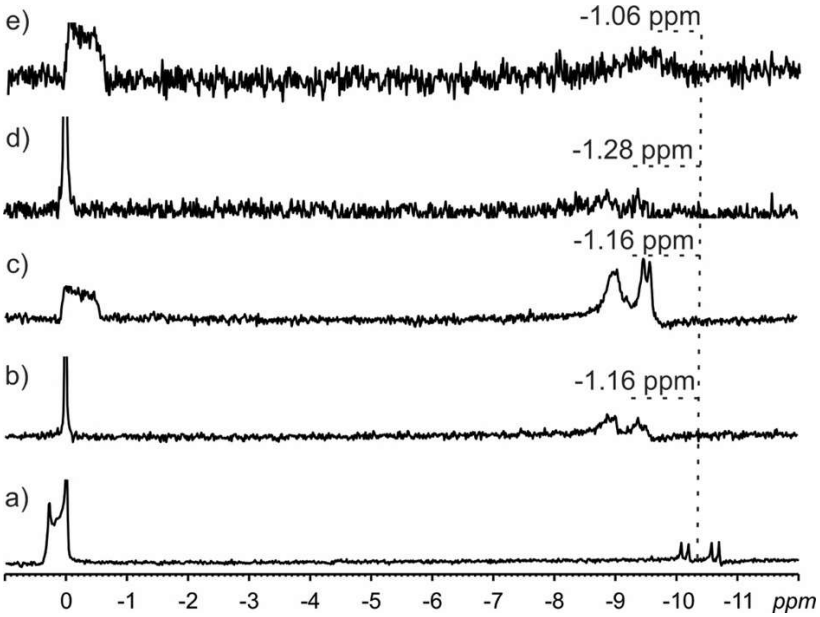

Appendix 3.18: ^{31}P NMR spectra (D_2O/[D_6]DMSO 9/1 v/v, 298 K) of (a) ATP, and equimolar mixtures of (b) ATP@C3OHNAR(Br)$_4$, (c) ATP@CyNAR(Br)$_4$, (d) ATP@BnNAR(Br)$_4$ and (e) ATP@NpNAR(Br)$_4$. The displaced anions are represented in parentheses. The dash lines give an indication of the signal changes in ppm.

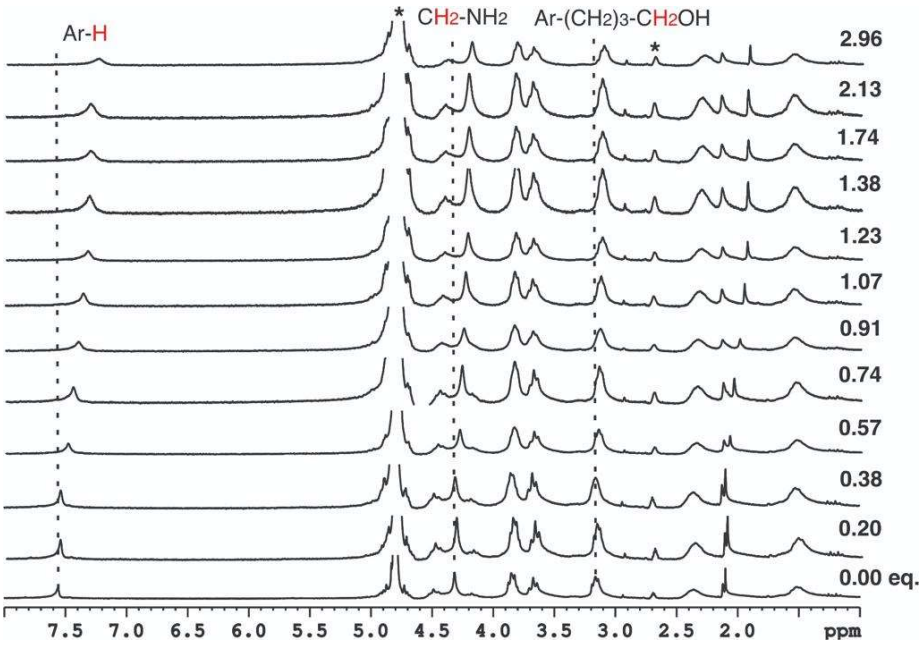

Appendix 3.19: ^1H NMR titration spectra (D_2O, 298 K) of C3OH-NAR(Br)$_4$ showing signal changes per equivalence of pyrophosphate added.

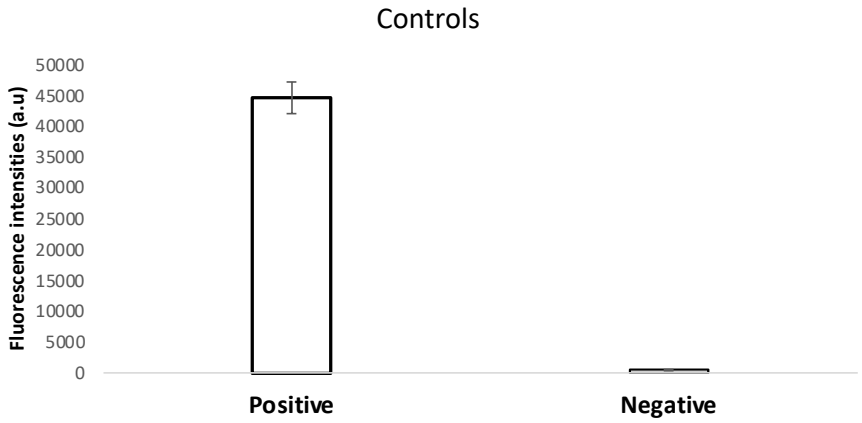

Appendix 4.1 Bar chart of fluorescence intensities of positive and negative controls of the Proteostat dye. Error bars are the standard deviations of the mean of triplicate measurements.

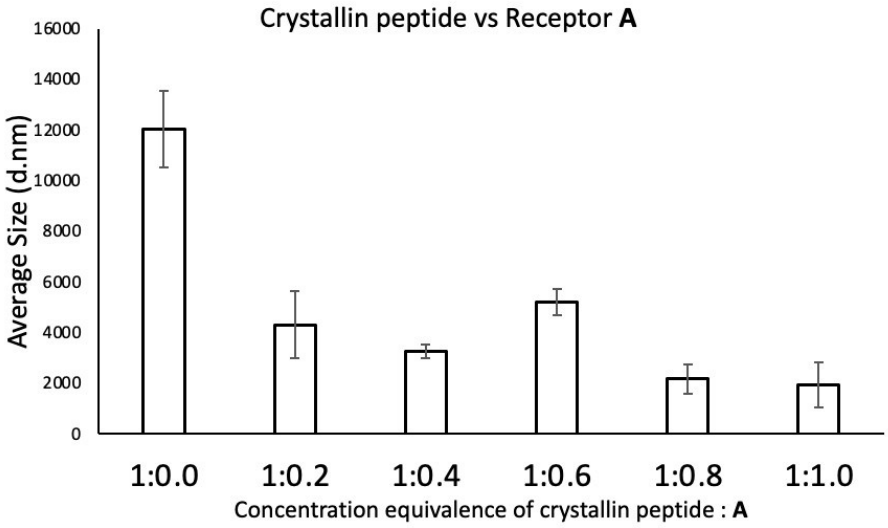

Appendix 4.2. Bar chart of Z-average size (d.nm) different concentration ratio of receptor A into 1 equivalence of αA66-80 crystallin peptide. Error bars are the standard deviations of the mean of triplicate measurements.

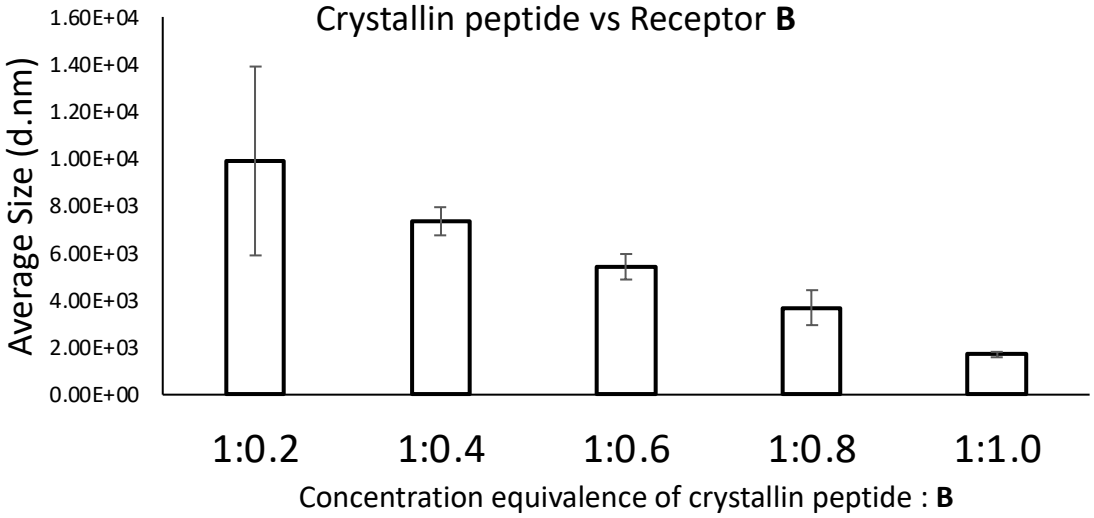

Appendix 4.3. Bar chart of Z-average size (d.nm) of different concentration ratio of receptor B into 1 equivalence of αA66-80 crystallin peptide. Error bars are the standard deviations of the mean of triplicate measurements.

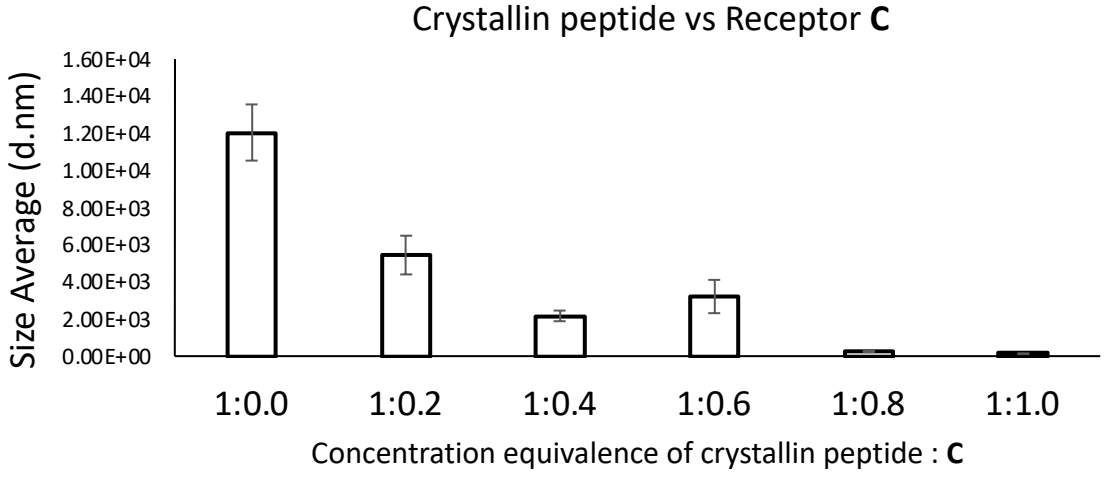

Appendix 4.4. Bar chart of Z-average size (d.nm) of different concentration ratio of receptor C into 1 equivalence of αA66-80 crystallin peptide. Error bars are the standard deviations of the mean of triplicate measurements.

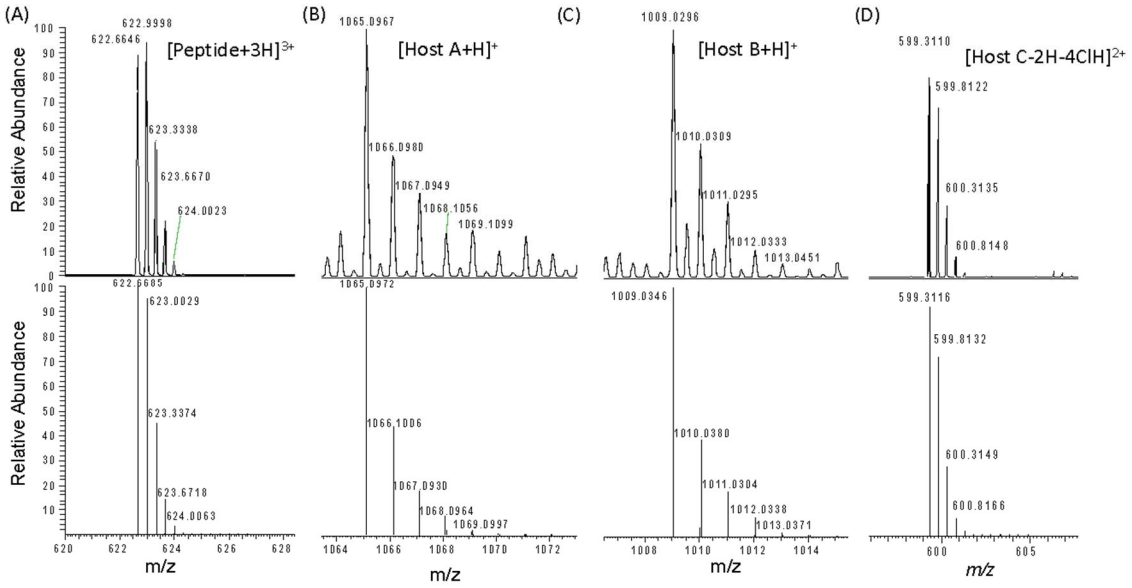

Appendix 4.5. Positive mode ESI-MS spectra of (A) the α66-80 crystallin peptide, (B) Host A, (C) Host B and (D) Host C with their respective theoretical isotope distributions.

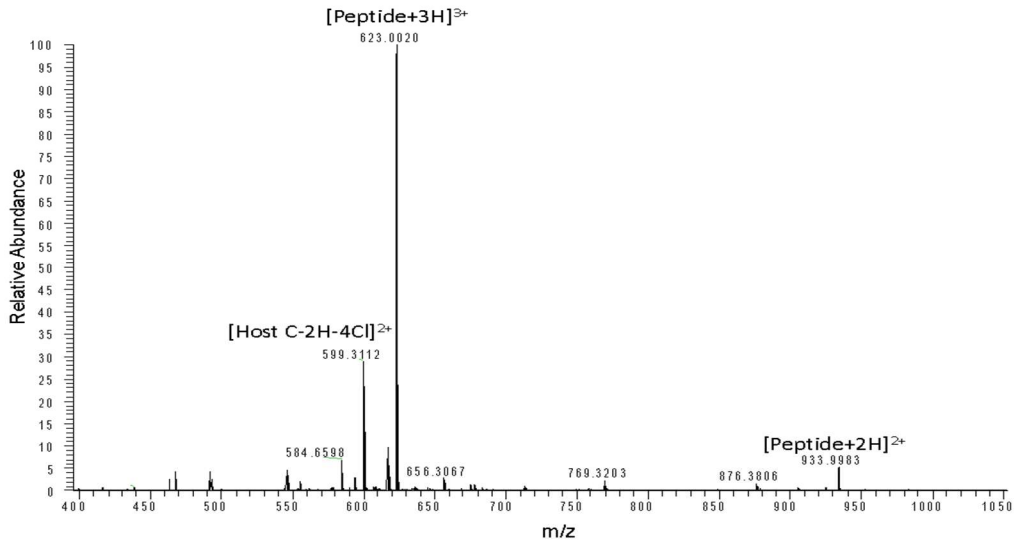

Appendix 4.6. Positive mode ESI mass spectrum of host C + peptide mix after incubation for 72 hours at 37 ºC. Peaks associated with the free peptide and free host are labeled.

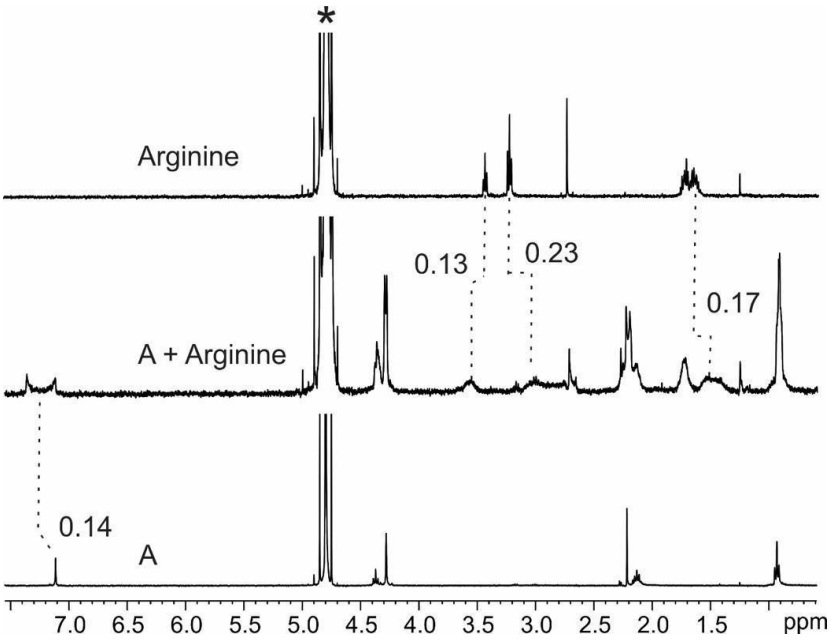

Appendix 4.7. ^{1}H NMR spectra (D_2O, 298 K) of (a) receptor A, equimolar mixtures of (b) arginine@A and (c) arginine. The dash lines give an indication of the signal changes in ppm. Asterisks is the residual NMR solvent.

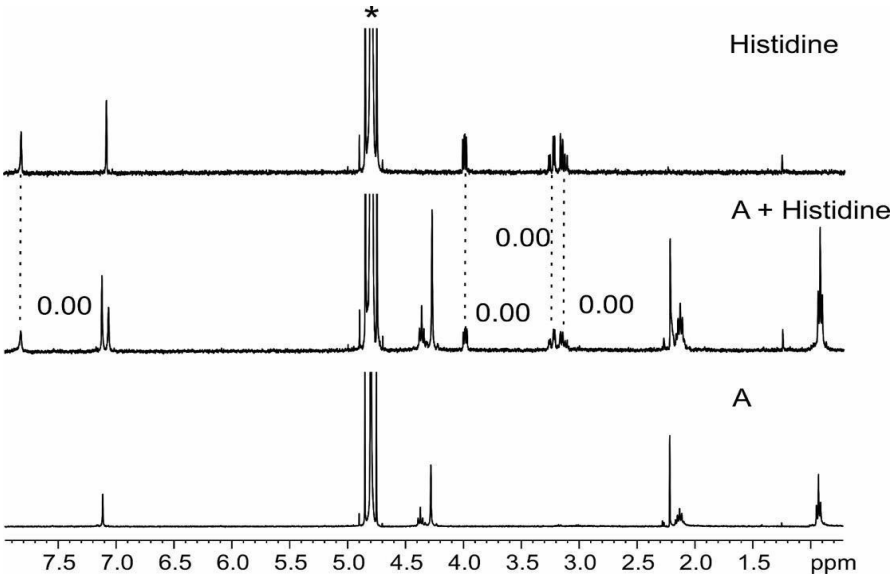

Appendix 4.8. ^{1}H NMR spectra (D_2O, 298 K) of (a) receptor A, equimolar mixtures of (b) histidine@A and (c) histidine. The dash lines give an indication of the signal changes in ppm. Asterisk is the residual NMR solvent.

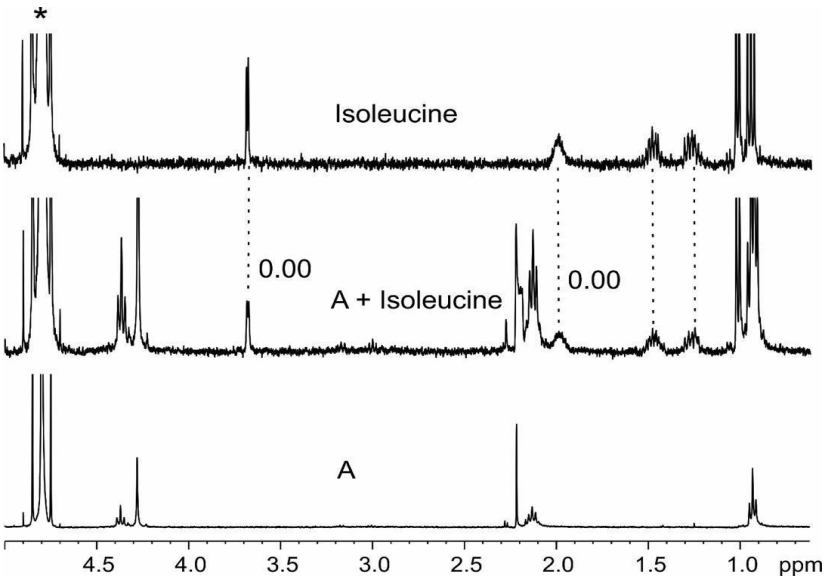

Appendix 4.9. ^{1}H NMR spectra (D_2O, 298 K) of (a) receptor A, equimolar mixtures of (b) isoleucine@A and (c) Isoleucine. The dash lines give an indication of the signal changes in ppm. Asterisk is the residual NMR solvent.

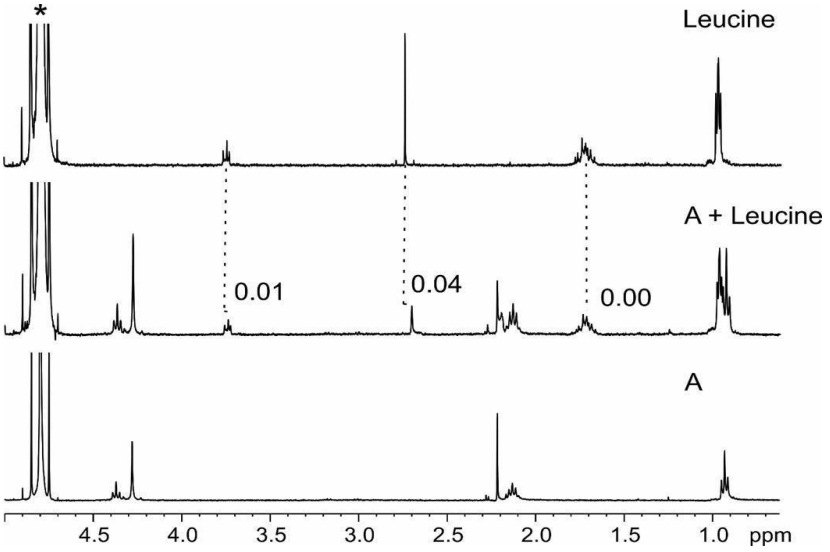

Appendix 4.10. ^{1}H NMR spectra (D_2O, 298 K) of (a) receptor A, equimolar mixtures of (b) leucine@A and (c) leucine. The dash lines give an indication of the signal changes in ppm. Asterisk is the residual NMR solvent.

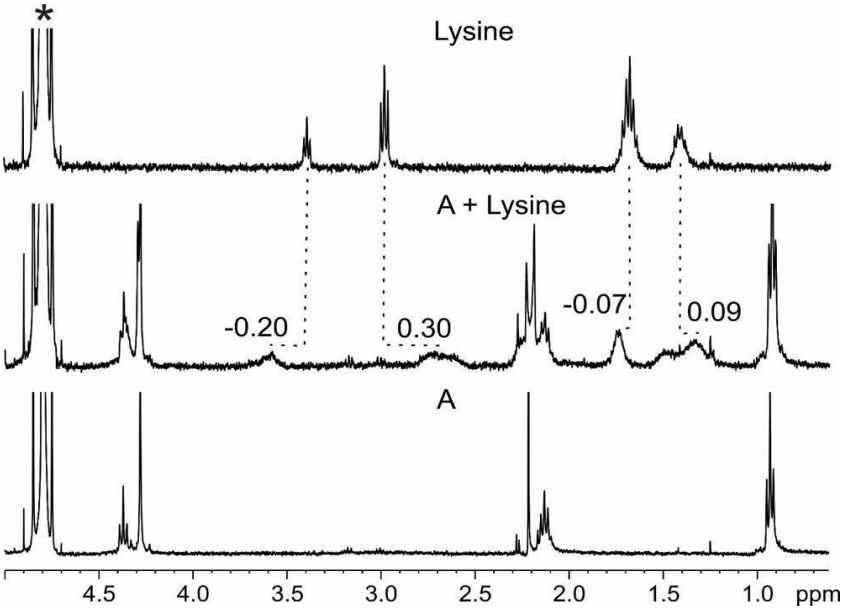

Appendix 4.11. ^{1}H NMR spectra (D_2O, 298 K) of (a) receptor A, equimolar mixtures of (b) lysine@A and (c) lysine. The dash lines give an indication of the signal changes in ppm. Asterisk is the residual NMR solvent.

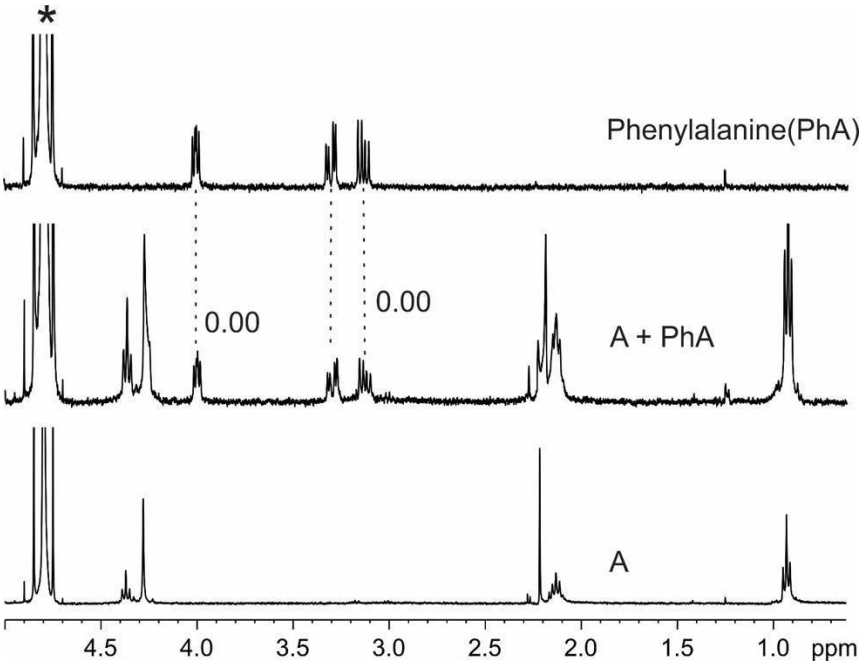

Appendix 4.12. ^{1}H NMR spectra (D_2O, 298 K) of (a) receptor A, equimolar mixtures of (b) phenylalanine@A and (c) phenylalanine. The dash lines give an indication of the signal changes in ppm. Asterisk is the residual NMR solvent.

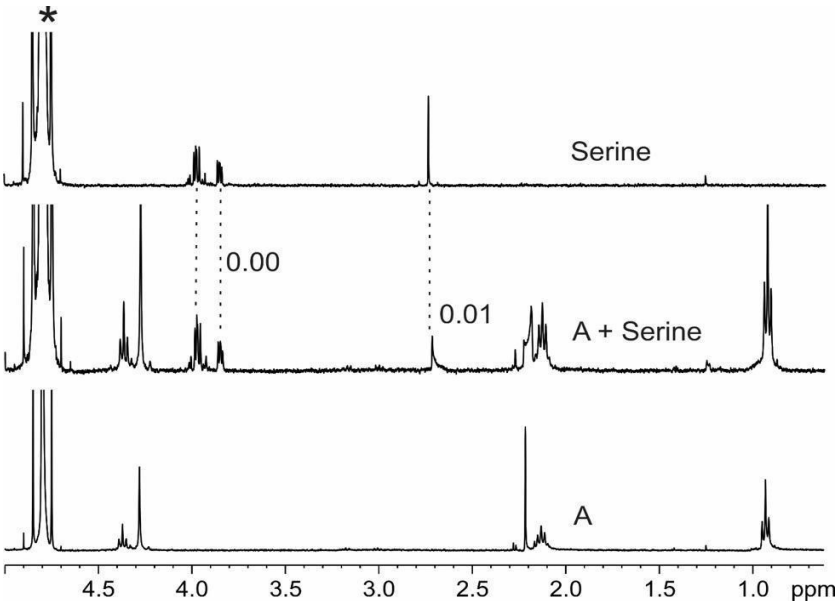

Appendix 4.13. ^{1}H NMR spectra (D_2O, 298 K) of (a) receptor A, equimolar mixtures of (b) serine@A and (c) serine. The dash lines give an indication of the signal changes in ppm. Asterisk is the residual NMR solvent.

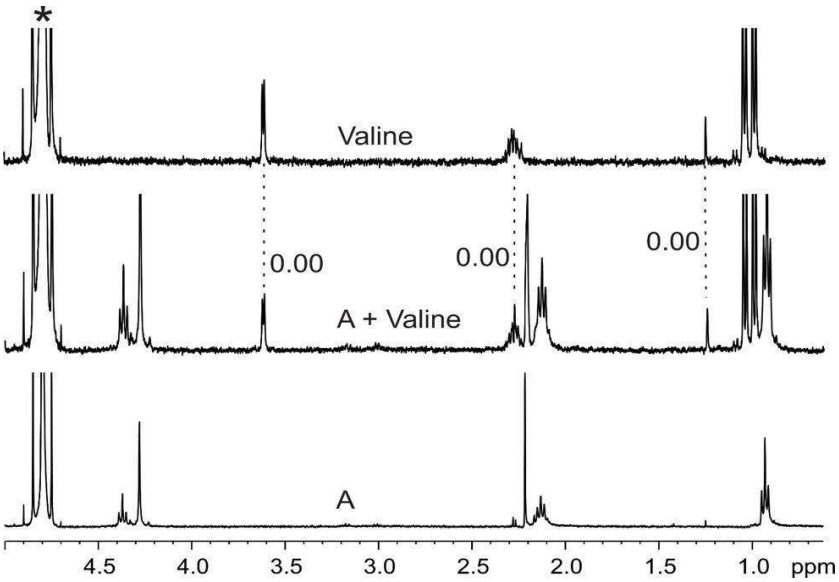

Appendix 4.14. ^{1}H NMR spectra (D_2O, 298 K) of (a) receptor A, equimolar mixtures of (b) valine@A and (c) valine. The dash lines give an indication of the signal changes in ppm. Asterisk is the residual NMR solvent.

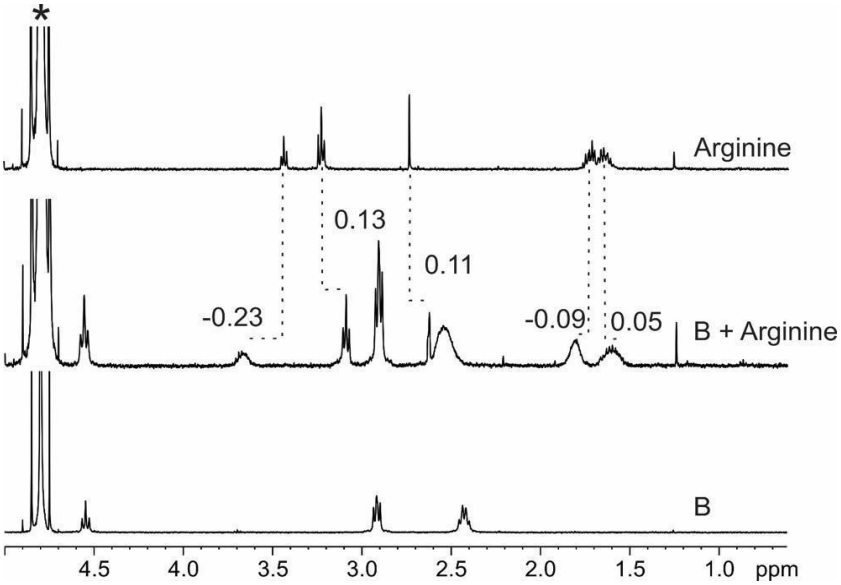

Appendix 4.15. ^{1}H NMR spectra (D_2O, 298 K) of (a) receptor B, equimolar mixtures of (b) arginine@B and (c) arginine. The dash lines give an indication of the signal changes in ppm. Asterisk is the residual NMR solvent.

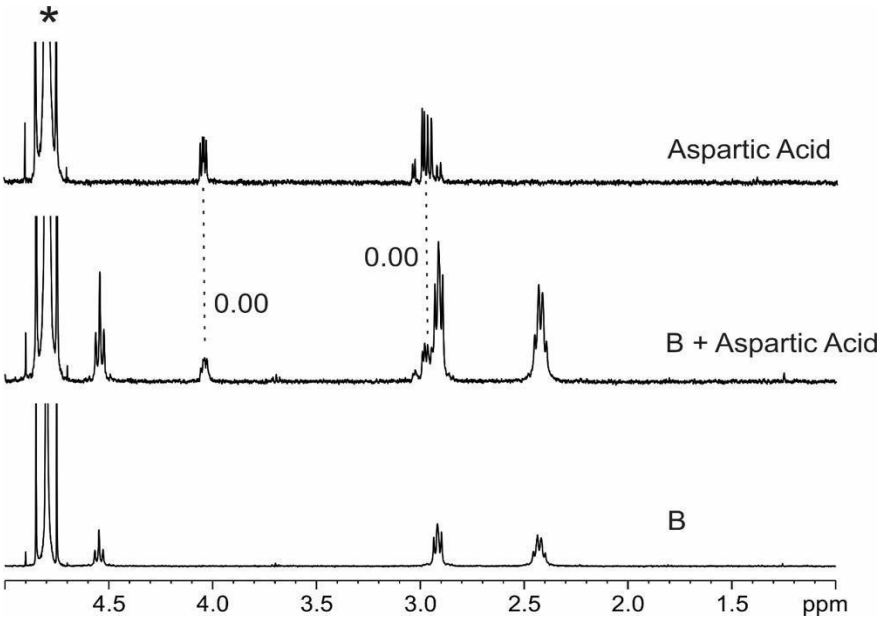

Appendix 4.16. ^{1}H NMR spectra (D_2O, 298 K) of (a) receptor B, equimolar mixtures of (b) aspartic acid@B and (c) aspartic acid. The dash lines give an indication of the signal changes in ppm. Asterisk is the residual NMR solvent.

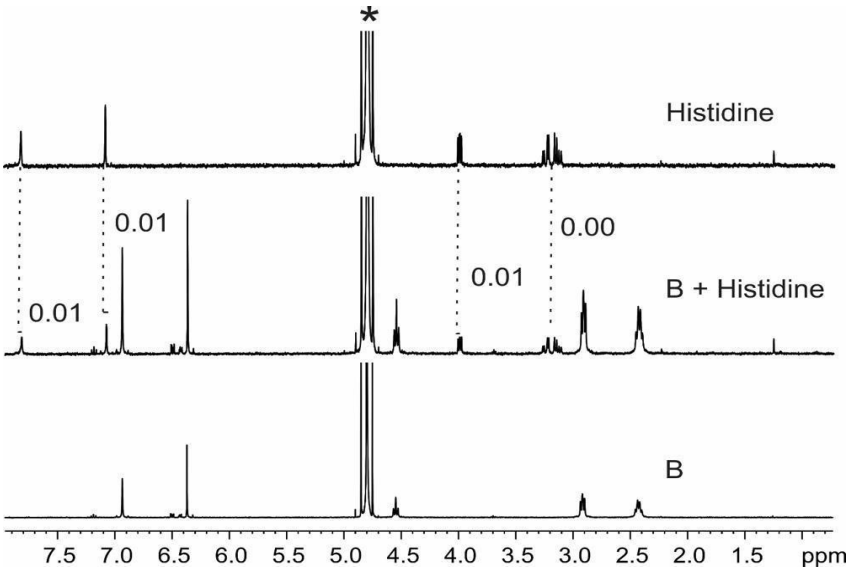

Appendix 4.17. ^{1}H NMR spectra (D_2O, 298 K) of (a) receptor B, equimolar mixtures of (b) histidine@B and (c) histidine. The dash lines give an indication of the signal changes in ppm. Asterisk is the residual NMR solvent.

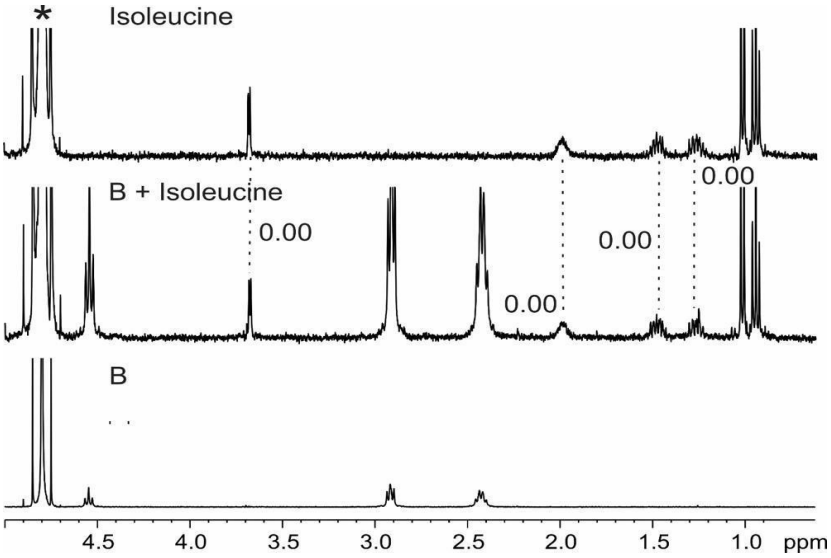

Appendix 4.18. ^{1}H NMR spectra (D_2O, 298 K) of (a) receptor B, equimolar mixtures of (b) isoleucine@B and (c) isoleucine. The dash lines give an indication of the signal changes in ppm. Asterisk is the residual NMR solvent.

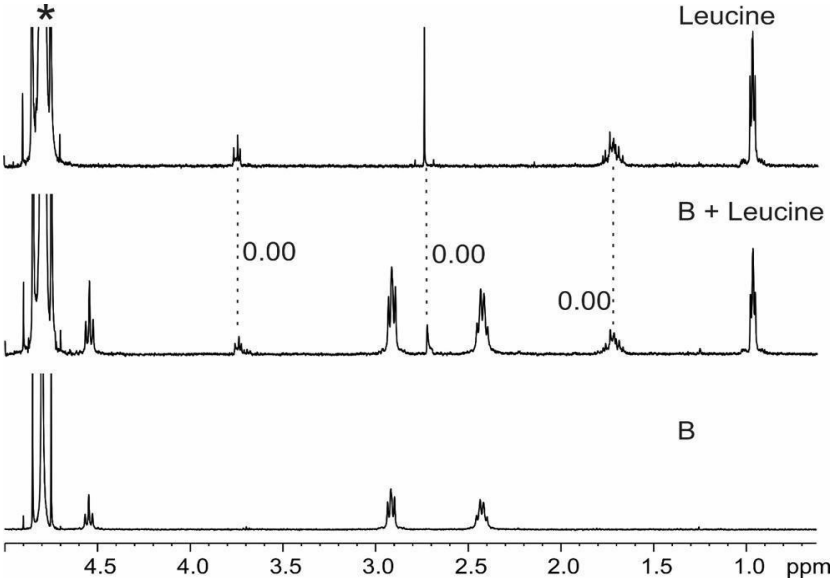

Appendix 4.19. ^{1}H NMR spectra (D_2O, 298 K) of (a) receptor B, equimolar mixtures of (b) leucine@B and (c) leucine. The dash lines give an indication of the signal changes in ppm. Asterisk is the residual NMR solvent.

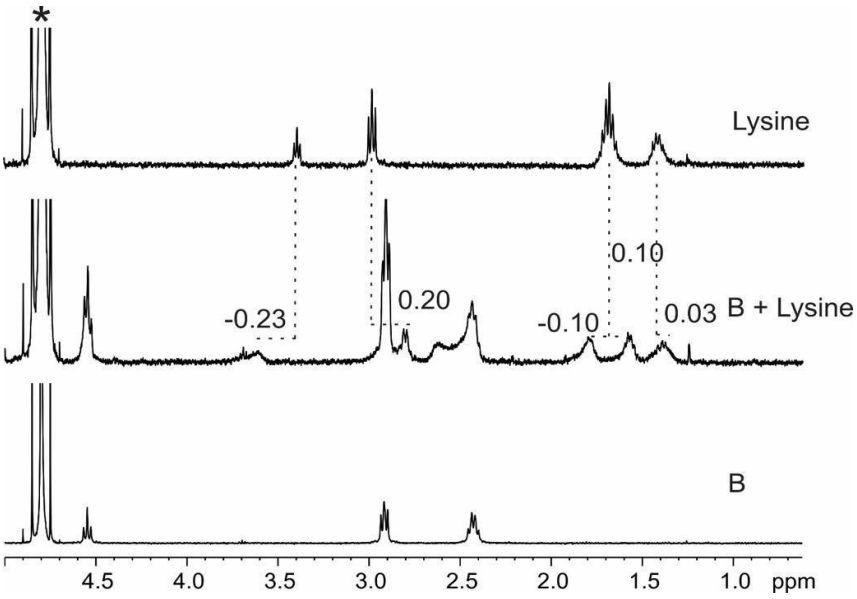

Appendix 4.20. ^{1}H NMR spectra (D_2O, 298 K) of (a) receptor B, equimolar mixtures of (b) lysine@B and (c) lysine. The dash lines give an indication of the signal changes in ppm. Asterisk is the residual NMR solvent.

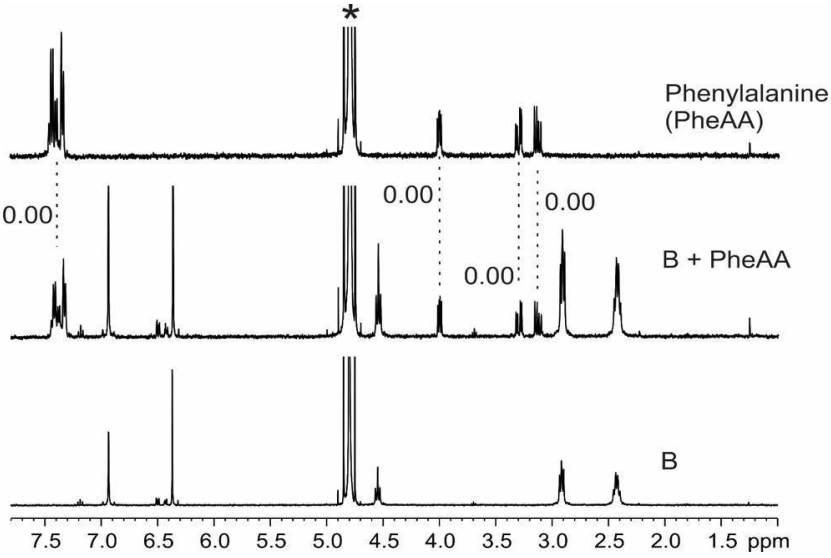

Appendix 4.21. ^{1}H NMR spectra (D_2O, 298 K) of (a) receptor B, equimolar mixtures of (b) phenylalanine@B and (c) phenylalanine. The dash lines give an indication of the signal changes in ppm. Asterisk is the residual NMR solvent.

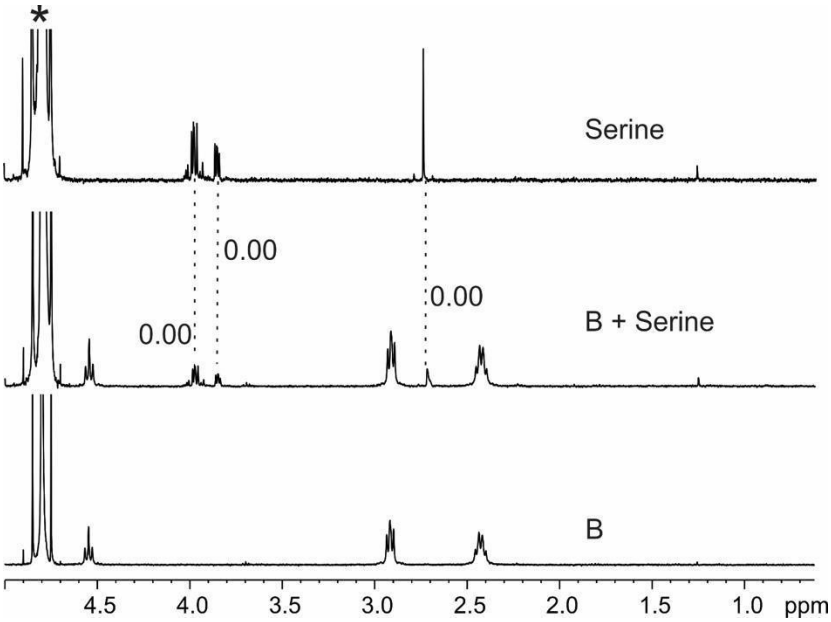

Appendix 4.22. ^{1}H NMR spectra (D_2O, 298 K) of (a) receptor B, equimolar mixtures of (b) serine@B and (c) serine. The dash lines give an indication of the signal changes in ppm. Asterisk is the residual NMR solvent.

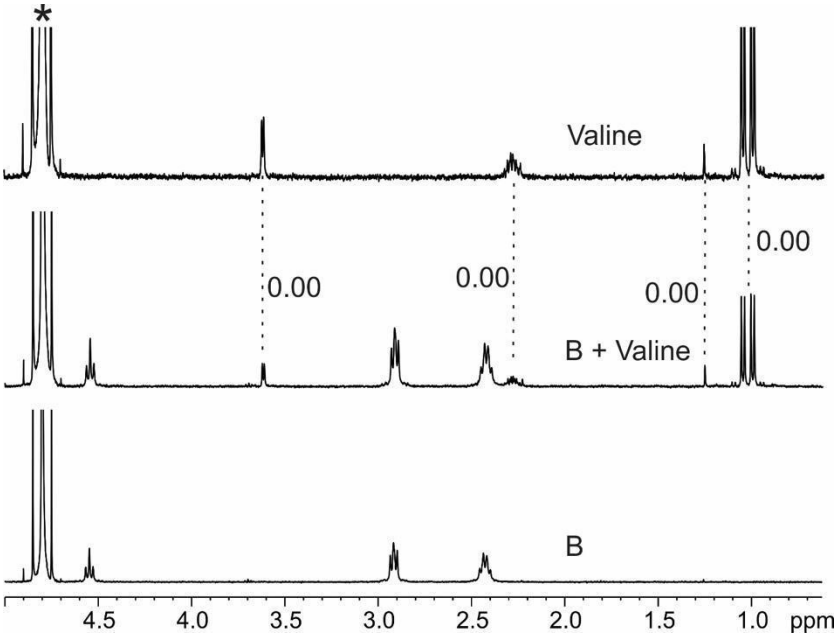

Appendix 4.23. ^{1}H NMR spectra (D_2O, 298 K) of (a) receptor B, equimolar mixtures of (b) valine@B and (c) valine. The dash lines give an indication of the signal changes in ppm. Asterisk is the residual NMR solvent.

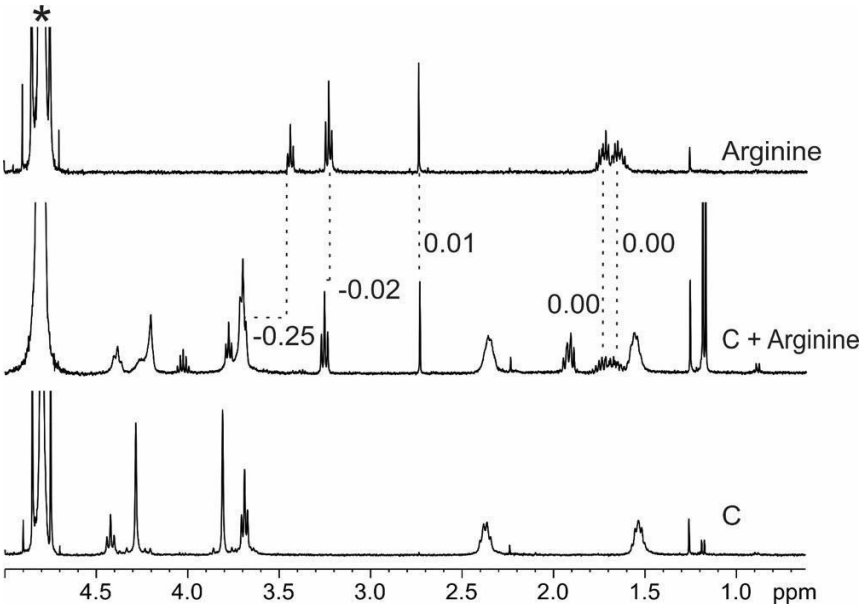

Appendix 4.24. ^{1}H NMR spectra (D_2O, 298 K) of (a) receptor C, equimolar mixtures of (b) arginine@C and (c) arginine. The dash lines give an indication of the signal changes in ppm. Asterisk is the residual NMR solvent.

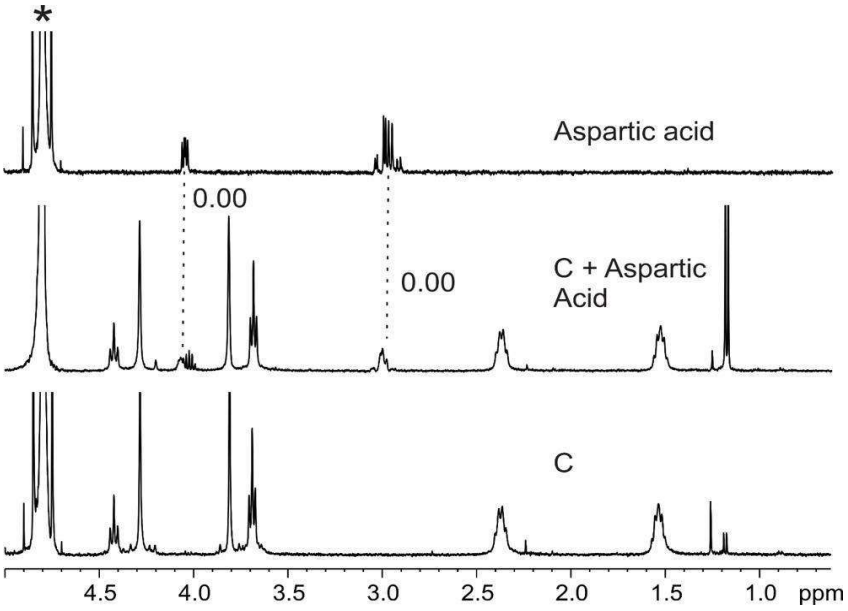

Appendix 4.25. ^{1}H NMR spectra (D_2O, 298 K) of (a) receptor C, equimolar mixtures of (b) aspartic acid@C and (c) aspartic acid. The dash lines give an indication of the signal changes in ppm. Asterisk is the residual NMR solvent.

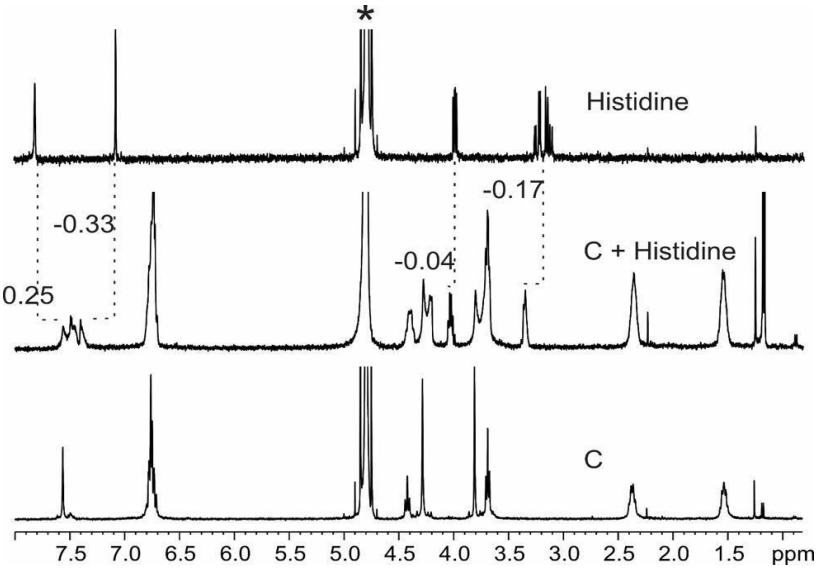

Appendix 4.26. ^{1}H NMR spectra (D_2O, 298 K) of (a) receptor C, equimolar mixtures of (b) histidine@C and (c) histidine. The dash lines give an indication of the signal changes in ppm. Asterisk is the residual NMR solvent.

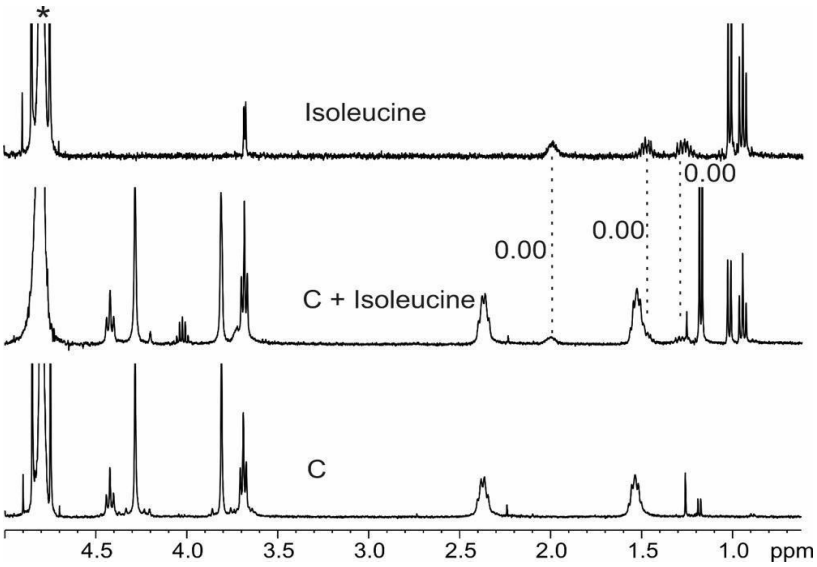

Appendix 4.27. ^{1}H NMR spectra (D_2O, 298 K) of (a) receptor C, equimolar mixtures of (b) isoleucine@C and (c) isoleucine. The dash lines give an indication of the signal changes in ppm. Asterisk is the residual NMR solvent.

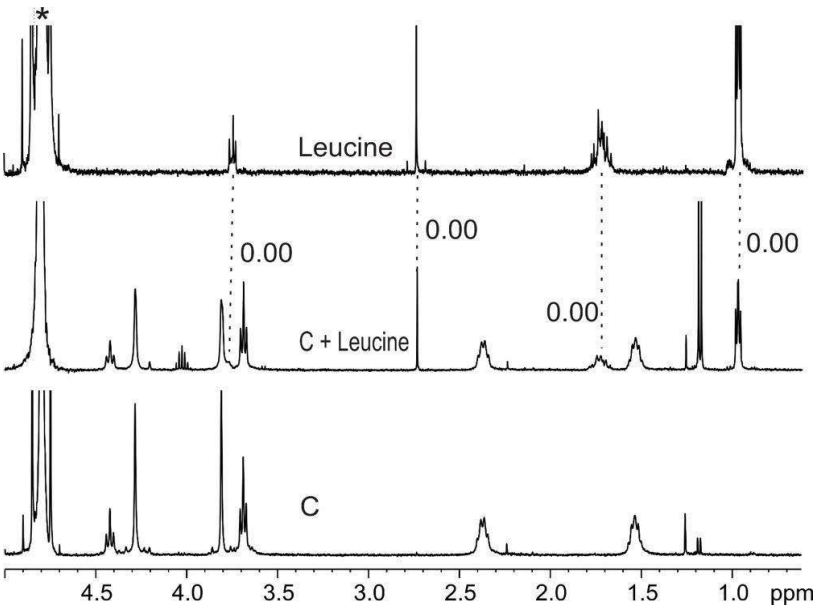

Appendix 4.28. ^{1}H NMR spectra (D_2O, 298 K) of (a) receptor C, equimolar mixtures of (b) leucine@C and (c) leucine. The dash lines give an indication of the signal changes in ppm. Asterisk is the residual NMR solvent.

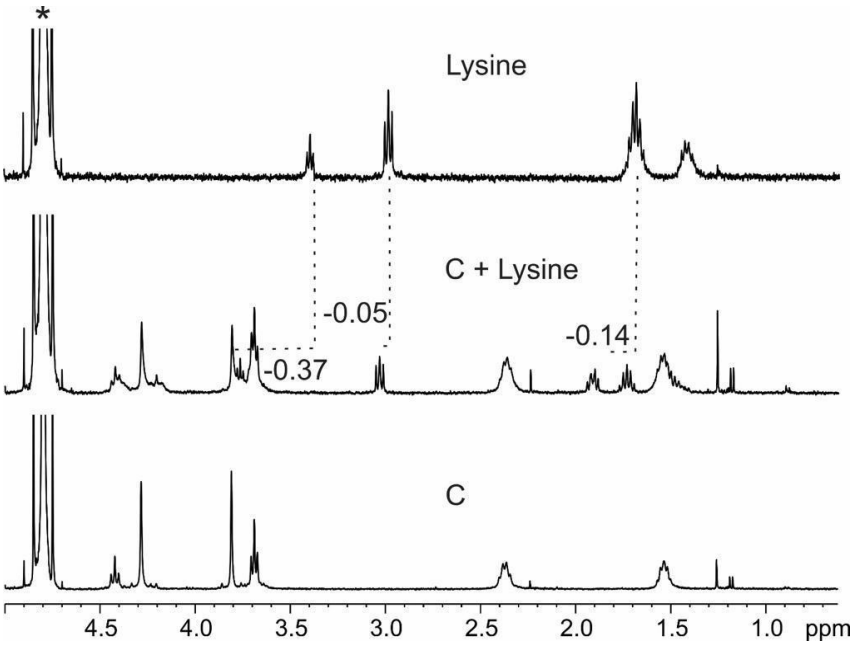

Appendix 4.29. ^{1}H NMR spectra (D_2O, 298 K) of (a) receptor C, equimolar mixtures of (b) lysine@C and (c) lysine. The dash lines give an indication of the signal changes in ppm. Asterisk is the residual NMR solvent.

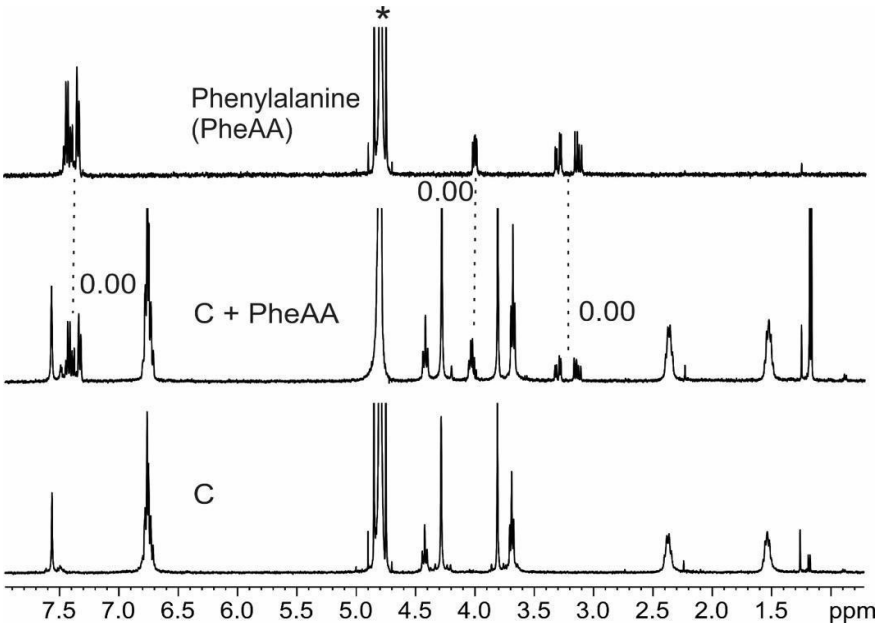

Appendix 4.30. ^{1}H NMR spectra (D_2O, 298 K) of (a) receptor C, equimolar mixtures of (b) phenylalanine@C and (c) phenylalanine. The dash lines give an indication of the signal changes in ppm. Asterisk is the residual NMR solvent.

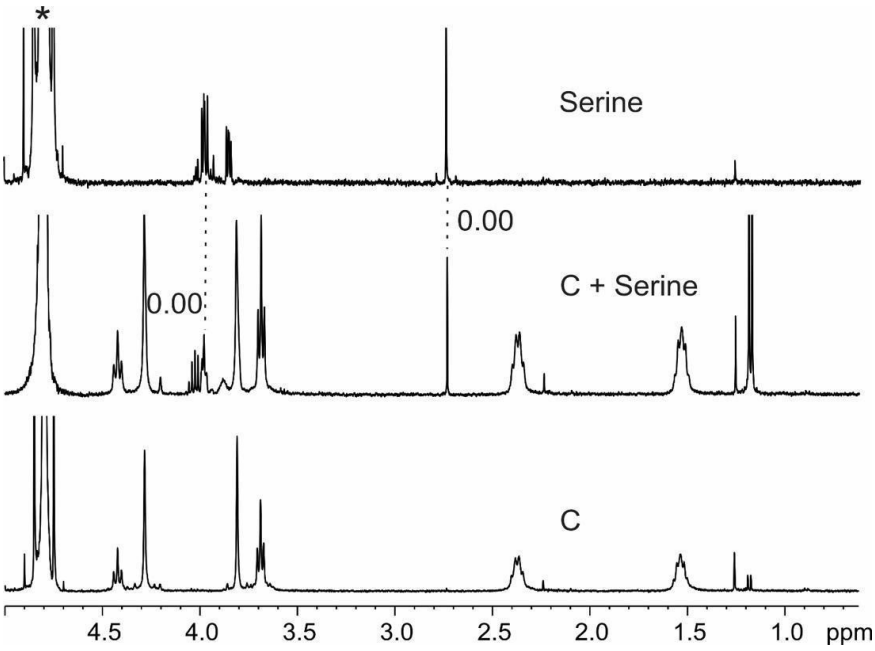

Appendix 4.31. ^{1}H NMR spectra (D_2O, 298 K) of (a) C, equimolar mixtures of (b) serine@C and (c) serine. The dash lines give an indication of the signal changes in ppm. Asterisk is the residual NMR solvent

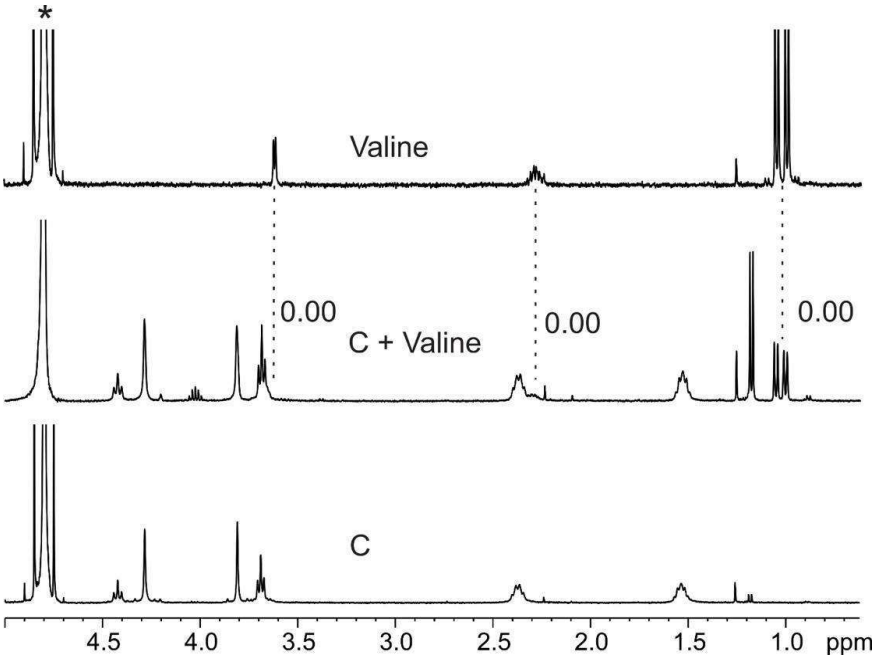

Appendix 4.32. ^{1}H NMR spectra (D_2O, 298 K) of (a) receptor C, equimolar mixtures of (b) valine@C and (c) valine. The dash lines give an indication of the signal changes in ppm. Asterisk is the residual NMR solvent.

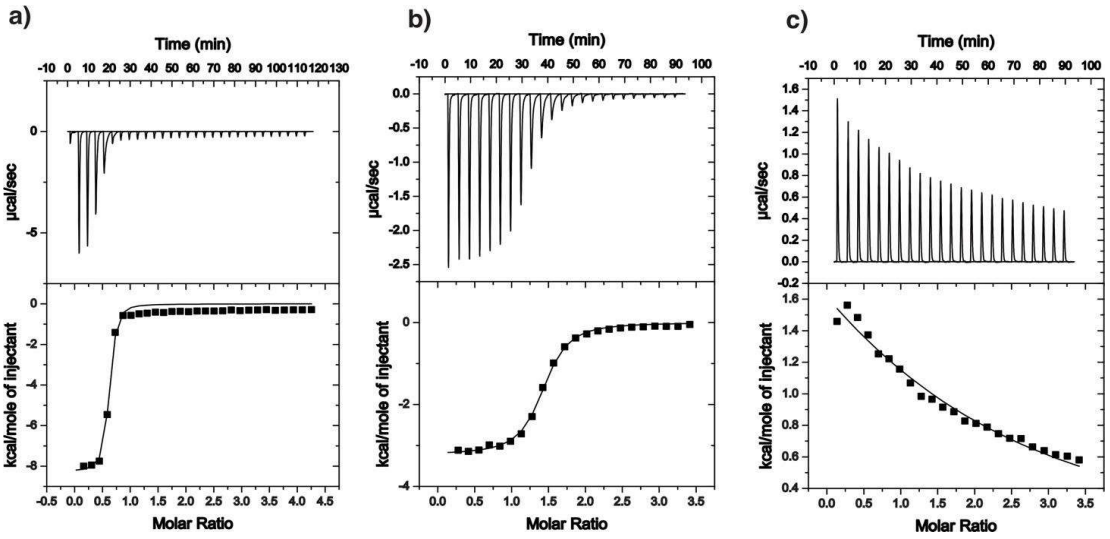

Appendix 4.33. ITC traces of the titration of crystallin peptide with receptors A, B and C (a, b and c respectively) at 298 K in water. All the data were fitted to a one-site binding model.

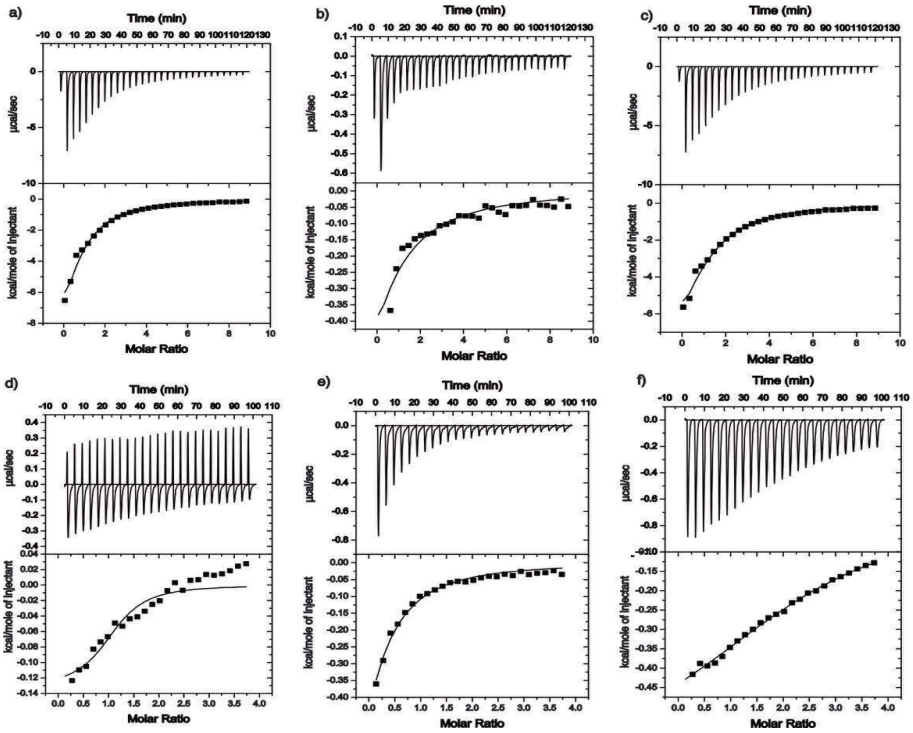

Appendix 4.34. ITC traces of the titration of receptor A with amino acids at 298 K. The data was fitted to a one-site binding model for (a) arginine@A, (b) histidine@A, and (c) lysine@A in water. (d) arginine@A, (e) histidine@A, and lysine@A were in 10mM tris buffer at pH 7.4.

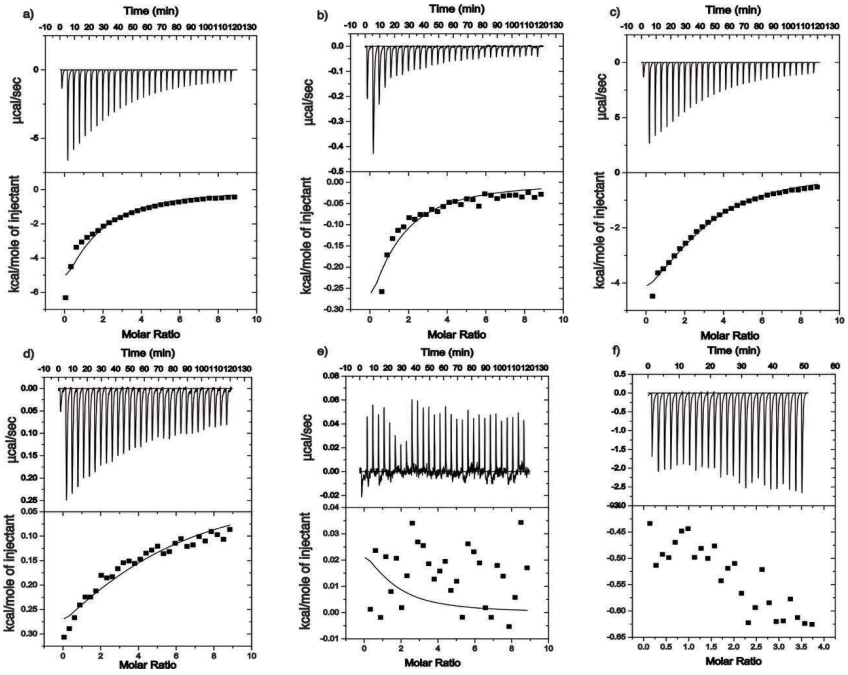

Appendix 4.35. ITC traces of the titration of receptor B with amino acids at 298 K. The data was fitted to a one site binding model for (a) arginine@B, (b) histidine@B and (c) lysine@B in water. (d) arginine@B, (e) histidine@B and lysine@B were in 10mM tris buffer at pH 7.4.

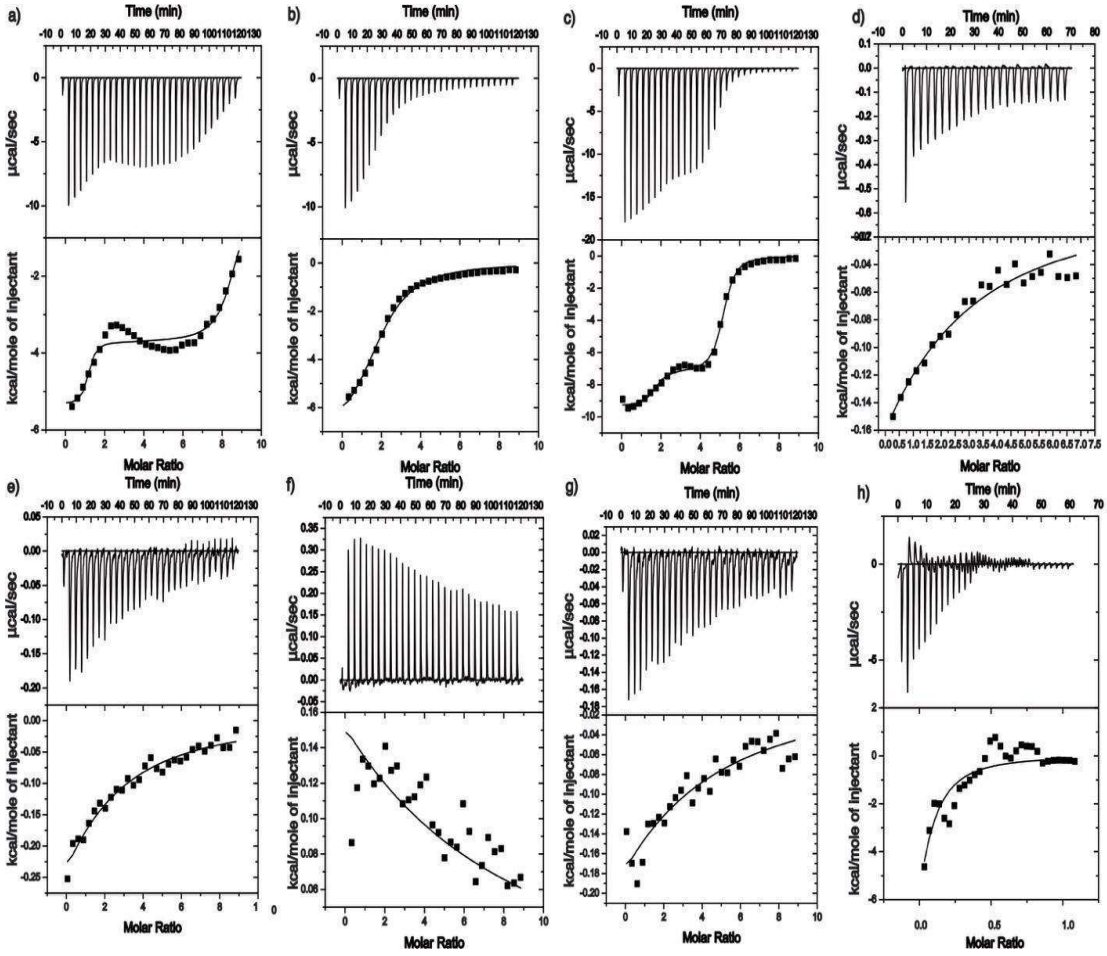

Appendix 4.36. ITC traces of the titration of receptor C with amino acids at 298 K. The data was fitted to a one site binding model for (a) arginine@C, (b) histidine@C and (c) lysine@C in water. (d) arginine@C, (e) histidine@C and lysine@C were in 10mM tris buffer at pH 7.4

Appendix 4.37 Interaction parameters between receptors **A**, **B** and **C** and selected amino acids in Tris buffer. All the data shown were fitted to one set of sites binding model at 298K.

Complex	K_1 $(\times 10^3)\ M^{-1}$	ΔH_1 kcal/mol	$T\Delta S_1$ kcal/mol	ΔG_1 kcal/mol
A•				
Arginine	7.27±1.28	-15.70±3.85	-10.43	-5.27
Lysine	5.89± 0.88	-12.07±2.04	-6.45	-5.62
Histidine	2.94±0.39	-2.59±0.16	6.91	-9.50
B•				
Arginine	1.42±0.73	-0.60±0.26	3.70	-4.30
Lysine	-	-	-	-
Histidine	-	-	-	-
C•				
Arginine	1.66±0.13	-1.07±0.05	3.31	-4.38
Lysine	0.78±0.12	-1.40±0.14	2.55	-3.95
Histidine	-	-	-	-
Aspartic Acid	-	-	-	-

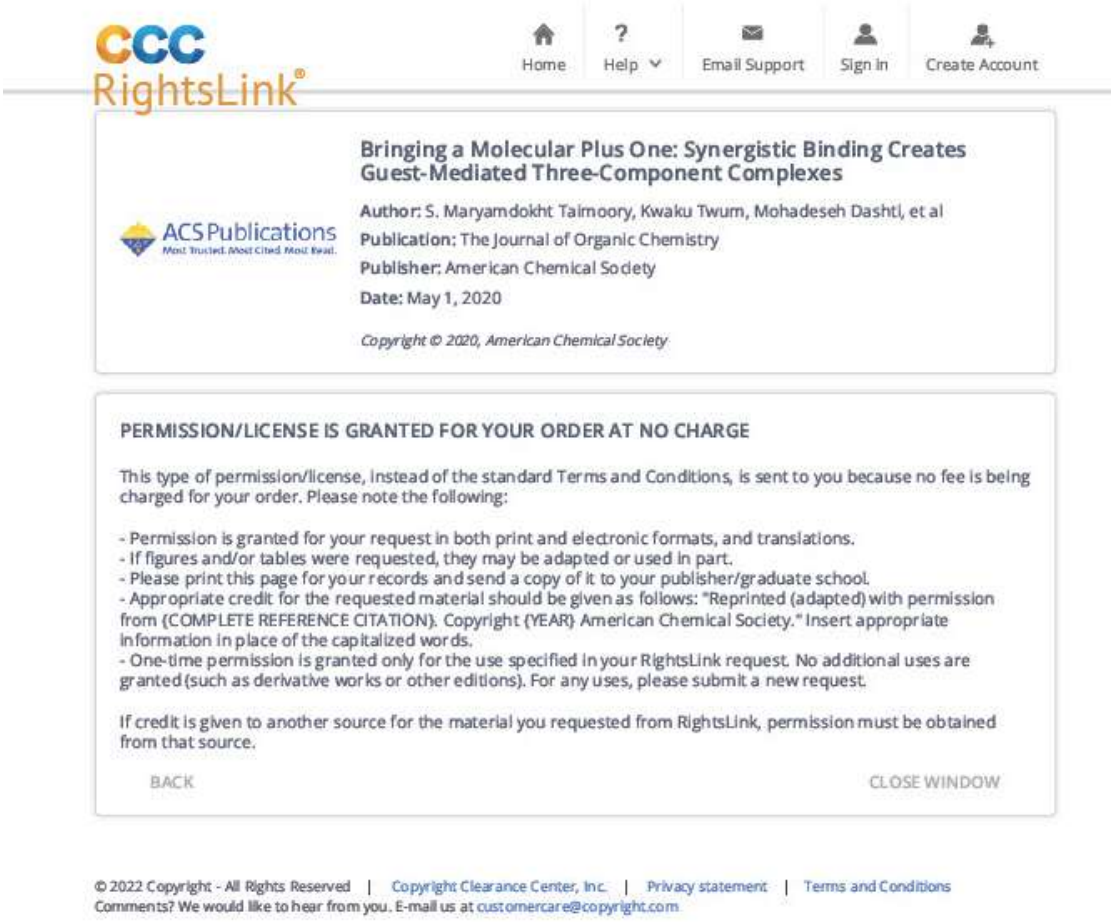

Appendix 5: Screenshot of copyright permission for publication 4.

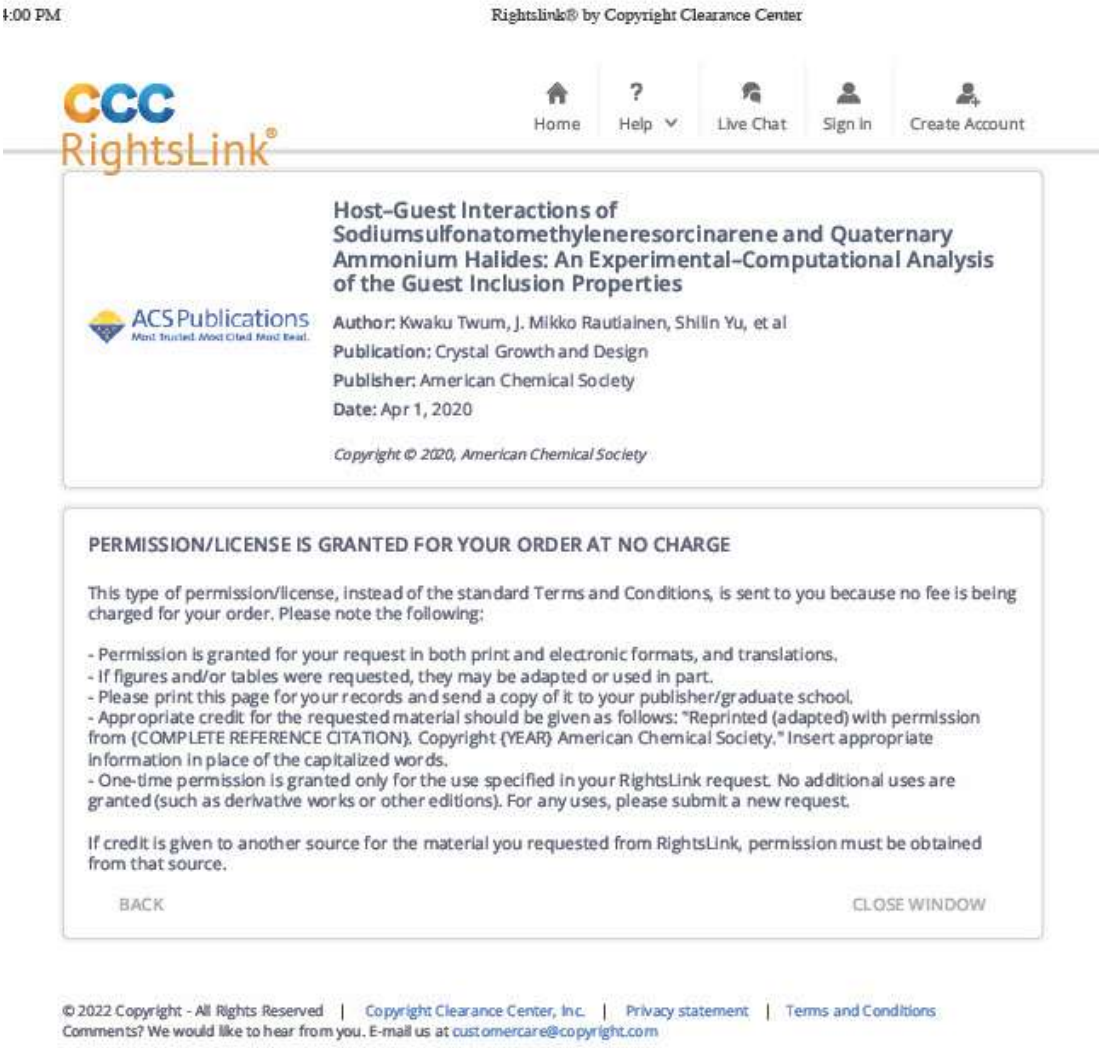

Appendix 6: Screenshot of copyright permission for publication 3.

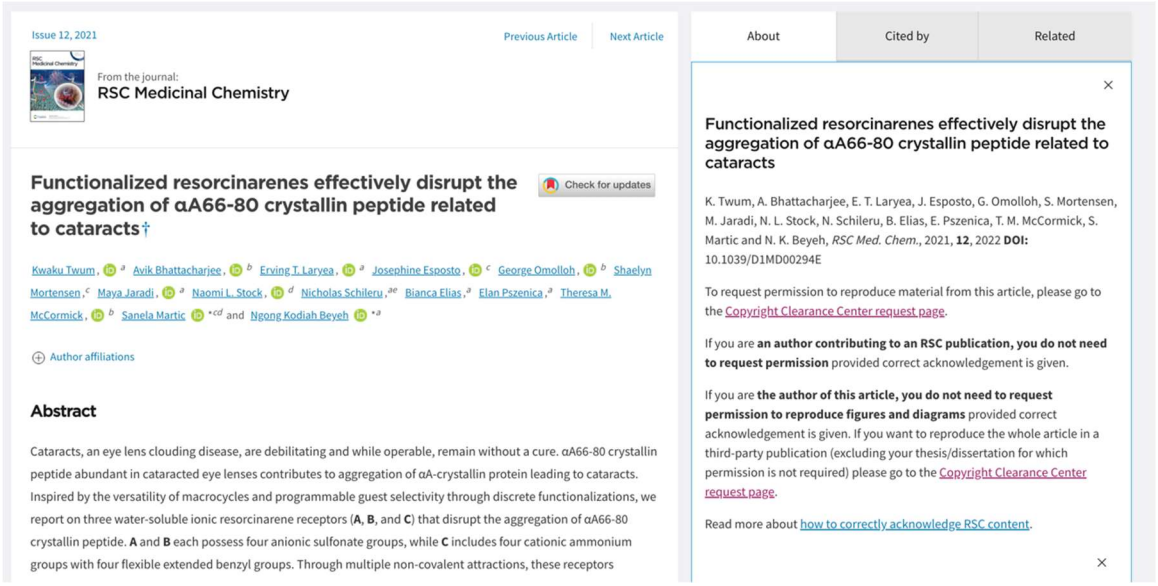

Appendix 8: Screenshot of copyright permission for publication 2.

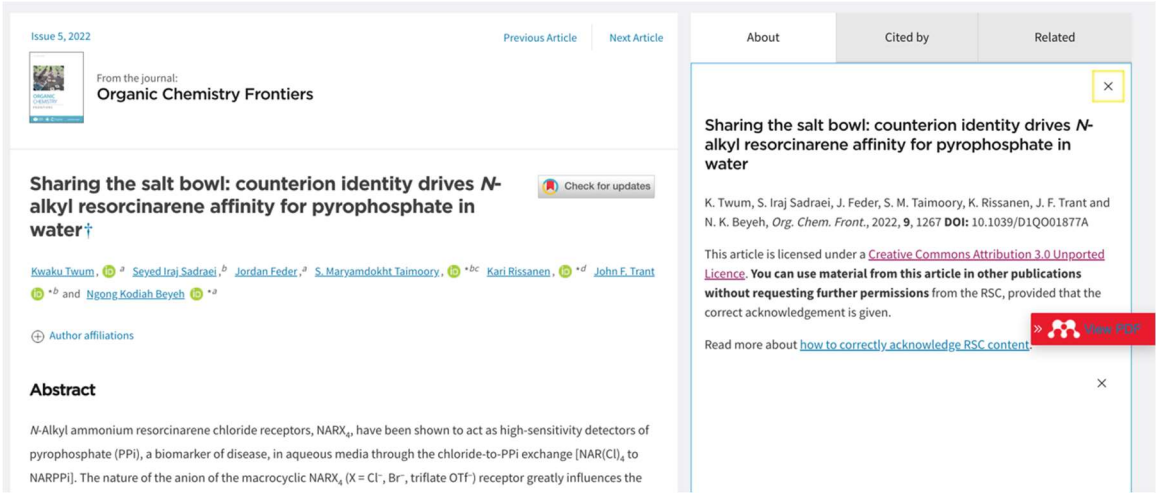

Appendix 7: Screenshot of copyright permission for publication 1.

REFERENCES

(1) Lehn, J. M. Supramolecular Chemistry. *Science (1979)* **1993**, *260* (5115), 1762–1763.

(2) Stupp, S. I.; Palmer, L. C. Supramolecular Chemistry and Self-Assembly in Organic Materials Design. *Chemistry of Materials* **2014**, *26* (1), 507–518.

(3) Chambers, J. P.; Arulanandam, B. P.; Matta, L. L.; Weis, A.; Valdes, J. J. Biosensor Recognition Elements. *Current Issues in Molecular Biology*. 2008, pp 1–12.

(4) Li, Z. T.; Hou, J. L.; Li, C.; Yi, H. P. Shape-Persistent Aromatic Amide Oligomers: New Tools for Supramolecular Chemistry. *Chem Asian J* **2006**, *1* (6), 766–778.

(5) Hasell, T.; Wu, X.; Jones, J. T. A.; Bacsa, J.; Steiner, A.; Mitra, T.; Trewin, A.; Adams, D. J.; Cooper, A. I. Triply Interlocked Covalent Organic Cages. *Nat Chem* **2010**, *2* (9), 750–755.

(6) Nagendrappa, G. Hermann Emil Fischer: Life and Achievements. *Resonance 2011 16:7* **2011**, *16* (7), 606–618.

(7) Latimer, W. M.; Rodebush, W. H. Polarity and Ionization from the Standpoint of the Lewis Theory of Valence. *J Am Chem Soc* **1920**, *42* (7), 1419–1433.

(8) Valastyan, J. S.; Lindquist, S. Mechanisms of Protein-Folding Diseases at a Glance. *DMM Disease Models and Mechanisms* **2014**, *7* (1), 9–14.

(9) Rt S M Vlli Ken, R. E.; Mulliken, R. S. Structures of Complexes Formed by Halogen Molecules with Aromatic and with Oxygenated Solvents. *J Am Chem Soc* **1950**, *72* (1), 600–608.

(10) Hassel, O. Structural Aspects of Interatomic Charge-Transfer Bonding. *Science (1979)* **1970**, *170* (3957), 497–502.

(11) Pedersen, C. J. The Discovery of Crown Ethers. *Science (1979)* **1988**, *241* (4865), 536–540.

(12) Izatt, R. M. Charles J. Pedersen: Innovator in Macrocyclic Chemistry and Co-Recipient of the 1987 Nobel Prize in Chemistry. *Chem Soc Rev* **2007**, *36* (2), 143–147.

(13) Kida, M.; Kubo, M.; Ujihira, T.; Ebata, T.; Abe, M.; Inokuchi, Y. Selective Probing of Potassium Ion in Solution by Intramolecular Excimer Fluorescence of Dibenzo-Crown Ethers. *ChemPhysChem* **2018**, *19* (11), 1331–1335.

(14) Gómez-López, M.; Preece, J. A.; Stoddart, J. F. The Art and Science of Self-Assembling Molecular Machines. *Nanotechnology* **1996**, *7* (3), 183.

(15) Ikkala, O.; ten Brinke, G. Functional Materials Based on Self-Assembly of Polymeric Supramolecules. *Science (1979)* **2002**, *295* (5564), 2407–2409.

(16) Vickers, M. S.; Beer, P. D. Anion Templated Assembly of Mechanically Interlocked Structures. *Chem Soc Rev* **2007**, *36* (2), 211–225.

(17) Lehn, J. M. Supramolecular Chemistry: From Molecular Information towards Self-Organization and Complex Matter*. *Reports on Progress in Physics* **2004**, *67* (3), 249.

(18) Cheong, W. J.; Yang, S. H.; Ali, F. Molecular Imprinted Polymers for Separation Science: A Review of Reviews. *J Sep Sci* **2013**, *36* (3), 609–628.

(19) Kolesnichenko, I. v.; Anslyn, E. v. Practical Applications of Supramolecular Chemistry. *Chem Soc Rev* **2017**, *46* (9), 2385–2390.

(20) Lehn, J. M. Supramolecular Chemistry: Receptors, Catalysts, and Carriers. *Science (1979)* **1985**, *227* (4689), 849–856.

(21) Xue, M.; Yang, Y.; Chi, X.; Zhang, Z.; Huang, F. Pillararenes, a New Class of Macrocycles for Supramolecular Chemistry. *Acc Chem Res* **2012**, *45* (8), 1294–1308.

(22) Curtis, N. F. The Advent of Macrocyclic Chemistry. **2012**, *24* (7), 439–447.

(23) Diederich, F.; Stang, P. J.; Tykwinski, R. R. (Rik R.). Modern Supramolecular Chemistry : Strategies for Macrocycle Synthesis. **2008**, 400.

(24) Mortensen, K. T.; Osberger, T. J.; King, T. A.; Sore, H. F.; Spring, D. R. Strategies for the Diversity-Oriented Synthesis of Macrocycles. *Chem Rev* **2019**, *119* (17), 10288–10317.

(25) Pedersen, C. J. The Discovery of Crown Ethers (Noble Lecture). *Angewandte Chemie International Edition in English* **1988**, *27* (8), 1021–1027.

(26) Flink, S.; van Veggel, F. C. J. M.; Reinhoudt, D. N. Recognition of Cations by Self-Assembled Monolayers of Crown Ethers. *Journal of Physical Chemistry B* **1999**, *103* (31), 6515–6520.

(27) Krakowiak, K. E.; Bradshaw, J. S.; Zamecka-Krakowiak, D. J. Synthesis of Aza-Crown Ethers. *Chem Rev* **1989**, *89* (4), 929–972.

(28) Siswanta, D.; Nagatsuka, K.; Yamada, H.; Kumakura, K.; Hisamoto, H.; Shichi, Y.; Toshima, K.; Suzuki, K. Structural Ion Selectivity of Thia Crown Ether Compounds with a Bulky Block Subunit and Their Application as an Ion-Sensing Component for an Ion-Selective Electrode. *Anal Chem* **1996**, *68* (23), 4166–4172.

(29) Gokel, G. W.; Leevy, W. M.; Weber, M. E. Crown Ethers: Sensors for Ions and Molecular Scaffolds for Materials and Biological Models. *Chem Rev* **2004**, *104* (5), 2723–2750.

(30) Saaid, M.; Saad, B.; Rahman, I. A.; Ali, A. S. M.; Saleh, M. I. Extraction of Biogenic Amines Using Sorbent Materials Containing Immobilized Crown Ethers. *Talanta* **2010**, *80* (3), 1183–1190.

(31) Smirnova, S. v.; Torocheshnikova, I. I.; Formanovsky, A. A.; Pletnev, I. v. Solvent Extraction of Amino Acids into a Room Temperature Ionic Liquid with Dicyclohexano-18-Crown-6. *Anal Bioanal Chem* **2004**, *378* (5), 1369–1375.

(32) Tang, W.; Ong, T. T.; Ng, S. C. Chiral Separation of Dansyl Amimo Acids in Capillary Electrophoresis Using Mono-(3-Methyl-Imidazolium)-β Cyclodextrin Chloride as Selector. *J Sep Sci* **2007**, *30* (9), 1343–1349.

(33) Durst, H. D.; Milano, M.; Kikta, E. J.; Connelly, S. A.; Grushka, E. Phenacyl Esters of Fatty Acids Via Crown Ether Catalysts for Enhanced Ultraviolet Detection in Liquid Chromatography. *Anal Chem* **1975**, *47* (11), 1797–1801.

(34) Yu, H. R.; Hu, J. Q.; Lu, X. H.; Ju, X. J.; Liu, Z.; Xie, R.; Wang, W.; Chu, L. Y. Insights into the Effects of 2:1 "Sandwich-Type" Crown-Ether/Metal-Ion Complexes in Responsive Host - Guest Systems. *Journal of Physical Chemistry B* **2015**, *119* (4), 1696–1705.

(35) Bereczki, R.; Gyurcsányi, R. E.; Ágai, B.; Tóth, K. Synthesis and Characterization of Covalently Immobilized Bis-Crown Ether Based Potassium Ionophore. *Analyst* **2005**, *130* (1), 63–70.

(36) Şahin Gül, D.; Ogutcu, H.; Hayvalı, Z. Investigation of Photophysical Behaviours and Antimicrobial Activity of Novel Benzo-15-Crown-5 Substituted Coumarin and Chromone Derivatives. *J Mol Struct* **2020**, *1204*, 127569.

(37) Zhang, X. X.; Izatt, R. M.; Bradshaw, J. S.; Krakowiak, K. E. Approaches to Improvement of Metal Ion Selectivity by Cryptands. *Coord Chem Rev* **1998**, *174* (1), 179–189.

(38) Hossain, Md. A.; Saeed, M. A. Binding and Selectivity of Halides with Macrocyclic Polyamines. *J Miss Acad Sci* **2009**, *54* (3–4), 230.

(39) Landini, D.; Maia, A.; Montanari, F.; Tundo, P. Lipophilic [2.2.2] Cryptands as Phase-Transfer Catalysts. Activation and Nucleophilicity of Anions in Aqueous-Organic Two-Phase Systems and in Organic Solvents of Low Polarity. *J Am Chem Soc* **1979**, *101* (10), 2526–2530.

(40) Takeda, Y. The Solvent Extraction of Metal Ions by Crown Compounds. **1984**, 1–38.

(41) Murray-Rust, P.; Biirgi, H. B.; Dunitz, J. D.; Crystallogr, A. Calixarenes. *Acc Chem Res* **1983**, *16* (5), 161–170.

(42) Timmerman, P.; Verboom, W.; Reinhoudt, D. N. Resorcinarenes. *Tetrahedron* **1996**, *52* (8), 2663–2704.

(43) Sliwa, W.; Kozlowski, C. *Calixarenes and Resorcinarenes: Synthesis, Properties and Applications*; 2009.

(44) Kurkov, S. v.; Loftsson, T. Cyclodextrins. *Int J Pharm* **2013**, *453* (1), 167–180.

(45) Brewster, M. E.; Loftsson, T. Cyclodextrins as Pharmaceutical Solubilizers. *Advanced Drug Delivery Reviews*. 2007, pp 645–666.

(46) Jansook, P.; Kurkov, S. v.; Loftsson, T. Cyclodextrins as Solubilizers: Formation of Complex Aggregates. *J Pharm Sci* **2010**, *99* (2), 719–729.

(47) Carrier, R. L.; Miller, L. A.; Ahmed, I. The Utility of Cyclodextrins for Enhancing Oral Bioavailability. *Journal of Controlled Release*. 2007, pp 78–99.

(48) Stoddart, J. F. Cyclodextrins, Off-the-Shelf Components for the Construction of Mechanically Interlocked Molecular Systems. *Angewandte Chemie International Edition in English* **1992**, *31* (7), 846–848.

(49) Hapiot, F.; Tilloy, S.; Monflier, E. Cyclodextrins as Supramolecular Hosts for Organometallic Complexes. *Chem Rev* **2006**, *106* (3), 767–781.

(50) Smolková-Keulemansová, E. Cyclodextrins as Stationary Phases in Chromatography. *J Chromatogr A* **1982**, *251* (1), 17–34.

(51) del Valle, E. M. M. Cyclodextrins and Their Uses: A Review. *Process Biochemistry* **2004**, *39* (9), 1033–1046.

(52) Song, N.; Yang, Y. W. Applications of Pillarenes, an Emerging Class of Synthetic Macrocycles. *Science China Chemistry 2014 57:9* **2014**, *57* (9), 1185–1198.

(53) Tao, H.; Cao, D.; Liu, L.; Kou, Y.; Wang, L.; Meier, H. Synthesis and Host-Guest Properties of Pillar[6]Arenes. *Science China Chemistry 2011 55:2* **2011**, *55* (2), 223–228.

(54) Cao, D.; Meier, H. Synthesis of Pillar[6]Arenes and Their Host-Guest Complexes. *Synthesis (Germany)* **2015**, *47* (8), 1041–1056.

(55) Ogoshi, T.; Ueshima, N.; Sakakibara, F.; Yamagishi, T. A.; Haino, T. Conversion from Pillar[5]Arene to Pillar[6-15]Arenes by Ring Expansion and Encapsulation of C60 by Pillar[n]Arenes with Nanosize Cavities. *Org Lett* **2014**, *16* (11), 2896–2899.

(56) Li, Q.; Zhu, H.; Huang, F. Pillararene-Based Supramolecular Functional Materials. *Trends Chem* **2020**, *2* (9), 850–864.

(57) Freeman, W. A.; Mock, W. L.; Shih, N. Y. Cucurbituril. *J Am Chem Soc* **1981**, *103* (24), 7367–7368.

(58) Burnett, C. A.; Witt, D.; Fettinger, J. C.; Isaacs, L. Acyclic Congener of Cucurbituril: Synthesis and Recognition Properties. *Journal of Organic Chemistry* **2003**, *68* (16), 6184–6191.

(59) Assaf, K. I.; Nau, W. M. Cucurbiturils: From Synthesis to High-Affinity Binding and Catalysis. *Chem Soc Rev* **2014**, *44* (2), 394–418.

(60) Kim, K.; Selvapalam, N.; Ho Ko, Y.; Min Park, K.; Kim, D.; Kim, J. Functionalized Cucurbiturils and Their Applications. *Chem Soc Rev* **2007**, *36* (2), 267–279.

(61) Biesaga, M.; Pyrzyńska, K.; Trojanowicz, M. Porphyrins in Analytical Chemistry. A Review. *Talanta* **2000**, *51* (2), 209–224.

(62) Bonkovsky, H. L.; Guo, J. T.; Hou, W.; Li, T.; Narang, T.; Thapar, M. Porphyrin and Heme Metabolism and the Porphyrias. *Compr Physiol* **2013**, *3* (1), 365–401.

(63) Mauzerall, D. Porphyrins, Chlorophyll, and Photosynthesis. *Photosynthesis I,* **1977**, 117–124.

(64) Huang, H.; Song, W.; Rieffel, J.; Emerging Applications of Porphyrins in Photomedicine, *Frontiers in physics*, **2015**, 3, 23

(65) Beyeh, N. K.; Kogej, M.; Åhman, A.; Rissanen, K.; Schalley, C. A. Flying Capsules: Mass Spectrometric Detection of Pyrogallarene and Resorcinarene Hexamers. *Angewandte Chemie - International Edition* **2006**, *45* (31), 5214–5218.

(66) Winkler, H. D. F.; Dzyuba, E. v.; Sklorz, J. A. W.; Beyeh, K.; Rissanenb, K.; Schalley, C. A. Gas-Phase H/D-Exchange Reactions on Resorcinarene and Pyrogallarene Capsules: Proton Transport through a One-Dimensional Grotthuss Mechanism. *Chem Sci* **2011**, *2* (4), 615–624.

(67) Kodiah Beyeh, N.; Aumanen, J.; Åhman, A.; Luostarinen, M.; Mansikkamäki, H.; Nissinen, M.; Korppi-Tommola, J.; Rissanen, K. Dansylated Resorcinarenes. *New Journal of Chemistry* **2007**, *31* (3), 370–376.

(68) Beyeh, N. K.; Valkonen, A.; Rissanen, K. Encapsulation of Tetramethylphosphonium Cations.

(69) Kalenius, E.; Kekäläinen, T.; Neitola, R.; Beyeh, K.; Rissanen, K.; Vainiotalo, P. Size- and Structure-Selective Noncovalent Recognition of Saccharides by Tetraethyl and Tetraphenyl Resorcinarenes in the Gas Phase. *Chemistry – A European Journal* **2008**, *14* (17), 5220–5228.

(70) Beyeh, N. K.; Weimann, D. P.; Kaufmann, L.; Schalley, C. A.; Rissanen, K. Ion-Pair Recognition of Tetramethylammonium Salts by Halogenated Resorcinarenes. *Chemistry – A European Journal* **2012**, *18* (18), 5552–5557.

(71) Kodiah Beyeh, N.; Göth, M.; Kaufmann, L.; Schalley, C. A.; Rissanen, K. The Synergetic Interplay of Weak Interactions in the Ion-Pair Recognition of Quaternary and Diquaternary Ammonium Salts by Halogenated Resorcinarenes. *European J Org Chem* **2014**, *2014* (1), 80–85.

(72) Turunen, L.; Beyeh, N. K.; Pan, F.; Valkonena, A.; Rissanen, K. Tetraiodoethynyl Resorcinarene Cavitands as Multivalent Halogen Bond Donors. *Chemical Communications* **2014**, *50* (100), 15920–15923.

(73) Turunen, L.; Pan, F.; Beyeh, N. K.; Cetina, M.; Trant, J. F.; Ras, R. H. A.; Rissanen, K. Halogen-Bonded Solvates of Tetrahaloethynyl Cavitands. *CrystEngComm* **2017**, *19* (35), 5223–5229.

(74) Turunen, L.; Warzok, U.; Puttreddy, R.; Beyeh, N. K.; Schalley, C. A.; Rissanen, K. [N···I+···N] Halogen-Bonded Dimeric Capsules from Tetrakis(3-Pyridyl)Ethylene Cavitands. *Angewandte Chemie International Edition* **2016**, *55* (45), 14033–14036.

(75) Beyeh, N. K.; Cetina, M.; Rissanen, K. Halogen Bonded Analogues of Deep Cavity Cavitands. *Chemical Communications* **2014**, *50* (16), 1959–1961.

(76) Kodiah Beyeh, N.; Valkonen, A.; Rissanen, K. Piperazine Bridged Resorcinarene Cages. *Org Lett* **2010**, *12* (7), 1392–1395.

(77) Beyeh, N. K.; Pan, F.; Bhowmik, S.; Mäkelä, T.; Ras, R. H. A.; Rissanen, K. N-Alkyl Ammonium Resorcinarene Salts as High-Affinity Tetravalent Chloride Receptors. *Chemistry – A European Journal* **2016**, *22* (4), 1355–1361.

(78) Beyeh, N. K.; Ala-Korpi, A.; Pan, F.; Jo, H. H.; Anslyn, E. v.; Rissanen, K. Cooperative Binding of Divalent Diamides by N-Alkyl Ammonium Resorcinarene Chlorides. *Chemistry – A European Journal* **2015**, *21* (26), 9556–9562.

(79) Pan, F.; Beyeh, N. K.; Rissanen, K. Concerted Halogen-Bonded Networks with N-Alkyl Ammonium Resorcinarene Bromides: From Dimeric Dumbbell to Capsular Architectures. *J Am Chem Soc* **2015**, *137* (32), 10406–10413.

(80) Välimäki, S.; Gustavsson, L.; Beyeh, N. K.; Linko, V.; Kostiainen, M. A. Halogen-Bond-Mediated Self-Assembly of Polymer–Resorcinarene Complexes. *Macromol Rapid Commun* **2019**, *40* (14), 1900158.

(81) Hunter, C. A.; Anderson, H. L. What Is Cooperativity? *Angewandte Chemie International Edition* **2009**, *48* (41), 7488–7499.

(82) von Krbek, L. K. S.; Schalley, C. A.; Thordarson, P. Assessing Cooperativity in Supramolecular Systems. *Chem Soc Rev* **2017**, *46* (9), 2622–2637.

(83) Mahadevi, A. S.; Sastry, G. N. Cooperativity in Noncovalent Interactions. *Chem Rev* **2016**, *116* (5), 2775–2825.

(84) Atwood, J. L.; Gokel, G. W.; Barbour, L. *Comprehensive Supramolecular Chemistry II*; Elsevier Science, 2017.

(85) Steed, J. W. The Role of Co-Crystals in Pharmaceutical Design. *Trends Pharmacol Sci* **2013**, *34* (3), 185–193.

(86) Schultheiss, N.; Newman, A. Pharmaceutical Cocrystals and Their Physicochemical Properties. *Cryst Growth Des* **2009**, *9* (6), 2950–2967.

(87) Shan, N.; Zaworotko, M. J. The Role of Cocrystals in Pharmaceutical Science. *Drug Discov Today* **2008**, *13* (9), 440–446.

(88) Duggirala, N. K.; Perry, M. L.; Almarsson, Ö.; Zaworotko, M. J. Pharmaceutical Cocrystals: Along the Path to Improved Medicines. *Chem. Commun.* **2016**, *52* (4), 640–655.

(89) Almarsson, Ö.; Peterson, M. L.; Zaworotko, M. The A to Z of Pharmaceutical Cocrystals: A Decade of Fast-Moving New Science and Patents. *Pharm Pat Anal* **2012**, *1* (3), 313–327.

(90) Landenberger, K. B.; Matzger, A. J. Cocrystals of 1,3,5,7-Tetranitro-1,3,5,7-Tetrazacyclooctane (HMX). *Cryst Growth Des* **2012**, *12* (7), 3603–3609.

(91) Landenberger, K. B.; Matzger, A. J. Cocrystal Engineering of a Prototype Energetic Material: Supramolecular Chemistry of 2,4,6-Trinitrotoluene. *Cryst Growth Des* **2010**, *10* (12), 5341–5347.

(92) Bolton, O.; Matzger, A. J. Improved Stability and Smart-Material Functionality Realized in an Energetic Cocrystal. *Angewandte Chemie International Edition* **2011**, *50* (38), 8960–8963.

(93) Bolton, O.; Simke, L. R.; Pagoria, P. F.; Matzger, A. J. High Power Explosive with Good Sensitivity: A 2:1 Cocrystal of CL-20:HMX. *Cryst Growth Des* **2012**, *12* (9), 4311–4314.

(94) Guo, D.; An, Q.; Zybin, S. V; Goddard III, W. A.; Huang, F.; Tang, B. The Co-Crystal of TNT/CL-20 Leads to Decreased Sensitivity toward Thermal Decomposition from First Principles Based Reactive Molecular Dynamics. *J. Mater. Chem. A* **2015**, *3* (10), 5409–5419.

(95) Park, L. Y.; Hamilton, D. G.; McGehee, E. A.; McMenimen, K. A. Complementary C3-Symmetric Donor−Acceptor Components: Cocrystal Structure and Control of Mesophase Stability. *J Am Chem Soc* **2003**, *125* (35), 10586–10590.

(96) Attias, A.-J.; Cavalli, C.; Donnio, B.; Guillon, D.; Hapiot, P.; Malthête, J. Columnar Mesophase from a New Disclike Mesogen Based on a 3,5-Dicyano-2,4,6-Tristyrylpyridine Core. *Chemistry of Materials* **2002**, *14* (1), 375–384.

(97) Bisson, A. P.; Hunter, C. A.; Morales, J. C.; Young, K. Cooperative Interactions in a Ternary Mixture. *Chemistry – A European Journal* **1998**, *4* (5), 845–851.

(98) Topić, F.; Rissanen, K. Systematic Construction of Ternary Cocrystals by Orthogonal and Robust Hydrogen and Halogen Bonds. *J Am Chem Soc* **2016**, *138* (20), 6610–6616.

(99) Tothadi, S.; Desiraju, G. R. Designing Ternary Cocrystals with Hydrogen Bonds and Halogen Bonds. *Chem. Commun.* **2013**, *49* (71), 7791–7793.

(100) Aakeröy, C. B.; Desper, J.; Smith, M. M. Constructing{,} Deconstructing{,} and Reconstructing Ternary Supermolecules. *Chem. Commun.* **2007**, No. 38, 3936–3938.

(101) Tothadi, S.; Mukherjee, A.; Desiraju, G. R. Shape and Size Mimicry in the Design of Ternary Molecular Solids: Towards a Robust Strategy for Crystal Engineering. *Chem. Commun.* **2011**, *47* (44), 12080–12082.

(102) Botta, B.; Cassani, M.; D'Acquarica, I.; Subissati, D.; Monache, G. Z. and G. D. Resorcarenes: Hollow Building Blocks for the Host-Guest Chemistry. *Current Organic Chemistry*. 2005, pp 1167–1202.

(103) Sliwa, W.; Kozlowski, C. *Calixarenes and Resorcinarenes*; Wiley, 2009.

(104) Schneider, H.-J.; Schneider, U. The Host-Guest Chemistry of Resorcinarenes. *Journal of inclusion phenomena and molecular recognition in chemistry* **1994**, *19* (1–4), 67–83.

(105) McIldowie, M. J.; Mocerino, M.; Ogden, M. I. A Brief Review of C n -Symmetric Calixarenes and Resorcinarenes. *Supramol Chem* **2010**, *22* (1), 13–39.

(106) Rebek, J. Molecular Behavior in Small Spaces. *Acc Chem Res* **2009**, *42* (10), 1660–1668.

(107) Wagner, B. D. Hydrogen Bonding of Excited States in Supramolecular Host–Guest Inclusion Complexes. *Phys. Chem. Chem. Phys.* **2012**, *14* (25), 8825–8835.

(108) Rest, C.; Kandanelli, R.; Fernández, G. Strategies to Create Hierarchical Self-Assembled Structures via Cooperative Non-Covalent Interactions. *Chem. Soc. Rev.* **2015**, *44* (8), 2543–2572.

(109) Shivanyuk, A. Selective Formation of Heterodimeric Resorcinarene Capsules. *Tetrahedron* **2005**, *61* (2), 349–352.

(110) Evan-Salem, T.; Baruch, I.; Avram, L.; Cohen, Y.; Palmer, L. C.; Rebek, J. Resorcinarenes Are Hexameric Capsules in Solution. *Proceedings of the National Academy of Sciences* **2006**, *103* (33), 12296–12300.

(111) Adriaenssens, L.; Ballester, P. Hydrogen Bonded Supramolecular Capsules with Functionalized Interiors: The Controlled Orientation of Included Guests. *Chem Soc Rev* **2013**, *42* (8), 3261–3277.

(112) Rauwald, U.; Scherman, O. A. Supramolecular Block Copolymers with Cucurbit[8]Uril in Water. *Angewandte Chemie International Edition* **2008**, *47* (21), 3950–3953.

(113) Al'tshuler, G. N.; Fedyaeva, O. N.; Ostapova, E. V. The Reaction OfC-Phenylcalix[4]Resorcinarene-Based Polymer with Quaternary Ammonium and Potassium Cations. *Russian Chemical Bulletin* **2000**, *49* (8), 1468–1470.

(114) Fujimura, T.; Ramasamy, E.; Ishida, Y.; Shimada, T.; Takagi, S.; Ramamurthy, V. Sequential Energy and Electron Transfer in a Three-Component System Aligned on a Clay Nanosheet. *Phys. Chem. Chem. Phys.* **2016**, *18* (7), 5404–5411.

(115) Yusof, N. N. M.; Kikuchi, Y.; Kobayashi, T. Predominant Hosting Lead(II) in Ternary Mixtures of Heavy Metal Ions by a Novel of Diethylaminomethyl-Calix[4]Resorcinarene. *International Journal of Environmental Science and Technology* **2014**, *11* (4), 1063–1072.

(116) Beyeh, N. K.; Pan, F.; Rissanen, K. Hierarchical Ordering in Ternary Co-Crystals of C60, N-Benzyl Ammonium Resorcinarene Bromide and Solvent Molecules. *Cryst Growth Des* **2014**, *14* (12), 6161–6165.

(117) Appel, E. A.; Biedermann, F.; Rauwald, U.; Jones, S. T.; Zayed, J. M.; Scherman, O. A. Supramolecular Cross-Linked Networks via Host−Guest Complexation with Cucurbit[8]Uril. *J Am Chem Soc* **2010**, *132* (40), 14251–14260.

(118) Rauwald, U.; Biedermann, F.; Deroo, S.; Robinson, C. V; Scherman, O. A. Correlating Solution Binding and ESI-MS Stabilities by Incorporating Solvation Effects in a Confined Cucurbit[8]Uril System. *J Phys Chem B* **2010**, *114* (26), 8606–8615.

(119) Sindelar, V.; Cejas, M. A.; Raymo, F. M.; Chen, W.; Parker, S. E.; Kaifer, A. E. Supramolecular Assembly of 2,7-Dimethyldiazapyrenium and Cucurbit[8]Uril: A New Fluorescent Host for Detection of Catechol and Dopamine. *Chemistry – A European Journal* **2005**, *11* (23), 7054–7059.

(120) Nguyen, N.; Clements, A. R.; Pattabiraman, M. Using Non-Covalent Interactions to Direct Regioselective 2+2 Photocycloaddition within a Macrocyclic Cavitand. *New J. Chem.* **2016**, *40* (3), 2433–2443.

(121) Puttreddy, R.; Beyeh, N. K.; Rissanen, K. Inclusion Complexes of C <inf>ethyl</Inf>-2-Methylresorcinarene and Pyridine N-Oxides: Breaking the C-I···O-N^+ Halogen Bond by Host-Guest Complexation. *CrystEngComm* **2016**, *18* (5).

(122) Puttreddy, R.; Beyeh, N. K.; Ras, R. H. A.; Trant, J. F.; Rissanen, K. Endo -/ Exo - And Halogen-Bonded Complexes of Conformationally Rigid C -Ethyl-2-Bromoresorcinarene and Aromatic N -Oxides. *CrystEngComm* **2017**, *19* (30).

(123) Puttreddy, R.; Beyeh, N. K.; Ras, R. H. A.; Trant, J. F.; Rissanen, K. Endo-/Exo- and Halogen-Bonded Complexes of Conformationally Rigid C-Ethyl-2-Bromoresorcinarene and Aromatic N-Oxides. *CrystEngComm* **2017**, *19* (30), 4312–4320.

(124) Puttreddy, R.; Beyeh, N. K.; Kalenius, E.; Ras, R. H. A.; Rissanen, K. 2-Methylresorcinarene: A Very High Packing Coefficient in a Mono-Anion Based Dimeric Capsule and the X-Ray Crystal Structure of the Tetra-Anion. *Chemical Communications* **2016**, *52* (52).

(125) Beyeh, N. K. N. K.; Puttreddy, R. Methylresorcinarene: A Reaction Vessel to Control the Coordination Geometry of Copper(Ii) in Pyridine N-Oxide Copper(Ii) Complexes. *Dalton Transactions* **2015**, *44* (21), 9881–9886.

(126) Nissinen, M.; Rissanen, K. Crystal Engineering Studies of the Complexes of Ethyl Resorcinarene with Aromatic Nitrogen Heterocycles. *Supramol Chem* **2003**, *15* (7–8), 581–590.

(127) Cohen, Y.; Avram, L.; Frish, L. Diffusion NMR Spectroscopy in Supramolecular and Combinatorial Chemistry: An Old Parameter—New Insights. *Angewandte Chemie International Edition* **2005**, *44* (4), 520–554.

(128) Avram, L.; Cohen, Y.; Rebek Jr., J. Recent Advances in Hydrogen-Bonded Hexameric Encapsulation Complexes. *Chem. Commun.* **2011**, *47* (19), 5368–5375.

(129) Avram, L.; Cohen, Y. Diffusion NMR of Molecular Cages and Capsules. *Chem. Soc. Rev.* **2015**, *44* (2), 586–602.

(130) Avram, L.; Cohen, Y. Spontaneous Formation of Hexameric Resorcinarene Capsule in Chloroform Solution as Detected by Diffusion NMR. *J Am Chem Soc* **2002**, *124* (51), 15148–15149.

(131) Timmerman, P.; Verboom, W.; Reinhoudt, D. N. Resorcinarenes. *Tetrahedron* **1996**, *52* (8), 2663–2704. https://doi.org/http://dx.doi.org/10.1016/0040-4020(95)00984-1.

(132) Jasat, A.; Sherman, J. C. Carceplexes and Hemicarceplexes. *Chem Rev* **1999**, *99* (4), 931–968. https://doi.org/10.1021/cr960048o.

(133) Neri, P.; Sessler, J. L.; Wang, M. X. *Calixarenes and Beyond*; Springer International Publishing, 2016.

(134) Böhmer, V. Calixarenes, Macrocycles with (Almost) Unlimited Possibilities. *Angewandte Chemie International Edition in English* **1995**, *34* (7), 713–745.

(135) Gramage-Doria, R.; Armspach, D.; Matt, D. Metallated Cavitands (Calixarenes, Resorcinarenes, Cyclodextrins) with Internal Coordination Sites. *Coord Chem Rev* **2013**, *257* (3), 776–816.

(136) Kobayashi, K.; Yamanaka, M. Self-Assembled Capsules Based on Tetrafunctionalized Calix[4]Resorcinarene Cavitands. *Chem Soc Rev* **2015**, *44* (2), 449–466.

(137) Kobayashi, K.; Asakawa, Y.; Kikuchi, Y.; Toi, H.; Aoyama, Y. CH-.Pi. Interaction as an Important Driving Force of Host-Guest Complexation in Apolar Organic Media. Binding of Monools and Acetylated Compounds to Resorcinol Cyclic Tetramer as Studied by Proton NMR and Circular Dichroism Spectroscopy. *J Am Chem Soc* **1993**, *115* (7), 2648–2654.

(138) Mahalakshmi, L.; Das, P. P.; Guru Row, T. N. Self Assembly of C-Methyl Resorcin[4]Arene with Coumarin and Thiocoumarin: A Nanotubular Array with a near Perfect Lock and Key Fit. *Journal of Chemical Sciences* **2008**, *120* (1), 39–44.

(139) Ma, B.-Q.; Coppens, P. Symmetry Mismatching as a Tool in the Synthesis of Complex Supramolecular Solids with Multiple Cavities. *Cryst Growth Des* **2004**, *4* (2), 211–213.

(140) Ma, B.-Q.; Zhang, Y.; Coppens, P. Multiple Structures in Supramolecular Solids: Benzophenone Embedded in Three Different C-Methylcalix[4]Resorcinarene/Bipyridine Frameworks. *Cryst Growth Des* **2001**, *1* (4), 271–275.

(141) Pfeiffer, C. R.; Atwood, S. G.; Samadello, L.; Atwood, J. L. Investigating Properties and Trends of Cocrystals Composed of Pyrogallol[4]Arenes and Anthracene-Based Fluorescent Probes. *Cryst Growth Des* **2015**, *15* (6), 2958–2978.

(142) Atwood, J. L.; Szumna, A. Cation–Pi Interactions in Neutral Calix[4]Resorcinarenes. *Journal of Supramolecular Chemistry* **2002**, *2* (4–5), 479–482.

(143) Barnes, C. L.; Bosch, E. Self-Assembly of C-Methyl Calix[4]Resorcinarene with 5,5{\textasciiacutex}-Bipyrimidine. *J Chem Crystallogr* **2007**, *37* (11), 783–786.

(144) Jiang, S.; Patil, R. S.; Barnes, C. L.; Atwood, J. L. Application of Cocrystallization for the Separation of C-Ethylresorcin[6]Arene from C-Ethylresoricn[4]Arene. *Cryst Growth Des* **2017**, *17* (8), 4060–4063.

(145) Zhou, J.; Chen, M.; Diao, G. Assembling Gold and Platinum Nanoparticles on Resorcinarene Modified Graphene and Their Electrochemical Applications. *J. Mater. Chem. A* **2013**, *1* (6), 2278–2285.

(146) Shen, M.; Sun, Y.; Han, Y.; Yao, R.; Yan, C. Strong Deaggregating Effect of a Novel Polyamino Resorcinarene Surfactant on Gold Nanoaggregates under Microwave Irradiation. *Langmuir* **2008**, *24* (22), 13161–13167.

(147) Sun, Y.; Yao, Y.; Yan, C.-G.; Han, Y.; Shen, M. Selective Decoration of Metal Nanoparticles inside or Outside of Organic Microstructures via Self-Assembly of Resorcinarene. *ACS Nano* **2010**, *4* (4), 2129–2141.

(148) Tripp, S. L.; Pusztay, S. V; Ribbe, A. E.; Wei, A. Self-Assembly of Cobalt Nanoparticle Rings. *J Am Chem Soc* **2002**, *124* (27), 7914–7915.

(149) Liu, W.; Yang, H.; Wu, W.; Gao, H.; Xu, S.; Guo, Q.; Liu, Y.; Xu, S.; Cao, S. Calix[4]Resorcinarene-Based Branched Macromolecules for All-Optical Photorefractive Applications. *J. Mater. Chem. C* **2016**, *4* (45), 10684–10690.

(150) Xu, S.; Fang, C.; Wu, Y.; Wu, W.; Guo, Q.; Zeng, J.; Wang, X.; Liu, Y.; Cao, S. Photorefractive Hyper-Structured Molecular Glasses Constructed by Calix[4]Resorcinarene Core and Carbazole-Based Methine Nonlinear Optical Chromophore. *Dyes and Pigments* **2017**, *142*, 8–16.

(151) Beyeh, N. K.; Díez, I.; Taimoory, S. M.; Meister, D.; Feig, A. I.; Trant, J. F.; Ras, R. H. A.; Rissanen, K. High-Affinity and Selective Detection of Pyrophosphate in Water by a Resorcinarene Salt Receptor. *Chem. Sci.* **2018**, *9* (5), 1358–1367.

(152) Haines, S. R.; Harrison, R. G. Novel Resorcinarene-Based PH-Triggered Gelator. *Chem. Commun.* **2002**, No. 23, 2846–2847.

(153) Li, N.; Harrison, R. G.; Lamb, J. D. Application of Resorcinarene Derivatives in Chemical Separations. *J Incl Phenom Macrocycl Chem* **2014**, *78* (1), 39–60.

(154) M., B. T.; Qi, Z.; Konrad, T. Iminium Catalysis inside a Self-Assembled Supramolecular Capsule: Modulation of Enantiomeric Excess. *Angewandte Chemie International Edition* **2016**, *55* (27), 7698–7701.

(155) Zhang, Q.; Catti, L.; Tiefenbacher, K. Catalysis inside the Hexameric Resorcinarene Capsule. *Acc Chem Res* **2018**, *51* (9), 2107–2114.

(156) Zhang, Q.; Rinkel, J.; Goldfuss, B.; Dickschat, J. S.; Tiefenbacher, K. Sesquiterpene Cyclizations Catalysed inside the Resorcinarene Capsule and Application in the Short Synthesis of Isolongifolene and Isolongifolenone. *Nat Catal* **2018**, *1* (8), 609–615.

(157) Zhang, Q.; Catti, L.; Kaila, V. R. I.; Tiefenbacher, K. To Catalyze or Not to Catalyze: Elucidation of the Subtle Differences between the Hexameric Capsules of Pyrogallolarene and Resorcinarene. *Chem Sci* **2017**, *8* (2), 1653–1657.

(158) Patel, M. B.; Valand, N. N.; Modi, N. R.; Joshi, K. V; Harikrishnan, U.; Kumar, S. P.; Jasrai, Y. T.; Menon, S. K. Effect of P-Sulfonatocalix[4]Resorcinarene (PSC[4]R) on the Solubility and Bioavailability of a Poorly Water Soluble Drug Lamotrigine (LMN) and Computational Investigation. *RSC Adv.* **2013**, *3* (36), 15971–15981.

(159) Hoskins C, Papachristou A, Ho TMH, Hine J, C. A. Investigation into Drug Solubilisation Potential of Sulfonated Calix[4] Resorcinarenes. *J Nanomed Nanotechnol* **2016**, *7*, 370.

(160) Sanabria, E.; Esteso, M. Á.; Pérez-Redondo, A.; Vargas, E.; Maldonado, M. Synthesis and Characterization of Two Sulfonated Resorcinarenes: A New Example of a Linear Array of Sodium Centers and Macrocycles. *Molecules* **2015**, *20* (6), 9915–9928.

(161) Jang, Y.-M.; Yu, C.-J.; Kim, J.-S.; Kim, S.-U. Ab Initio Design of Drug Carriers for Zoledronate Guest Molecule Using Phosphonated and Sulfonated Calix[4]Arene and Calix[4]Resorcinarene Host Molecules. *J Mater Sci* **2018**, *53* (7), 5125–5139.

(162) Galindres, D. M.; Ribeiro, A. C. F.; Valente, A. J. M.; Esteso, M. A.; Sanabria, E.; Vargas, E. F.; Verissimo, L. M. P.; Leaist, D. G. Ionic Conductivities and Diffusion Coefficients of Alkyl Substituted Sulfonated Resorcinarenes in Aqueous Solutions. *J Chem Thermodyn* **2019**, *133*, 223–228.

(163) Kazakova, E. K.; Makarova, N. A.; Ziganshina, A. U.; Muslinkina, L. A.; Muslinkin, A. A.; Habicher, W. D. Novel Water-Soluble Tetrasulfonatomethylcalix[4]Resorcinarenes. *Tetrahedron Lett* **2000**, *41* (51), 10111–10115.

(164) Syakaev, V. V; Kazakova, E. Kh.; Morozova, J. E.; Shalaeva, Y. V; Latypov, S. K.; Konovalov, A. I. Guest Controlled Aggregation of Amphiphilic Sulfonatomethylated Calix[4]Resorcinarenes in Aqueous Solutions. *J Colloid Interface Sci* **2012**, *370* (1), 19–26.

(165) Shalaeva, Y. V; Morozova, J. E.; Syakaev, V. V; Kazakova, E. K.; Ermakova, A. M.; Nizameev, I. R.; Kadirov, M. K.; Konovalov, A. I. Supramolecular Nanoscale Systems Based on Amphiphilic Tetramethylensulfonatocalix[4]Resorcinarenes and Cationic Polyelectrolyte with Controlled Guest Molecule Binding. *Supramol Chem* **2017**, *29* (4), 278–289.

(166) Amirov, R. R.; Nugaeva, Z. T.; Mustafina, A. R.; Fedorenko, S. V; Morozov, V. I.; Kazakova, E. K.; Habicher, W. D.; Konovalov, A. I. Aggregation and Counter Ion Binding Ability of Sulfonatomethylcalix[4]Resorcinarenes in Aqueous Solutions. *Colloids Surf A Physicochem Eng Asp* **2004**, *240* (1), 35–43.

(167) Counterion Effect on Sulfonatocalix[n]Arene Recognition . *Pure and Applied Chemistry* . 2019.

(168) Mustafina, A. R.; Fedorenko, S. V; Makarova, N. A.; Kazakova, E. K. H.; Bazhanova, Z. G.; Kataev, V. E.; Konovalov, A. I. The Inclusion Properties of a New Watersoluble Sulfonated Calix[4]Resorcinarene towards Alkylammonium and N-Methylpyridinium Cations. *J Incl Phenom Macrocycl Chem* **2001**, *40* (1), 73–76.

(169) Sanabria, E.; Esteso, M. Á.; Vargas, E.; Maldonado, M. Experimental Comparative Study of Solvent Effects on the Structure of Two Sulfonated Resorcinarenes. *J Mol Liq* **2018**, *254*, 391–397.

(170) Hong, M.; Zhang, Y.-M.; Liu, Y. Selective Binding Affinity between Quaternary Ammonium Cations and Water-Soluble Calix[4]Resorcinarene. *J Org Chem* **2015**, *80* (3), 1849–1855.

(171) Kobayashi, K.; Asakawa, Y.; Kato, Y.; Aoyama, Y. Complexation of Hydrophobic Sugars and Nucleosides in Water with Tetrasulfonate Derivatives of Resorcinol Cyclic Tetramer Having a Polyhydroxy Aromatic Cavity: Importance of Guest-Host CH-.Pi. Interaction. *J Am Chem Soc* **1992**, *114* (26), 10307–10313.

(172) Kashapov, R. R.; Pashirova, T. N.; Kharlamov, S. V; Ziganshina, A. Yu.; Ziltsova, E. P.; Lukashenko, S. S.; Zakharova, L. Ya.; Habicher, W. D.; Latypov, S. K.; Konovalov, A. I. Novel Self-Assembling System Based on Resorcinarene and Cationic Surfactant. *Phys. Chem. Chem. Phys.* **2011**, *13* (35), 15891–15898.

(173) Korshin, D. E.; Kashapov, R. R.; Murtazina, L. I.; Mukhitova, R. K.; Kharlamov, S. V; Latypov, S. K.; Ryzhkina, I. S.; Ziganshina, A. Y.; Konovalov, A. I. Self-Assembly of an Aminoalkylated Resorcinarene in Aqueous Media: Host–Guest Properties. *New J. Chem.* **2009**, *33* (12), 2397–2401.

(174) Bucur, C. B.; Sui, Z.; Schlenoff, J. B. Ideal Mixing in Polyelectrolyte Complexes and Multilayers: Entropy Driven Assembly. *J Am Chem Soc* **2006**, *128* (42), 13690–13691.

(175) Mansikkamäki, H.; Nissinen, M.; Rissanen, K. Noncovalent Π···π-Stacked Exo-Functional Nanotubes: Subtle Control of Resorcinarene Self-Assembly. *Angewandte Chemie* **2004**, *116* (10), 1263–1266.

(176) Mansikkamaki, H.; Schalley, C. A.; Nissinen, M.; Rissanen, K. Weak Interactions between Resorcinarenes and Diquaternary Alkyl Ammonium Cations. *New Journal of Chemistry* **2005**, *29* (1), 116–127.

(177) Mansikkamäki, H.; Schalley, C. A.; Nissinen, M.; Rissanen, K. Weak Interactions between Resorcinarenes and Diquaternary Alkyl Ammonium Cations. *New J. Chem.* **2005**, *29* (1), 116–127.

(178) Mansikkamäki, H.; Nissinen, M.; Rissanen, K. C-Methyl Resorcin[4]Arene Packing Motifs with Alkyl Ammonium Salts: From Molecular Capsules to Channels and Tubes. *CrystEngComm* **2005**, *7* (85), 519–526.

(179) Beyeh, N. K.; Weimann, D. P.; Kaufmann, L.; Schalley, C. A.; Rissanen, K. Ion-Pair Recognition of Tetramethylammonium Salts by Halogenated Resorcinarenes. *Chemistry – A European Journal* **2012**, *18* (18), 5552–5557.

(180) Palacios, M. A.; Nishiyabu, R.; Marquez, M.; Anzenbacher, P. Supramolecular Chemistry Approach to the Design of a High-Resolution Sensor Array for Multianion Detection in Water. *J Am Chem Soc* **2007**, *129* (24), 7538–7544.

(181) Hargrove, A. E.; Nieto, S.; Zhang, T.; Sessler, J. L.; Anslyn, E. V. Artificial Receptors for the Recognition of Phosphorylated Molecules. *Chemical Reviews*. NIH Public Access November 9, 2011, pp 6603–6782.

(182) Rostami, A.; Wei, C. J.; Guérin, G.; Taylor, M. S. Anion Detection by a Fluorescent Poly(Squaramide): Self-Assembly of Anion-Binding Sites by Polymer Aggregation. *Angewandte Chemie International Edition* **2011**, *50* (9), 2059–2062.

(183) Egawa, T.; Hirabayashi, K.; Koide, Y.; Kobayashi, C.; Takahashi, N.; Mineno, T.; Terai, T.; Ueno, T.; Komatsu, T.; Ikegaya, Y.; Matsuki, N.; Nagano, T.; Hanaoka, K. Red Fluorescent Probe for Monitoring the Dynamics of Cytoplasmic Calcium Ions. *Angewandte Chemie - International Edition* **2013**, *52* (14), 3874–3877.

(184) Zapata, F.; Caballero, A.; White, N. G.; Claridge, T. D. W.; Costa, P. J.; Félix, V.; Beer, P. D. Fluorescent Charge-Assisted Halogen-Bonding Macrocyclic Halo-Imidazolium Receptors for Anion Recognition and Sensing in Aqueous Media. *J Am Chem Soc* **2012**, *134* (28), 11533–11541.

(185) Ji, X.; Wu, R. T.; Long, L.; Guo, C.; Khashab, N. M.; Huang, F.; Sessler, J. L. Physical Removal of Anions from Aqueous Media by Means of a Macrocycle-Containing Polymeric Network. *J Am Chem Soc* **2018**, *140* (8), 2777–2780.

(186) Pan, F.; Beyeh, N. K.; Rissanen, K. Dimeric Resorcinarene Salt Capsules with Very Tight Encapsulation of Anions and Guest Molecules. *RSC Adv* **2015**, *5* (71), 57912–57916.

(187) Borissov, A.; Marques, I.; Lim, J. Y. C.; Félix, V.; Smith, M. D.; Beer, P. D. Anion Recognition in Water by Charge-Neutral Halogen and Chalcogen Bonding Foldamer Receptors. *J Am Chem Soc* **2019**, *141* (9), 4119–4129.

(188) Lee, D. H.; Kim, S. Y.; Hong, J. I. A Fluorescent Pyrophosphate Sensor with High Selectivity over ATP in Water. *Angewandte Chemie - International Edition* **2004**.

(189) White, N. G.; Carvalho, S.; Félix, V.; Beer, P. D. Anion Binding in Aqueous Media by a Tetra-Triazolium Macrocycle. *Org Biomol Chem* **2012**, *10* (34), 6951–6959.

(190) Gale, P. A.; Davis, J. T.; Quesada, R. Anion Transport and Supramolecular Medicinal Chemistry. *Chemical Society Reviews*. 2017.

(191) Busschaert, N.; Caltagirone, C.; Van Rossom, W.; Gale, P. A. Applications of Supramolecular Anion Recognition. *Chemical Reviews*. 2015.

(192) Langton, M. J.; Robinson, S. W.; Marques, I.; Félix, V.; Beer, P. D. Halogen Bonding in Water Results in Enhanced Anion Recognition in Acyclic and Rotaxane Hosts. *Nat Chem* **2014**, *6* (12), 1039–1043.

(193) Kyung, K. I. M. S.; Dong Hoon, L. E. E.; Hong, J. I. N.; Yoon, J. Chemosensors for Pyrophosphate. *Acc Chem Res* **2009**, *42* (1), 23–31.

(194) Amendola, V.; Fabbrizzi, L.; Mosca, L. Anion Recognition by Hydrogen Bonding: Urea-Based Receptors. *Chemical Society Reviews*. 2010.

(195) Tromans, R. A.; Carter, T. S.; Chabanne, L.; Crump, M. P.; Li, H.; Matlock, J. V.; Orchard, M. G.; Davis, A. P. A Biomimetic Receptor for Glucose. *Nat Chem* **2019**, *11* (1), 52–56.

(196) Zhang, Z.; Schreiner, P. R. (Thio)Urea Organocatalysis—What Can Be Learnt from Anion Recognition? *Chem Soc Rev* **2009**, *38* (4), 1187–1198.

(197) Kubik, S. Anion Recognition in Water. *Chem Soc Rev* **2010**, *39* (10), 3648–3663.

(198) Mustroph, A.; Hess, N.; Sasidharan, R. Hypoxic Energy Metabolism and Ppi as an Alternative Energy Currency. *Plant Cell Monographs* **2014**, *21*, 165–184.

(199) Wright, G. D.; Doherty, M. Calcium Pyrophosphate Crystal Deposition Is Not Always “wear and Tear” or Aging. *Ann Rheum Dis* **1997**, *56* (10), 586–588.

(200) Lee, D. H.; Kim, S. Y.; Hong, J.-I. A Fluorescent Pyrophosphate Sensor with High Selectivity over ATP in Water. *Angewandte Chemie* **2004**, *116* (36), 4881–4884.

(201) Lee, D. H.; Im, J. H.; Son, S. U.; Chung, Y. K.; Hong, J. I. An Azophenol-Based Chromogenic Pyrophosphate Sensor in Water. *J Am Chem Soc* **2003**, *125* (26), 7752–7753.

(202) Cheng, T.; Wang, T.; Zhu, W.; Chen, X.; Yang, Y.; Xu, Y.; Qian, X. Red-Emission Fluorescent Probe Sensing Cadmium and Pyrophosphate Selectively in Aqueous Solution. *Org Lett* **2011**.

(203) Kumari, N.; Huang, H.; Chao, H.; Gasser, G.; Zelder, F. A Disassembly Strategy for Imaging Endogenous Pyrophosphate in Mitochondria by Using an FeIII–Salen Complex. *ChemBioChem* **2016**, *17* (13), 1211–1215.

(204) Oshchepkov, A. S.; Mittapalli, R. R.; Fedorova, O. A.; Kataev, E. A. Naphthalimide-Based Polyammonium Chemosensors for Anions: Study of Binding Properties and Sensing Mechanisms. *Chemistry - A European Journal* **2017**, *23* (40), 9657–9665.

(205) Gunnlaugsson, T.; Davis, A. P.; O'Brien, J. E.; Glynn, M. Fluorescent Sensing of Pyrophosphate and Bis-Carboxylates with Charge Neutral PET Chemosensors. *Org Lett* **2002**, *4* (15), 2449–2452.

(206) Huang, X.; Guo, Z.; Zhu, W.; Xie, Y.; Tian, H. A Colorimetric and Fluorescent Turn-on Sensor for Pyrophosphate Anion Based on a Dicyanomethylene-4H-Chromene Framework. *Chemical Communications* **2008**, No. 41, 5143–5145.

(207) Cabarcos, O. M.; Weinheimer, C. J.; Lisy, J. M.; Xantheas, S. S. Microscopic Hydration of the Fluoride Anion. *Journal of Chemical Physics* **1999**, *110* (1), 5–8.

(208) Saint-Martin, H.; Ortega-Blake, I.; Leś, A.; Adamowicz, L. The Role of Hydration in the Hydrolysis of Pyrophosphate. A Monte Carlo Simulation with Polarizable-Type Interaction Potentials. *Biochimica et Biophysica Acta (BBA)/Protein Structure and Molecular* **1994**, *1207* (1), 12–23.

(209) Beyeh, N. K.; Pan, F.; Bhowmik, S.; Mäkelä, T.; Ras, R. H. A. A.; Rissanen, K. N-Alkyl Ammonium Resorcinarene Salts as High-Affinity Tetravalent Chloride Receptors. *Chemistry - A European Journal* **2016**, *22* (4), 1355–1361.

(210) Beyeh, N. K.; Valkonen, A.; Bhowmik, S.; Pan, F.; Rissanen, K. N-Alkyl Ammonium Resorcinarene Salts: Multivalent Halogen-Bonded Deep-Cavity Cavitands. *Organic Chemistry Frontiers* **2015**, *2* (4), 340–345.

(211) Beyeh, N. K.; Cetina, M.; Rissanen, K. Halogen Bonded Analogues of Deep Cavity Cavitands. *Chemical Communications* **2014**, *50* (16), 1959–1961.

(212) Beyeh, N. K.; Díez, I.; Taimoory, S. M.; Meister, D.; Feig, A. I.; Trant, J. F.; Ras, R. H. A.; Rissanen, K. High-Affinity and Selective Detection of Pyrophosphate in Water by a Resorcinarene Salt Receptor. *Chem Sci* **2018**, *9* (5), 1358–1367.

(213) Beyeh, N. K.; Rissanen, K. N-Alkyl Ammonium Resorcinarene Salts: A Versatile Family of Calixarene-Related Host Molecules. In *Calixarenes and Beyond*; Springer, 2016; pp 255–284.

(214) Graw, J. Genetics of Crystallins: Cataract and Beyond. *Experimental Eye Research*. Academic Press February 2, 2009, pp 173–189.

(215) Quinlan, R. A. A New Dawn for Cataracts. *Science (1979)* **2015**, *350* (6261), 636–637.

(216) Moreau, K. L.; King, J. A. Protein Misfolding and Aggregation in Cataract Disease and Prospects for Prevention. *Trends in Molecular Medicine*. 2012, pp 273–282.

(217) Kannan, R.; Santhoshkumar, P.; Mooney, B. P.; Sharma, K. K. The Aa66-80 Peptide Interacts with Soluble α-Crystallin and Induces Its Aggregation and Precipitation: A Contribution to Age-Related Cataract Formation. *Biochemistry* **2013**, *52* (21), 3638–3650.

(218) Santhoshkumar, P.; Raju, M.; Sharma, K. K. AA-Crystallin Peptide 66SDRDKFVIFLDVKHF80 Accumulating in Aging Lens Impairs the Function of α-Crystallin and Induces Lens Protein Aggregation. *PLoS One* **2011**, *6* (4).

(219) Raju, M.; Santhoshkumar, P.; Sharma, K. K. Lens Endogenous Peptide AA66-80 Generates Hydrogen Peroxide and Induces Cell Apoptosis. *Aging Dis* **2017**, *8* (1), 57–70.

(220) Derham, B. K.; Harding, J. J. Effect of Aging on the Chaperone-like Function of Human α-Crystallin Assessed by Three Methods. *Biochemical Journal* **1997**, *328* (3), 763–768.

(221) Warmack, R. A.; Shawa, H.; Liu, K.; Lopez, K.; Loo, J. A.; Horwitz, J.; Clarke, S. G. The L-Isoaspartate Modification within Protein Fragments in the Aging Lens Can Promote Protein Aggregation. *Journal of Biological Chemistry* **2019**, *294* (32), 12203–12219.

(222) Bisht, A.; Sharma, M.; Sharma, S.; Ali, M. E.; Panda, J. J. Carrier-Free Self-Built Aspirin Nanorods as Anti-Aggregation Agents towards Alpha-Crystallin-Derived Peptide Aggregates: Potential Implications in Non-Invasive Cataract Therapy. *J Mater Chem B* **2019**, *7* (44), 6945–6954.

(223) Xu, J.; Fu, Q.; Chen, X.; Yao, K. Advances in Pharmacotherapy of Cataracts. *Ann Transl Med* **2020**, *8* (22), 1552–1552.

(224) Allen, D.; Vasavada, A. Cataract and Surgery for Cataract. *Br Med J* **2006**, *333* (7559), 128–132.

(225) Douglas, T.; Young, M. Host-Guest Encapsulation of Materials by Assembled Virus Protein Cages. *Nature* **1998**, *393* (6681), 152–155.

(226) Välimäki, S.; Beyeh, N. K.; Linko, V.; Ras, R. H. A.; Kostiainen, M. A. A Supramolecular Host-Guest Complex for Heparin Binding and Sensing. *Nanoscale* **2018**, *10* (29), 14022–14030.

(227) Schrader, T.; Bitan, G.; Klärner, F. G. Molecular Tweezers for Lysine and Arginine-Powerful Inhibitors of Pathologic Protein Aggregation. *Chemical Communications* **2016**, *52* (76), 11318–11334.

(228) Sinha, S.; Lopes, D. H. J.; Du, Z.; Pang, E. S.; Shanmugam, A.; Lomakin, A.; Talbiersky, P.; Tennstaedt, A.; McDaniel, K.; Bakshi, R.; Kuo, P. Y.; Ehrmann, M.; Benedek, G. B.; Loo, J. A.; Klärner, F. G.; Schrader, T.; Wang, C.; Bitan, G. Lysine-Specific Molecular Tweezers Are Broad-Spectrum Inhibitors of Assembly and Toxicity of Amyloid Proteins. *J Am Chem Soc* **2011**, *133* (42), 16958–16969.

(229) Prabhudesai, S.; Sinha, S.; Attar, A.; Kotagiri, A.; Fitzmaurice, A. G.; Lakshmanan, R.; Ivanova, M. I.; Loo, J. A.; Klärner, F. G.; Schrader, T.; Stahl, M.; Bitan, G.; Bronstein, J. M. A Novel "Molecular Tweezer" Inhibitor of α-Synuclein Neurotoxicity in Vitro and in Vivo. *Neurotherapeutics* **2012**, *9* (2), 464–476.

(230) Kazakova, E. K.; Makarova, N. A.; Ziganshina, A. U.; Muslinkina, L. A.; Muslinkin, A. A.; Habicher, W. D. Novel Water-Soluble Tetrasulfonatomethylcalix[4]Resorcinarenes. *Tetrahedron Lett* **2000**, *41* (51), 10111–10115.

(231) Twum, K.; Rautiainen, J. M.; Yu, S.; Truong, K. N.; Feder, J.; Rissanen, K.; Puttreddy, R.; Beyeh, N. K. Host-Guest Interactions of Sodiumsulfonatomethyleneresorcinarene and Quaternary Ammonium Halides: An Experimental-Computational Analysis of the Guest Inclusion Properties. *Cryst Growth Des* **2020**, *20* (4), 2367–2376.

(232) Hong, M.; Zhang, Y. M.; Liu, Y. Selective Binding Affinity between Quaternary Ammonium Cations and Water-Soluble Calix[4]Resorcinarene. *Journal of Organic Chemistry* **2015**, *80* (3), 1849–1855.

(233) Kobayashi, K.; Asakawa, Y.; Kato, Y.; Aoyama, Y. Complexation of Hydrophobic Sugars and Nucleosides in Water with Tetrasulfonate Derivatives of Resorcinol Cyclic Tetramer Having a Polyhydroxy Aromatic Cavity: Importance of Guest-Host CH-.Pi. Interaction. *J Am Chem Soc* **2002**, *114* (26), 10307–10313.

(234) Oshinbolu, S.; Shah, R.; Finka, G.; Molloy, M.; Uden, M.; Bracewell, D. G. Evaluation of Fluorescent Dyes to Measure Protein Aggregation within Mammalian Cell Culture Supernatants. *Journal of Chemical Technology and Biotechnology* **2018**, *93* (3), 909–917.

(235) Chakrabortee, S.; Liu, Y.; Zhang, L.; Matthews, H. R.; Zhang, H.; Pan, N.; Cheng, C. R.; Guan, S. H.; Guo, D. A.; Huang, Z.; Zheng, Y.; Tunnacliffe, A. Macromolecular and Small-Molecule Modulation of Intracellular Aβ 42 Aggregation and Associated Toxicity. *Biochemical Journal* **2012**, *442* (3), 507–515.

(236) Regitz, C.; Fitzenberger, E.; Mahn, F. L.; Dußling, L. M.; Wenzel, U. Resveratrol Reduces Amyloid-Beta (Aβ1–42)-Induced Paralysis through Targeting Proteostasis in an Alzheimer Model of Caenorhabditis Elegans. *Eur J Nutr* **2016**, *55* (2), 741–747.

(237) McClure, S. M.; Ahl, P. L.; Blue, J. T. High Throughput Differential Scanning Fluorimetry (DSF) Formulation Screening with Complementary Dyes to Assess Protein Unfolding and Aggregation in Presence of Surfactants. *Pharm Res* **2018**, *35* (4), 1–10. https://doi.org/10.1007/s11095-018-2361-1.

(238) Burchard, W. Dynamic Light Scattering. *Polysaccharide Hydrogels: Characterization and Biomedical Applications* **2016**, *67* (12), 167–207.

(239) Freire, E.; Mayorga, O. L.; Straume, M. Isothermal Titration. *Anal Chem* **1990**, *62* (18), 950A-959A.